

Research Articles | Systems/Circuits

## Spinal glycine receptor alpha 3 cells communicate sensations of chemical itch in hairy skin

<https://doi.org/10.1523/JNEUROSCI.1585-23.2024>

Received: 22 August 2023  
Revised: 31 January 2024  
Accepted: 15 February 2024

Copyright © 2024 Weman et al.

This is an open-access article distributed under the terms of the [Creative Commons Attribution 4.0 International license](#), which permits unrestricted use, distribution and reproduction in any medium provided that the original work is properly attributed.

---

*This Early Release article has been peer reviewed and accepted, but has not been through the composition and copyediting processes. The final version may differ slightly in style or formatting and will contain links to any extended data.*

**Alerts:** Sign up at [www.jneurosci.org/alerts](http://www.jneurosci.org/alerts) to receive customized email alerts when the fully formatted version of this article is published.

1 **Spinal glycine receptor alpha 3 cells communicate sensations of chemical itch in**  
2 **hairy skin**

3 Abbreviated title: Spinal *Gla3* cells signal itch in hairy skin

4  
5 Hannah M. Weman<sup>1</sup>, Mikaela M. Ceder<sup>1</sup>, Aikeremu Ahemaiti<sup>1</sup>, Kajsa A. Magnusson<sup>1</sup>, Katharina  
6 Henriksson<sup>1</sup>, Linn Andréasson<sup>1</sup> and Malin C. Lagerström<sup>1</sup>

7 <sup>1</sup>Department of Immunology, Genetics and Pathology, Uppsala University, 751 08 Uppsala,  
8 Sweden

9 Corresponding author: [malin.lagerstrom@igp.uu.se](mailto:malin.lagerstrom@igp.uu.se){ Citation }

10  
11 **Author contributions**

12 Conceptualization: HMW, MCL; Methodology: HMW, MMC, AA, MCL; Validation: HMW,  
13 MMC, AA, KAM, MCL; Formal Analysis: HMW, MMC, AA; Investigation: HMW, MMC, AA,  
14 KAM, KH, LA; Resources: MCL; Data Curation: MCL; Visualization: HMW, MMC, AA, MCL;  
15 Supervision: HMW, MMC, MCL; Project Administration: HMW, MMC, MCL; Funding  
16 Acquisition: MMC, MCL; Writing-Original Draft: HMW, MMC, AA, MCL; Writing-Review &  
17 Editing: HMW, MMC, AA, KAM, KH, MCL. All authors have read and approved the final version.

18  
19 Number of pages: 77

20 Number of figures: 14

21 Number of tables: 2 + a key resource table (in material and methods)

22 Number of words for abstract: 164

23 Number of words for introduction: 440

24 Number of words for discussion: 1,603

25

## 26 **Conflict of interest**

27 The authors declare no conflict of interest.

28

## 29 **Acknowledgements**

30 We would like to express our gratitude to Jonne Rietdijk and Jon Jakobsson for technical assistance,  
31 Stina Lundberg for statistical analysis input, Elena Muscolino for proofreading and Caroline  
32 Öhman-Mägi for technical assistance prior to the 3D printing of the artificial hind paw. The 3D  
33 printing was performed at U-PRINT: Uppsala University's 3D-printing facility at the Disciplinary  
34 Domain of Medicine and Pharmacy. Uppsala University Behavioral Facility (UUBF) for virus  
35 facility and behavioral tests support, and the Biological Visualization (BioVis) core at the  
36 department of Immunology, Genetics and Pathology, Uppsala University, for confocal imaging  
37 support. We would like to thank the viral core facility (VCF, Charité, Berlin) for the production of  
38 the helper and pseudotyped rabies viruses. This work was supported by the Swedish Brain  
39 Foundation, the Swedish research council (2016-00851, 2022-00960), Knut och Alice Wallenbergs  
40 Stiftelse (2019.0047) (dorsal root stimulations), and Uppsala University.

42 **Abstract**

43 Glycinergic neurons regulate nociceptive and pruriceptive signaling in the spinal cord, and the  
44 identity and role of the glycine-regulated neurons are not fully known. Herein, we have  
45 characterized spinal glycine receptor alpha 3 (*Gla3*) subunit-expressing neurons in *Gla3*-Cre  
46 female and male mice. *Gla3*-Cre(+) neurons express *Gla3*, are located mainly in laminae III–VI,  
47 and respond to glycine. Chemogenetic activation of spinal *Gla3*-Cre(+) neurons induced  
48 biting/licking, stomping, and guarding behaviors, indicative of both a nociceptive and pruriceptive  
49 role for this population. Chemogenetic inhibition did not affect mechanical or thermal responses,  
50 but reduced behaviors evoked by compound 48/80 and chloroquine, revealing a pruriceptive role  
51 for these neurons. Spinal cells activated by compound 48/80 or chloroquine express *Gla3*, further  
52 supporting the phenotype. Retrograde tracing revealed that spinal *Gla3*-Cre(+) neurons receive  
53 input from afferents associated with pain and itch, and dorsal root stimulation validated the  
54 monosynaptic input. In conclusion, these results show that spinal *Gla3*(+) neurons contribute to  
55 acute communication of compound 48/80- and chloroquine-induced itch in hairy skin.

56

57

58 **Significance Statement**

59 Spinal glycinergic neurons regulate itch (pruriception), suggesting that components of the  
60 glycinergic system have great potential as drug targets to treat pruritus. Nonetheless, thus far, the  
61 pruriceptive roles of any of the glycine receptor (GLR) subunits have not been evaluated. Here, we  
62 successfully linked the *Gla3*-Cre populations to a pro-pruriceptive role in itch, indicating that  
63 GLRA3-expressing neurons may be a potential novel target for itch treatment. The spontaneous  
64 stomping and guarding behaviors observed from activating the *Gla3*-Cre populations are  
65 indicative of a role in sensory hypersensitivity and hence, raises questions regarding the  
66 hypersensitivity involvement of these populations for future investigations.

## 68 **Introduction**

69  
70 Spinal somatosensory circuits transmitting the sensation of pain and itch from the body are  
71 regulated locally by inhibitory inputs, including glycinergic transmission (Beyer et al., 1985;  
72 Yamamoto and Yaksh, 1993; Takazawa et al., 2017; Freitag et al., 2019). For instance, ablation of  
73 glycine transporter 2 (GLYT2) neurons results in mechanical, heat, and cold hyperalgesia, and  
74 behaviors associated with persistent itch, e.g. extensive localized biting (Foster et al., 2015).  
75 Conversely, selective activation of GLYT2 neurons *in vivo* reduces the sensitivity to mechanical-,  
76 heat-, and cold-induced pain, and the behavioral responses against chloroquine and histamine,  
77 suggesting that the glycinergic system is essential for controlling pain and itch transmission (Foster  
78 et al., 2015). In addition, the glycinergic system is activated by nociceptive counter stimuli, which  
79 decrease itch transmission in the spinal cord (Akiyama et al., 2011).

80 Glycinergic receptors (GLRs) are ligand-gated ion channels, which induce inward hyperpolarizing  
81 chloride currents upon binding of glycine (Lynch, 2004; Zeilhofer, 2005; Lein et al., 2007; Dutertre  
82 et al., 2012). In mice, the glycine receptor alpha 3 (*Glrα3*) gene is expressed in both excitatory and  
83 inhibitory spinal dorsal horn neuronal clusters (Häring et al., 2018; Zeisel et al., 2018; Ceder et al.,  
84 2023) and GLRA3 immunoreactivity is detected in the dorsal (Harvey et al., 2004; Wang et al.,  
85 2018; Werynska et al., 2021) and ventral horns of the spinal cord (Harvey et al., 2004; Wang et al.,  
86 2018). The other *Glr* genes; *Glrα1*, *Glrα2*, *Glrα4* and *Glrβ*, are also expressed in the dorsal horn of  
87 the spinal cord (Groemer et al., 2022). In addition to the expression in the spinal cord, *Glrα3* is  
88 detected in the amygdala, hypothalamus, nucleus accumbens, tegmentum, and brainstem, but not  
89 in the dorsal root ganglia (DRG) (Lein et al., 2007; Usoskin et al., 2015; McCracken et al., 2017;  
90 Häring et al., 2018; Tudeau et al., 2020; San Martin et al., 2021; Groemer et al., 2022). Expression  
91 analyses have shown that spinal cord injury decreases levels of GLRA3 in the dorsal spinal cord,

92 whereas zymosan A-induced inflammation increases GLRA3 levels (Berrocal et al., 2014;  
93 Mariqueo, 2020). Additionally, in an endometriosis mouse model, *Gla3* expression was found to  
94 be upregulated in the insula (Li et al., 2018), emphasizing this receptor subunit's role in pain and  
95 its potential as a novel pain treatment.

96 Thus far, studies have focused on examining the nociceptive role of the GLRA3 subunit. Herein,  
97 we investigated the molecular and electrophysiological characteristics, along with the sensory role  
98 of spinal *Gla3*-expressing cells in pruriceptive, mechanical, and thermal transmission, using a  
99 transgenic *Gla3*-Cre mouse line and *fos* measurements. Moreover, we established neuronal inputs  
100 to the population, using replication deficient rabies tracing and dorsal root stimulations.

101 **Materials and methods**

102

103 *Key Resources table*

| <b>Viral Vectors and Serotypes</b>    |                                |   |              |   |                          |
|---------------------------------------|--------------------------------|---|--------------|---|--------------------------|
|                                       | Vector                         | Source  | Company      | Lot and titer   | Injection                |
| <i>AAV8.hSyn-DIO-hM3D(Gq)-mCherry</i> | pAAV-hSyn-DIO-hM3D(Gq)-mCherry | The vector was a gift from Bryan Roth (Krashes et al., 2011) (Addgene viral prep #44361-AAV8; <a href="http://n2t.net/addgene:44361">http://n2t.net/addgene:44361</a> ; RRID:Addgene_44361) | Addgene, USA | first lot#: v27924 with titer: 2.2x 10 <sup>13</sup> GC/m<br>1; second lot # v78582 with titer: 2.1x 10 <sup>13</sup> GC/m<br>1 | One site                 |
| <i>AAV8.hSyn-DIO-hM4D(Gi)-mCherry</i> | pAAV-hSyn-hM4D(Gi)-mCherry     | The vector was a gift from Bryan Roth (Krashes et al., 2011) (Addgene viral prep #44362-AAV8;   | Addgene, USA | v86749 with titer: 1.8 x 10 <sup>13</sup> GC/ml   | Two sites (unilaterally) |



|                              |                       |  |                     |   |                               |
|------------------------------|-----------------------|--|---------------------|---|-------------------------------|
|                              |                       | <a href="http://n2t.net/addgene:44362">http://n2t.net/addgene:44362</a> ;<br>RRID:Addgene_44362)   |                     |   |                               |
| <i>AAV8.hSyn-DIO-mCherry</i> | pAAV-hSyn-DIO-mCherry | The vector was a gift from Bryan Roth (Addgene viral prep # 50459-AAV8;<br><a href="http://n2t.net/addgene:50459">http://n2t.net/addgene:50459</a> ;<br>RRID:Addgene_50459)  | Addgene, USA        | v61605<br>with titer:<br>2.2x<br>10 <sup>13</sup> GC/ml                   | One or two sites (unilateral) |
| <i>AAVDJ.EF1a-DIO-HTB</i>    | pAAV.EF1a-DIO-HTB     | The vector was a gift from Edward Callaway (Addgene plasmid # 44187;<br><a href="http://n2t.net/addgene:44187">http://n2t.net/addgene:44187</a> ;<br>RRID:Addgene_44187).<br>The vector was packaged into AAVDJ by Salk institute GT3 (Gene Transfer, Targeting, and Therapeutics) core facility (provided by John Naughton) with funding from NIH-NCI CCSG: | Salk institute, USA | lot date:<br>20/12-2018 with<br>titer:<br>1.09x<br>10 <sup>12</sup> VG/ml | Two sites (bilateral)         |

|   |  |   |                               |   |          |
|---|--|---|-------------------------------|---|----------|
|   |  | P30 014195, an NINDS R24 Core Grant and funding from NEI  |                               |   |          |
| <i>AAV8.Syn-flex-TVA.E66T-P2A-oG-WPRE3</i>                | <i>pAAV.Syn-flex-TVA.E66T-P2A-oG-WPRE3</i> | Charité, Germany, with technical assistance from Salk investigator John Naughton  | Charité, Germany              | BA-229a with titer: 3.98x 10 <sup>12</sup> VG/ml        | One site |
| <i>BRVenvA-Io Rabies Virus, pseudotyped EnvA, mCherry</i> | <i>pSADB19d G-mCherry</i>                  | Charité, Germany, the material was originally provided by Edward Callaway and distributed through Addgene (plasmid #32630, #32631, #32632, #32633, #32634) (Osakada et al., 2011) | Charité, Germany              | unknown, with titer: 1.00x 10 <sup>8</sup> particles/ml | One site |
| <b>Antibodies</b>   |  |   |                               |   |          |
| Antibody name   | Host animal                                | Dilution  | Company                       | Catalogue number  | Lot      |
| NEUN  | Mouse                                      | 1:500–1:1,000   | Millipore, USA                | MAB377  |          |
| PKC $\gamma$  | Rabbit polyclonal                          | 1:500   | Santa Cruz Biotechnology, USA | sc-211  |          |
| IB4   |  | 1:500–1:1,000   | Invitrogen, USA               | I32450  |          |

|                        |                      |                          |                             |             |           |
|------------------------|----------------------|--------------------------|-----------------------------|-------------|-----------|
| PAX2                   | Rabbit<br>polyclonal | 1:500                    | Covance/BioLegend, USA      | Poly19010   |           |
| GFP                    | Chicken              | 1:1,000                  | Aves Lab, USA               | GFP-1020    |           |
| NF200                  | Rabbit               | 1:1,000                  | Sigma-Aldrich, USA          | N4142       |           |
| TRKA                   | Rabbit<br>monoclonal | 1:1,000                  | Abcam, USA                  | ab8871      |           |
| CGRP                   | Rabbit<br>polyclonal | 1:1,000                  | Peninsula Laboratories, USA | T-4239.0050 |           |
| TH                     | Rabbit               | 1:1,000                  | Millipore, USA              | AB152       |           |
| SST                    | Rabbit<br>polyclonal | 1:500                    | Invitrogen, USA             | XJ371918    | PA5-85759 |
| Anti-rabbit<br>488     | Goat                 | 1:500                    | Jackson ImmunoResearch, USA | 111-095-144 |           |
| Anti-rabbit<br>647     | Donkey               | 1:200 (SST assay); 1:500 | Invitrogen, USA             | A31573      |           |
| Anti-mouse<br>488      | Donkey               | 1:200                    | Abcam, USA                  | ab150105    |           |
| Anti-mouse<br>647      | Donkey               | 1:200                    | Invitrogen, USA             | A31571      |           |
| Anti-chicken<br>488    | Donkey               | 1:500                    | Invitrogen, USA             | SA1-72000   |           |
| <b>RNAscope probes</b> |                      |                          |                             |             |           |

| Probe name     |  | Dilution | Company                           | Catalogue number | Channel |
|----------------|--|----------|-----------------------------------|------------------|---------|
| <i>fos</i>     |  | 1:50     | Advanced Cell<br>Diagnostics, USA | 31692            | C1      |
| <i>Glra3</i>   |  | 1:50     | Advanced Cell<br>Diagnostics, USA | 490591           | C2      |
| <i>mCherry</i> |  | 1:50     | Advanced Cell<br>Diagnostics, USA | 431201           | C2      |
| <i>Nppb</i>    |  | 1:50     | Advanced Cell<br>Diagnostics, USA | 425021           | C1      |
| <i>Mrgpra3</i> |  | 1:50     | Advanced Cell<br>Diagnostics, USA | 548161           | C3      |
| <i>Mrgprd</i>  |  | 1:50     | Advanced Cell<br>Diagnostics, USA | 417921           | C1      |
| <i>Trpm8</i>   |  | 1:50     | Advanced Cell<br>Diagnostics, USA | 420451           | C3      |
| <i>Trpv1</i>   |  | 1:50     | Advanced Cell<br>Diagnostics, USA | 313331           | C1      |
| <i>Vglut2</i>  |  | 1:50     | Advanced Cell<br>Diagnostics, USA | 319171           | C3      |
| <i>Viaat</i>   |  | 1:50     | Advanced Cell<br>Diagnostics, USA | 319191           | C3      |

104

105 *Animals*

106 Procedures related to the mice used in this study were approved by the local animal research ethical  
107 committee (Uppsala djurförsöksetiska nämnd) and followed the Swedish Animal Welfare Act  
108 (Svensk författningssamling (SFS) 2018:1192), The Swedish Animal Welfare Ordinance (SFS  
109 2019:66), and the Regulations and General Advice for Laboratory Animals (SJVFS 2019:9, Saknr  
110 L 150), permit numbers: 5.8.18-01428/2023, 5.2.18-17971/2019, 5.8.18-11551/2019, 5.8.18-  
111 19421/2019, 5.8.18-01217/2019, 5.8.18-01503/2023 and 5.8.18-03266/2023. The constitutive  
112 knock-in *Gla3*-Cre mouse line was generated by Cyagen, with the homology arms having been  
113 amplified from a bacterial artificial chromosome (BAC), for which the *Gla3* gene is located on  
114 chromosome 8 (GenBank: NM\_080438.2, Ensembl: ENSMUS00000038257). *Gla3*-Cre(+) mice  
115 were crossed with C57BL/6J mice (Taconic, Denmark) and *tdTomato* reporter mice  
116 (Gt(ROSA)26Sor<sup>tm14(CAG-tdTomato)Hze</sup>, Allen Brain Institute). The *Gla3*-Cre allele was kept  
117 hemizygous and both female and male mice were included in the analyses, unless otherwise stated.  
118 The mice were housed with littermates in approximately 501cm<sup>2</sup> cages (maximum 5 mice per cage)  
119 in room temperature ranging between 20–24°C and humidity of 45–65% on a 12-hour light:dark  
120 cycle with lights on at 6 am. All mice were provided food (Diet Pellets, Scanbur, Sweden) and tap  
121 water *ad libitum*.

122

### 123 *Genotyping by polymerase chain reaction*

124 Tissue biopsies from ear marking, taken at the age of 3–4 weeks, were incubated in 50µL of buffer,  
125 consisting of 25mM NaOH and 200µM ethylenediaminetetraacetic acid (EDTA), in a shaking  
126 block (BIOER Mixing Block MB-102, China, 300 speed) at 96°C for 25min, whereafter the  
127 samples were neutralized with 50µL of Tris-HCl (40mM), pH 8.0. The following primers were  
128 used to identify *Cre* and *tdTomato*, respectively; *Cre* 5'-acgagtgatgaggttcgcaaga-3' (forward,

129 mutant allele), 5'-accgacgatgaagcatgttag-3' (reverse, mutant allele), *tdTomato* 5'-  
130 ctgttctctgtacggcatgg-3' (forward, mutant allele), 5'-ggcattaaagcagcgtatcc-3' (reverse, mutant  
131 allele), 5'-aaggagctgcagtggagta-3' (forward, wild type allele), 5'-ccgaaaatctgtgggaagtc-3'  
132 (reverse, wild-type allele).

133

### 134 *Spinal Cord Viral Injections*

135 The viral injections into the spinal cord were performed for the chemogenetic sensory tests,  
136 monosynaptic retrograde tracing, and the electrophysiological recordings of adult *Gla3-Cre(+)*  
137 neurons. The injections were performed as previously described (Freitag et al., 2019); in brief,  
138 *Gla3-Cre* mice (>6 weeks old) were initially anesthetized in a 4% isoflurane (FORANE, Baxter,  
139 USA) box. When fully anesthetized, the mice were moved to a stereotaxic frame with a breathing  
140 mask, where the isoflurane concentration was kept at 1.5–2% throughout the entire procedure. To  
141 prevent eye damage, Oftagel was applied (Santen Oy, Tammerfors, Finland) and the body  
142 temperature was monitored and maintained at 35–37°C using a heating pad (FHC, Bowdoin,  
143 Maine, USA). Adjacent to the incision sites, the mice were administered subcutaneously with  
144 bupivacaine (Marcain®, 2mg/kg, AstraZenica AB, Cambridge, England). For post-surgery  
145 analgesia, the mice were administered subcutaneously with karprofen (Norocarp vet, 5mg/kg, N-  
146 vet, Uppsala, Sweden or Rimadyl® Bovis vet, 4mg/kg, Zoetis Finland Oy, Finland). Within 24h  
147 post-surgery, the mice were again administered 5mg/kg karprofen for post-surgery analgesia. The  
148 dorsal skin was shaved and cleaned with sterile saline (B Braun medical AB, Stockholm, Sweden)  
149 and chlorhexidine (Fresenius Kabi, Bad Humberg, Germany) before a 1cm skin incision was made  
150 to expose the T13 and L1 vertebrae. Sterile saline was continuously applied to keep the tissue  
151 moist. The connective tissue was gently separated along these vertebrae and a clamp was inserted

152 ventral of the L1 transverse process for stabilization of the spine. When stabilized, the posterior  
153 longitudinal ligament and ligament flavum connecting T13 and L1 were cut to expose the spinal  
154 cord. Thereafter, 500nl of the respective viral vector (*AAV8.hSyn-DIO-hM3D(Gq)-mCherry*  
155 (Krashes et al., 2011), *AAV8.hSyn-DIO-mCherry* or *AAVDJ.EF1a-DIO-HTB*) (please see Key  
156 Resources Table for detailed information) was injected into the L5/L6 spinal dorsal horn (as caudal  
157 as possible from zeroed midline, ML: 0.4mm, DV: 0.4mm, with needle eye directed rostrally),  
158 using a 10µl Nanofil Hamilton syringe (World Precision Instruments, Sarasota, Florida, USA) with  
159 a 34g beveled needle (World Precision Instruments), monitored by a micro syringe pump controller  
160 (World Precision Instruments) at 50nl/min. For injections of *AAV8.hSyn-DIO-hM4D(Gi)-mCherry*  
161 (Krashes et al., 2011), the virus was injected at two sites into the right dorsal horn (RC: 0/-0.5mm,  
162 ML: 0.3mm, DV: 0.6mm), with the eye of the needle pointing lateral. To prevent leakage and  
163 withdrawal of virus, the needle was left in the injection site for 5min. When the injection was  
164 completed, the spine was detached from the clamp and the skin and connective tissue were sutured  
165 and cleaned with sterile saline before the mice were removed from the breathing mask and  
166 administered subcutaneously with Buprenorfin (Vetergesic® Vet, Orion Pharma, Finland,  
167 0.05mg/kg). The mice were subsequently placed on a heating pad in their cages to wake up. The  
168 mice were subjected to behavioral experiments or sacrificed for tissue analyses after a minimum  
169 of 2–4 weeks to allow sufficient expression of viral genes.

170 Adult *Gla3-Cre* mice (7+7, 7 females, 7 males, 6–26 weeks old) for the Randall-Selitto test were  
171 injected with *AAV8.hSyn-DIO-hM4D(Gi)-mCherry* (Krashes et al., 2011) or *AAV8.hSyn-DIO-*  
172 *mCherry* between L1/L2 to target the sacral 2 (S2) segment, affecting the tail (Bennett et al., 1999).  
173 The virus was injected into the dorsal horn at two sites with the eye of the needle directing lateral

174 (RC: 0/-0.5mm, ML: 0.25mm, DV: 0.45mm). The mice were assessed to the Randall-Selitto test  
175 2–3 weeks after injection.

176 The injections for monosynaptic retrograde tracing of adult *Gla3-Cre* mice (*Gla3-Cre(+)*: 5  
177 females, 5 males, 7–15 weeks old; *Gla3-Cre(-)*: 3 females, 3 males, 7–17 weeks old) were  
178 conducted in the same manner as described above for the *AAV8.hSyn-DIO-hM3D(Gq)-mCherry*  
179 experiments. The mice were initially injected with helper virus (herein abbreviated as AAV8.Syn-  
180 flex-TVA-oG-GFP). To allow sufficient expression of the helper vector genes required for rabies  
181 virus host cell entry, the mice were injected with pseudotyped rabies virus *BRVenvA-1o Rabies*  
182 *Virus, pseudotyped EnvA, mCherry* (please see Key Resources Table for detailed information) 7–  
183 8 days after the helper virus injection. One week after the final injection, the mice were sacrificed.

184  
185 *Immunohistochemistry Tissue Preparation of Developmental and Adult Virally labelled Gla3-*  
186 *Cre(+) mice*

187 Adult *Gla3-Cre;tdTomato* mice (4 females, 7–23 weeks old) and virally spinal cord injected  
188 *Gla3-Cre.mCherry* mice (2 females, 2 males, 17–25 weeks old, from the behavioral experiments)  
189 were anesthetized in isoflurane (FORANE, Baxter, USA). All mice were subsequently injected  
190 intraperitoneally with 0.6ml (1:1) Ketamin (Ketalar, 10mg/ml, Pfizer, Sweden) and Medetomidine  
191 (Domitor, 1mg/ml, Orion Pharma, Sweden). When fully anaesthetized, the mice were perfused  
192 through the left ventricle with 1x PBS, followed by 4% formaldehyde (FA) (Histolab, Sweden).  
193 The spinal columns were isolated and placed in 1x PBS, followed by dissection of the tissue area  
194 of interest (spinal cord and dorsal root ganglia (DRG)). The tissues were placed in 4% FA  
195 (Histolab, Sweden) at 4°C overnight. The spinal cords and DRG were dehydrated for 24h in 15%  
196 sucrose and then for 24h in 30% sucrose for cryoprotection. The tissues were thereafter embedded



197 in optimal cutting temperature (OCT) medium (Bio-Optica, Milan, Italy) and snap-frozen on dry  
198 ice in -80°C isopentane (Sigma-Aldrich, USA), at which temperature the tissues were stored until  
199 sectioning. The spinal cords and DRG were sectioned into 16–18µm sections using a cryostat  
200 (Leica cryocut 1800, Leica, Germany) and the sections were collected on glass slides (Superfrost®  
201 Plus, Thermo Scientific, USA) as a series of six slides/series. The completed slides were stored at  
202 -80°C until further immunohistochemical analyses were performed.

203 In the tracing experiment, following brain dissections, the brains were fixated in 4% FA (Histolab,  
204 Sweden) at 4°C overnight and thereafter stored in 1x PBS at 4°C until vibratome sectioning. Upon  
205 sectioning, the brains were superficially and unilaterally cut with a razor blade to keep track of  
206 orientation, and subsequently mounted in 4% agarose. The brains were sliced into 70µm sections  
207 (Leica VT1000S, Leica, Germany), which were collected into wells as series of five wells/series  
208 with five sections/well. All sections were examined for traced mCherry(+) cells using a fluorescent  
209 stereomicroscope (Leica MZ16F, Leica, Germany). For documentation, the brain sections of one  
210 well/series (every fifth brain section) were mounted and embedded in Anti-Fade Fluorescence  
211 Mounting Medium (Abcam, UK) on glass slides and covered with glass cover slides (Menzel-  
212 Gläser, Germany) for imaging.

213

#### 214 *Immunohistochemistry*

215 All slides to be used for immunohistochemistry (*Gla3-Cre;tdTomato*: 4 females, 7–23 weeks old;  
216 *Gla3-Cre.mCherry*: 4 mice; 2 females, 2 males, 17–25 weeks old; traced *Gla3-Cre(+)*: 4 females,  
217 2 males, 9–17 weeks old) were placed at room temperature (RT) for 30min to thaw and dry before  
218 initializing the protocols. The assays were either PBS- (NEUN, PKCγ, IB4, NF200, TRKA, CGRP,

219 TH) or TBS- (PAX2, SST) based. In all assays, the sections were washed with 1x PBS/TBS for 4x  
220 10min before and after the primary antibody incubation. Prior to the primary antibody incubation,  
221 the sections were blocked with either supermix (0.25% gelatin and 0.5% TritonX-100 in 1x  
222 PBS/TBS, [NEUN, NF200, TRKA, CGRP, TH]) or blocking solution (5% donkey or goat serum  
223 in 1x PBS/TBS, [PKC $\gamma$ , IB4, PAX2, SST]) for 1h at RT. In the same solutions (supermix: [PKC $\gamma$ ,  
224 IB4, PAX2, SST]; blocking solution: [NEUN, NF200, TRKA, CGRP, TH]), the primary and  
225 secondary antibodies were incubated, in which the primary antibodies were incubated for 48h at  
226 4°C and the secondary antibodies with 200nM/ml DAPI for 2h at RT. As the final step, the sections  
227 were washed 4x 10min in 1x PBST/TBST (0.1% Tween20 in 1x PBS/TBS). After completion of  
228 protocols, the slides were embedded in Anti-Fade Fluorescence Mounting Medium (Abcam, UK)  
229 and covered with glass slides (Menzel-Gläser, Germany). The slides were left at 4°C to dry and  
230 were stored at this temperature until imaging. For antibody specifics, see Key Resources Table.

231

### 232 *In Situ Hybridization Tissue Preparation*

233 Adult *Gla3-Cre(+)* mice microinjected with AAVDJ.EF1a-DIO-HTB (3 females, 2 males, 7–11  
234 weeks) and mice included in the retrograde rabies tracing (1 female and 2 males, 14 weeks) in the  
235 L5/L6 spinal dorsal horn, were subjected to similar procedures as described previously (Freitag et  
236 al., 2021). The HTB protein is a histone-tagged GFP and this virus was used since the fluorescence  
237 could be detected after RNAscope protocol. In brief; 14 days post viral injection, the mice were  
238 anesthetized in isoflurane (FORANE, Baxter, USA), followed by intraperitoneal injection of 0.6ml  
239 (1:1) Ketamine (Ketalar, 10mg/ml, Pfizer, Sweden) and Medetomidine (Domitor, 1mg/ml, Orion  
240 Pharma, Sweden). To minimize the risk of contamination and altered gene expression, the mice

241 were perfused in autoclaved ice-cold 1x PBS. In the same solution, the spinal columns were quickly  
242 dissected and the spinal area containing the viral fluorescence was isolated. The tissues were  
243 immediately embedded in optimal cutting temperature (OCT) medium (Bio-Optica, Milan, Italy)  
244 and snap-frozen on dry ice in -80°C isopentane (Sigma-Aldrich, USA), at which temperature the  
245 tissues were stored until sectioning. The tissues were cryosectioned (Leica Cryocut 1800, Leica,  
246 Germany) into 12–14 µm sections and were collected onto Superfrost Plus (Thermo Scientific,  
247 USA) glass slides as series consisting of six slides with 7–8 sections/slide for the *Gla3-Cre(+)*  
248 AAVDJ.EF1a-DIO-HTB injected mice and eight slides with 3 sections/slide for the sensory  
249 stimulated C57BL/6J mice. To prevent mRNA degradation and contamination, the completed  
250 series were stored at -21°C until sectioning was finished. The slides were stored at -80°C until the  
251 RNAscope Fluorescent Multiplex kit (Advanced Cell Diagnostics (ACD), USA, cat #: 320850)  
252 protocol commenced.

253

#### 254 *Fluorescent In Situ Hybridization*

255 The fluorescent *in situ* hybridization was performed using the RNAscope Fluorescent Multiplex  
256 kit (ACD, USA, cat# 320850) in accordance with ACD guidelines for fresh frozen tissues, with  
257 minor modifications (Wang et al., 2012) on sections from *Gla3-Cre*.HTB and sensory stimulated  
258 C57BL/6J mice. In brief, as performed previously (Freitag et al., 2021), the slides to be used were  
259 taken from -80°C and immediately fixated in 4% FA (Histolab, Sweden) for 15min at RT before  
260 being washed in autoclaved 1x PBS for 2min. The tissues were thereafter dehydrated in a step-wise  
261 increase of EtOH concentration; 3min in 50%, 3min in 70% and 2x 5min in 100% (Merck KGaA,  
262 Germany). The slides were placed at RT for 5min to dry, whereafter a hydrophobic barrier was  
263 made around the chosen sections (3 sections/mouse), using an ImmeEdge pen (Vector

264 Laboratories, USA). The sections were incubated in Protease IV for 30–40min at RT, followed by  
265 3x 5min washing in autoclaved 1x PBS. The sections were incubated in target probes (for specifics  
266 see Key Resources Table) 1:50 in probe diluent (ACD, USA, cat# 300041) for 2h at 40°C in a  
267 hybridization oven (HybEZ™ II Oven, ACD, USA). The following amplification steps were  
268 performed at 40°C in the hybridization oven and the sections were washed 2x 2min in RT washing  
269 buffer between each amplification step: AMP 1-FL for 30min, AMP 2-FL for 15min, AMP 3-FL  
270 for 30min and AMP 4-FL for 15min. The coloring step using AMP 4-FL was performed to enable  
271 the combination with the viral fluorescence. Lastly, the slides were washed 2x 2min in washing  
272 buffer before 30sec incubations in DAPI and mounting in Anti-Fade Fluorescence Mounting  
273 Medium (Abcam, UK). The slides were covered with glass slides (Menzel-Gläser, Germany) and  
274 were left at 4°C to dry. The slides were stored at this temperature until imaging.

275

#### 276 *Image Acquisition and Quantification*

277 Images of immunohistochemistry treated sections were acquired using a wide field Olympus  
278 BX61WI fluorescence microscope (Olympus, Japan) with a 10x objective, for which the brightness  
279 and contrast were optimized for each channel during image acquisition and quantification. The  
280 RNAscope treated sections were acquired with wide field 20x magnification with the Olympus  
281 BX61WI fluorescence microscope (Olympus, Japan) or an Axio Imager.Z2 (ZEISS, Germany),  
282 where each channel was set to be automatically optimized for each image, but had to be further  
283 optimized during image analysis. Here, the optimal intensity and contrast was set for one image  
284 (reference image) and the settings of the other images were set to match the reference image. The  
285 images were manually quantified using the Fiji (ImageJ 1.52f) Cell Counter plugin.

286 *Immunohistochemistry spinal cord:* All *Gla3-Cre.tdTomato* (2 females, n sections/mouse: 3) or

287 *Gla3-Cre.mCherry* (2 females and 2 males, n sections/mouse: 3–5) mice with DAPI overlap were  
288 quantified depending on layer location (IB4: outer lamina II; PKC $\gamma$ : inner lamina II) and marker  
289 protein (NEUN) co-expression. *Immunohistochemistry retrograde rabies tracing, spinal cord:*  
290 *Gla3-Cre(+)* mice: A DAPI cell with overlap of helper virus GFP and rabies virus mCherry was  
291 considered a starter cell, and a DAPI cell with only mCherry overlap was considered a presynaptic  
292 traced cell. The co-expression of starter and traced cells was quantified for NEUN and PAX2 (5  
293 females, 5 males, n section/mouse/assay: 2–11); *Gla3-Cre(-)* mice: The overlap of helper virus  
294 GFP and rabies virus mCherry with DAPI overlap was quantified (3 females, 3 males, every sixth  
295 section analyzed). *Immunohistochemistry retrograde rabies tracing, DRG:* The overlap of traced  
296 mCherry DAPI+ cells with NF200, TRKA, CGRP, IB4, TH and SST was quantified (NF200: 2  
297 females, 2 males, n sections/mice: 2–5; TRKA: 2 females, 2 males, n section/mice: 1–8; CGRP: 1  
298 female, 2 males, n sections/mice: 2–5; IB4: 3 females, 1 male, n sections/mice: 2–5; TH: 4 females,  
299 2 males, n sections/mice: 1–7; SST: 2 females, 1 male, n sections/mice: 3–5). *Brain scanning for*  
300 *mCherry(+)* traced cells in *Gla3-Cre(+)* and *Gla3-Cre(-)* mice: Whole brain section images were  
301 acquired in the mCherry (500ms) and widefield black & white (15% light source intensity, 5ms)  
302 channels of every fifth section, using tiles (ZEISS, Germany) to scan for mCherry(+) traced cells  
303 (*Gla3-Cre(+)*: 5 females, 5 males; *Gla3-Cre(-)*: 3 females, 3 males). *RNAScope, Gla3-Cre.HTB:*  
304 All *Gla3-Cre.HTB* cells with DAPI overlap were considered cells and one read of the targeted  
305 probe could be visualized as one dot. A *Gla3-Cre.HTB* cell was considered to be expressing the  
306 targeted gene (*Gla3*, *Vglut2* or *Viaat*) if the overlapping #dots  $\geq 3$  (3 females and  
307 2 males, n sections/mouse: 2–4). One section from the *Gla3/Viaat* assay was excluded  
308 due to weak signal from both probes. *RNAScope, retrograde rabies tracing DRG:* DAPI cell was  
309 considered expressing the targeted gene (*mCherry*, *Nppb*, *Mrgpra3*, *Mrgprd*, *Trpv1*, *Trpm8*) if

310 the #dots $\geq$ 3 (*Nppb*: 1 female and 1 male, n sections/mice:4–6; *Mrgprd* and *Mrgpra3*: 1 female  
311 and 1 male, n sections/mice:4–6, *Trpv1* and *Trpm8*: 2 females and 1 male, n sections/mice:2–6).  
312 RNAscope, *fos* expression in *Gla3* expressing cells following sensory stimulation: The  
313 experimenter was blinded to the treatment received by the mouse and the *Vglut2/Viaat* probes, so  
314 no randomization was needed in the quantification. A DAPI cell was considered to express the  
315 targeted gene (*Gla3*, *fos* and *Vglut2* or *Viaat*) if the #dots $\geq$ 3 and #dots $\geq$ 5 for *fos* (3  
316 mice/stimulus, n sections/mouse: 3). One section from the scratch analysis was excluded due to  
317 poor tissue quality. To obtain a high resolution, two images of each dorsal horn were acquired and  
318 later merged together using Adobe Photoshop 22.3 to a composited representative image of the  
319 dorsal horn. The result is presented as percentage $\pm$ SEM.

320

### 321 *Electrophysiology*

322 For patch-clamp recordings, spinal cord transverse slices were made from *Gla3-Cre;tdTomato*  
323 mice (13 females, 11 males, 4–35 weeks old) according to a previously described protocol (Freitag  
324 et al., 2019). For root stimulations, the spinal cord was cut at a 60° angle and the slice thickness  
325 was increased to 400 $\mu$ m in order to get transverse slices with attached dorsal roots. After  
326 incubation, the slice was transferred to a recording chamber, where *Gla3-Cre;tdTomato* neurons  
327 were visualized via a fluorescent LED light source (CoolLED system, UK) on a Prime BSI Express  
328 scientific sCMOS camera (Teledyne Photometrics, USA) through 60x or 10x water-immersion  
329 objectives (LUMPlan FI, 0.90 numerical aperture (NA), Olympus, Japan). Borosilicate glass  
330 capillaries (GC150F-10 Harvard Apparatus, USA) were used to pull patch electrodes (6-10M $\Omega$ )  
331 with a flaming/brown micropipette puller (P-1000, Shutter Instrument, USA). The internal solution

332 of patch pipettes (in mM): 130 K-gluconate, 40 HEPES, 1.02 MgCl<sub>2</sub>, 2.17 MgATP, 0.34 NaGTP,  
333 with pH adjusted to 7.2 using 1M KOH. Liquid junction potential was corrected before each  
334 recording. Whole-cell patch-clamp signals were amplified with a MultiClamp 700B amplifier  
335 (Molecular Devices, USA), digitalized at 20kHz with Digidata 1440A (Molecular Devices, USA),  
336 low pass filtered at 10kHz, and acquired in WinWCP software (Dr. J. Dempster, University of  
337 Strathclyde, Glasgow, UK).

338 When the whole cell configuration was achieved, action potentials were induced, in the current  
339 clamp mode via current steps from 0–150pA with increments of 10pA (pulse duration 500ms), to  
340 monitor the viability and the firing pattern of the patched neuron. The rheobase was determined by  
341 using 1pA increment current steps (pulse duration 500ms). The neuron was then held at -60mV in  
342 the voltage clamp mode. When a stable baseline was achieved in a continuous voltage clamp  
343 recording, 300μM glycine was applied through the perfusion system to the recording chamber to  
344 verify the expression of GLRs on the patched neuron. The hyperpolarization was then blocked by  
345 10μM strychnine to further confirm that the response was due to the expression of GLRs.

346 In root stimulation experiments, the dorsal root was identified using the 10x objective and sucked  
347 into a suction pipette. The stimulating electric pulses were applied via the suction pipette from an  
348 A365 Stimulus Isolator (World Precision Instruments, USA). Stimulation pulses with a duration of  
349 0.2ms were used for activation of the dorsal root, while in some cases 0.5ms pulse durations were  
350 used to activate the C-fiber. The conduction velocities of different afferent fibers were used to  
351 determine monosynaptic inputs (Pan et al., 2019). Further confirmation followed by none failure  
352 responses with consistent onset latencies, in which patched cells responded to a minimum of 10  
353 consecutive root stimulations at 1Hz and the latency variation was less than 1ms (Pinto et al., 2008;  
354 Pan et al., 2019). Data analyses were done by Clampfit 10.3 (Molecular Devices, USA), Mini

355 Analysis (Synaptosoft, USA), and GraphPad Prism (GraphPad Software, USA). No neurons were  
356 excluded in the post analysis.

357

### 358 *Cell filling*

359 Neurobiotin™ Tracer (Vector Laboratories, USA) was added into the intracellular solution  
360 (4mg/ml) and diffused into the target *Gla3-Cre;tdTomato* cells during patch-clamp recording. The  
361 diffusion of Neurobiotin™ was further assisted by injecting depolarizing current pulses (0.2–  
362 0.5nA, duration 150ms) into the cell at 2Hz for 10–15min. After the filling, the patch pipette was  
363 carefully detached from the cell and removed from the recording chamber. The excessive  
364 Neurobiotin™ in the tissue was removed by perfusing the slice for at least 15 more min after the  
365 removal of the pipette. The slice was then transported into an Eppendorf tube and fixed in 4% FA  
366 (Histolab, Sweden) overnight at 4 °C. Fixed slices were washed with 1x PBS (Fisher BioReagents,  
367 USA) 4x10min before the staining. Slices were stained for PKC $\gamma$  using the same procedure  
368 described in previous immunohistochemistry section. Additionally, streptavidin Alexa Flour 488  
369 conjugate (Invitrogen, USA) was added to the primary antibody staining solution with 1:1000  
370 dilution ratio for Neurobiotin™ staining. The mounted slice was imaged using a ZEISS LSM700  
371 confocal microscope (ZEISS, Germany) with 10x and 20x objectives. The morphology of a filled  
372 neuron was reconstructed using the Simple Neurite Tracer plug-in in the NIH ImageJ software  
373 (National Institutes of Health, Bethesda, Maryland, USA).

374

375 *Basal behavioral observation after chemogenetic activation or inhibition of Gla3-Cre(+) neurons*



376 *Gla3-Cre(+)* mice (*Gla3-Cre.hM3Dq* and *Gla3-Cre.mCherry*: 7+8 mice, 7 females and 8 males;  
377 *Gla3-Cre.hM4Di* and *Gla3-Cre.mCherry*: 8+8 mice, 11 females, 5 males) unilaterally injected in  
378 L5 with AAV8.hsyn-DIO-hM3D(Gq)-mCherry, AAV8.hsyn-DIO-hM4D(Gi)-mCherry or  
379 AAV8.hsyn-DIO-mCherry were acclimatized to a plastic cylinder arena (diameter: 19cm, height:  
380 29cm, surface area: 283cm<sup>2</sup>) with a mirror to obtain a 360° view for 20min. The mice were injected  
381 intraperitoneally with 0.1mg/kg of freshly prepared Clozapine N-oxide (CNO) (AK Scientific,  
382 USA, 0.02mg/ml dissolved in 0.02% DMSO in sterile saline). The basal behavior of the mice  
383 following CNO administration was recorded for 30min (for *Gla3-Cre.hM3Dq* recordings) or  
384 60min (for *Gla3-Cre.hM4Di* recordings). The duration and frequency of targeted behaviors were  
385 analyzed for the total recording time. The same experimenter scored all the behavior recordings  
386 and was blinded for the viral vectors used during the experiments. The licking/biting of the  
387 ipsilateral paw were scored as one behavior, for which the episodes were scored when contact  
388 between the paw and face could be clearly visualized. The guarding and stomping behaviors were  
389 also scored. Guarding was defined as the time the mouse spent sitting still with its paw in the air.  
390 Stomping was interpreted as a mouse rapidly lifting and lowering the hind paw while being either  
391 still or in movement. No mice were excluded from the analysis

392

### 393 *Injections of saline or pruritogens*

394 Two days prior to the stimulus recording, the right calves of the mice were shaved and cleaned  
395 with sterile saline. Adult *Gla3-Cre(+)* mice injected with AAV8.hsyn-DIO-hM4D(Gi)-mCherry  
396 or control AAV8.hsyn-DIO-mCherry were injected with 0.1mg/kg freshly prepared CNO (AK  
397 Scientific, USA, 0.02mg/ml dissolved in 0.02% DMSO in sterile saline) and thereafter returned to

398 their respective home cages. After 30min, the mice were placed in a plastic cylinder arena with a  
399 mirror to obtain a 360° view for 10min to acclimatize to the set up. The mice were subsequently  
400 injected subcutaneously in the dorsolateral calf with either 10µl of saline (8+8 mice; 9 females, 7  
401 males), 20µg compound 48/80 (Sigma-Aldrich, USA, cat# c2313, dissolved in sterile saline; 8+8  
402 mice; 8 females, 8 males), or 10mM chloroquine phosphate (Sigma-Aldrich, USA, cat# PHR1258,  
403 dissolved in sterile saline, 8+8 mice; 9 females, 7 males). The mice were returned to the plastic  
404 cylinder area and recorded for 30min. Licking of the calf is indicative of pain, while biting  
405 demonstrates itch (LaMotte et al., 2011). However, since we had difficulties separating these  
406 behaviors while scoring, the total duration and frequency of licking/biting towards the injected calf  
407 was scored as one behavior. These episodes were scored when contact between the calf and face  
408 could be clearly visualized. No mice were excluded from the analysis

409

#### 410 *Randall-Selitto test*

411 Two days prior to the experiment, a plastic cylinder (Model 84, IITC Life Science, USA) was  
412 placed in each home cage to acclimatize the mice to the setup. Adult *Gla3-Cre(+)* mice (7+7 mice;  
413 7 females, 7 males) injected with either AAV8.hsyn-DIO-hM4D(Gi)-mCherry or AAV8.hsyn-  
414 DIO-mCherry between L1/L2 were intraperitoneally administered 0.1mg/kg freshly prepared CNO  
415 (AK Scientific, USA, 0.02mg/ml dissolved in 0.02% DMSO in sterile saline) and thereafter  
416 returned to their respective home cages. Ten min later, the mice were allowed to enter the plastic  
417 cylinder and were placed in the Randall-Selitto setup (Analgesy-meter, UGO Basile, Italy) for  
418 approximately 30min. When 40min had passed since the CNO injection, the mechanical threshold  
419 (g), at which pressure the mouse retracted its tail, was measured twice per mouse at different

420 locations on the tail with at least 5min between the measurements. One female and one male  
421 injected with AAV8.hsyn-DIO-hM4D(Gi)-mCherry were excluded from the analysis due to lack  
422 of mCherry expression in the post hoc verification step.

423

#### 424 *Hargreaves test*

425 Adult *Gla3-Cre(+)* mice (8+8 mice; 11 females, 5 males) injected with AAV8.hsyn-DIO-  
426 hM4D(Gi)-mCherry or control AAV8.hsyn-DIO-mCherry were initially acclimatized for 60min in  
427 the Hargreaves set up (transparent acrylic glass chambers on glass floor). Baseline thermal  
428 sensitivity was measured by directing the Hargreaves heat source (IITC Life Science, Woodland  
429 Hills, CA, USA), guided by a light pointer, to the plantar surface of the right hind paw, for which  
430 the time from turning on the thermal source until the mouse withdrew/flinched its paw was noted.  
431 The cut-off time was set to 20sec to avoid tissue damage and the withdrawal time was measured  
432 twice with at least 5min intervals in between each measurement. After completed measurements,  
433 the mice were injected intraperitoneally with 0.1mg/kg freshly prepared CNO (AK Scientific,  
434 USA, 0.02mg/ml dissolved in 0.02% DMSO in sterile saline) and placed back into the Hargreaves  
435 setup. Forty min after the CNO administration, the withdrawal time measurement was repeated.  
436 No mice were excluded from the analysis

437

#### 438 *Acetone drop test*

439 Adult *Gla3-Cre(+)* mice (8+8 mice; 8 females, 8 males) injected with either AAV8.hsyn-DIO-  
440 hM4D(Gi)-mCherry or AAV8.hsyn-DIO-mCherry were allowed 60min acclimatization to the

441 gridded surface. Forty minutes before the first measurement, the mice were injected  
442 intraperitoneally with 0.1mg/kg freshly prepared CNO (AK Scientific, USA, 0.02mg/ml dissolved  
443 in 0.02% DMSO in sterile saline), and returned to the setup. The mice were subjected to a drop of  
444 acetone solution (9:1 acetone in water, Labscan, Dublin, Ireland) on the plantar surface of the right  
445 hind paw, where the total duration of sensory aversive behaviors, including lifting, flinching, and  
446 licking/biting of the paw, was recorded. The stimulation was performed twice with at least 5min  
447 intervals in between each application of the acetone solution. No mice were excluded from the  
448 analysis

449

450 *Sensory stimulation for fos detection*

451 *Pruritic stimulation of urethane anesthetized mice:* To detect activation of *Gla3* expressing cells  
452 following sensory stimulation, adult C57BL/6J mice (10–14 weeks old, 3 mice/stimulus, 15 mice  
453 in total) were initially anesthetized with 2g/kg urethane (Sigma-Aldrich, USA, cat# U2500,  
454 125mg/ml in sterile saline) through intraperitoneal injection to minimize neuronal activity caused  
455 by prurito- and nocifensive behavior. To prevent eye-damage and dehydration, Oftagel (Santen Oy,  
456 Finland) was applied to eyes and the mouse was injected subcutaneously with 0.5ml saline. To  
457 maintain body temperature, a glove filled with body temperature water, that was continuously  
458 replaced to sustain temperature, was placed next to the mouse. When the mouse had been fully  
459 anesthetized for 10min, the mouse was subjected to the stimulus. For pruritic stimulations, the mice  
460 were injected subcutaneously into the right dorsolateral calf either with 10 $\mu$ l saline (1 female and  
461 2 males), or a pruritic substance: 20 $\mu$ g compound 48/80 (Sigma-Aldrich, USA, cat# c2313,  
462 dissolved in sterile saline, 1 female and 2 males), or 20mM chloroquine (Sigma-Aldrich, USA,  
463 cat# PHR1258, dissolved in sterile saline, 1 female and 2 males). *Noxious mechanical stimulation*

464 *of urethane anesthetized mice*: the mouse was either subjected to pinching (1 female and 2 males)  
465 or scratching (2 females and 1 male) of the skin on the right dorsolateral calf. The pinching was  
466 performed 5x for 5sec using tweezers, with 5sec resting periods in between each pinching episode.  
467 The scratching was conducted for 30sec with 2Hz and approximately 300mN (30.6g), using an  
468 artificial mouse claw in scratch position. Forty min after application of the stimulus, the mouse was  
469 injected intraperitoneally with 0.05ml Ketamine (Ketalar, 10mg/ml, Pfizer, Sweden) and 0.05ml  
470 Medetomidine (Domitor, 1mg/ml, Orion Pharma, Sweden), followed by perfusion and tissue  
471 preparation for RNAscope, as described above. *Hargreaves stimulation for fos detection in awake*  
472 *mice*: adult C57BL/6J mice (2 females and 1 male, 11–17 weeks old) were subjected to the same  
473 Hargreaves protocol as described above for baseline measurements. After completed stimulation,  
474 40min was allowed to pass until the mouse was injected intraperitoneally with 0.7–0.8ml Ketamine  
475 (Ketalar, 10mg/ml, Pfizer, Sweden) and Medetomidine (Domitor, 1mg/ml, Orion Pharma, Sweden)  
476 (1:1), followed by perfusion and tissue preparation for RNAscope, as described above. Same mice  
477 but separate sections have been used in a manuscript under revision. No mice were excluded from  
478 the analysis.

479

#### 480 *Experimental Design and Statistical Analyses*

481 All behavioral testing was performed a minimum of 2–4 weeks after viral injection to allow  
482 sufficient expression of viral vector genes. *Gla3-Cre.hM3Dq* mice were only included in one basal  
483 behavioral analysis/mouse, except for 2 (*Gla3-Cre.hM3Dq*) + 3 (*Gla3-Cre.mCherry*) mice that  
484 also were subjected to an initial analysis (one CNO injection, data not shown) a few weeks prior to  
485 establish a proper CNO concentration. *Gla3-Cre.hM4Di* mice were included in maximum four

486 behavioral tests (including basal recording) with a minimum of one week between the tests. The  
487 basal recording was conducted first and the following tests were not conducted in a specific order.  
488 *Gtra3-Cre.mCherry* mice were included in maximum four behavioral tests (including basal  
489 recording) with a minimum of one week between the tests. The tests were not conducted in a  
490 specific order. The mice were returned to their home cages after each completed behavioral test.  
491 No mice were excluded from the behavioral analyses presented. No randomization was used. Mice  
492 were arbitrary assigned to different treatments (e.g., injections of viral vectors) based on sex. All  
493 the behavior experiments were conducted by the same female experimenter, who was blinded to  
494 viral vectors (control vs chemogenetic). In the acetone and Randall-Selitto tests, an additional  
495 female experimenter was conducting the experiment (also blinded to the viral vector injected), so  
496 no randomization was needed or possible. Reporter expression was validated and documented in  
497 all mice after chemogenetic behavioral testing to ensure presence of DREADD (designer receptors  
498 exclusively activated by designer drugs) or control vector at the correct spinal segments. The  
499 experimental groups were matched to the best extent in terms of sex and littermates. In the sensory  
500 stimulation tests to examine *fos*, the mice were arbitrary assigned to the different stimuli, but we  
501 ensured that both sexes were used in the testing.

502 The number of mice per behavioral and *in situ* experiment was not based on any statistical  
503 calculations prior to the experiments. Sample sizes are in line with similar studies in the field  
504 (Bourane et al., 2015; Foster et al., 2015; Häring et al., 2018). All data were analyzed in GraphPad  
505 Prism (version 9 or 10). The normal distribution of the mean data per mouse was analyzed using  
506 the Shapiro-Wilk normality test ( $\alpha=.05$ ). To compare mean values, either a two-tailed student t-test  
507 or Mann-Whitney u test was performed. In the basal hM3Dq experiment, for which the mean value  
508 of the control mCherry groups was zero for stomping and guarding behaviors, a Chi-square test

509 was performed to compare the mean values between these groups. In order to compare the mean  
510 values between multiple parameters (viral vector and pre/post CNO injection) in the Hargreaves  
511 test and to compare the differences in the number of the targeted cells following saline, compound  
512 48/80, and chloroquine injections, a one-way ANOVA with Šídák's multiple comparisons test was  
513 used. The results are presented as mean $\pm$ SEM.

JNeurosci Accepted Manuscript

514 **Results**

515

516 *Gla3-Cre;tdTomato* neurons are predominantly located in laminae III–IV and the adult *Gla3-*  
517 *Cre* population consists of a major excitatory and a minor inhibitory population

518 First, immunohistochemistry was used to examine the anatomical location and molecular  
519 characteristics of the spinal *Gla3-Cre* population using the *tdTomato* reporter line (Figure 1A–C).  
520 Immunostaining for the neuronal marker NEUN (Figure 1A) showed that almost all *tdTomato*(+)  
521 cells were neurons (98.7±0.2%, 1637/1659). The neurons were most frequently found in the dorsal  
522 horn (dorsal horn: laminae I–VI, 89.1±2.3%, 1528/1713; ventral horn: laminae VII–X, 10.9±2.3%,  
523 185/1713), especially in laminae III–IV (44.2±2.1%, 753/1713) and laminae V–VI (23.4±1.6%,  
524 405/1713). Smaller *tdTomato*(+) populations were found in lamina I (4.8±0.6%, 78/1713), the  
525 outer lamina II defined by IB4 staining (Todd, 2017) (4.7±0.7%, 80/1713), and the inner lamina II  
526 defined by PKC $\gamma$  (Polgár et al., 1999; Peirs et al., 2014) (12.1±1.6%, 212/1713), in which  
527 52.4±5.2% (117/212) of the cells were *tdTomato*(+)PKC $\gamma$ (+) (Figure 1B–B'). Collectively, the  
528 *Gla3-Cre;tdTomato* neurons were located throughout the spinal cord (Figure 1C) and were most  
529 commonly found in laminae III–IV.

530 Single-cell RNA sequencing (scRNAseq) has identified *Gla3* in both excitatory SCGLU10 and  
531 Glut9, and in inhibitory Gaba8–9 spinal dorsal horn neuronal clusters among others (Häring et al.,  
532 2018; Zeisel et al., 2018). To further examine the molecular characteristics of the *Gla3-Cre*  
533 population and to address adult *Gla3-Cre* expression, fluorescent *in situ* hybridization using the  
534 RNAscope approach (Wang et al., 2012) was performed. Said method targeted *Gla3*, the  
535 excitatory marker *Vglut2* (*Vesicular glutamate transporter 2*, *Slc17a6*), and the inhibitory marker  
536 *Viaat* (*Vesicular inhibitory amino acid transporter*, *Slc32a1*) in adult AAVDJ.Ef1a-DIO-HTB



537 labelled *Gla3*-Cre(+) neurons (Figure 1D–H). HTB is a histone-tagged protein that was used due  
538 to its ability to be detected following the RNAscope protocol. *Gla3* was expressed by  $74.8\pm 1.8\%$   
539 (436/571) of the *Gla3*-Cre.HTB(+) cells in the analysis also targeting *Vglut2* and by  $71.7\pm 4.3\%$   
540 (235/342) of the *Gla3*-Cre.HTB(+) cells in the analysis also targeting *Viaat*. These findings  
541 indicated that the mouse line and Cre-dependent virus mark the *Gla3*(+) population (Figure 1E–  
542 H). In the *Vglut2*-examining assay (Figure 1E–E’), *Vglut2*(+) and *Gla3*(+)*Vglut2*(+) were found  
543 in  $74.5\pm 2.8\%$  (437/571) and  $70.6\pm 2.8\%$  (318/517) of the *Gla3*-Cre.HTB(+) population,  
544 respectively (Figure 1F). Meanwhile, *Viaat*(+) was found in  $34.4\pm 3.3\%$  (116/342) and  
545 *Gla3*(+)*Viaat*(+) in  $28.0\pm 3.75\%$  (89/342) of the *Gla3*-Cre.HTB(+) neurons (Figure 1G–H).  
546 These results suggest that the adult spinal *Gla3*-Cre population consists of *Gla3*-expressing  
547 neurons found in a major *Vglut2*(+) excitatory population and a smaller *Viaat*(+) inhibitory  
548 population.

549  
550 *Gla3*-Cre;*tdTomato* neurons respond to glycine and the populations display a heterogeneous  
551 firing pattern

552 Patch-clamp recordings were used to examine electrophysiological properties of *Gla3*-Cre(+) neurons.  
553 The recorded *Gla3*-Cre;*tdTomato* neurons had an average resting membrane potential of  
554  $-59.9\pm 1.2\text{mV}$ , input resistance of  $879\pm 70.1\text{M}\Omega$ , and membrane capacitance of  $55.1\pm 4.3\text{pF}$  (Table  
555 1). All recorded neurons fired action potentials (APs) upon electrical stimulation of 500ms duration  
556 and increments of 10pA (Figure 2A). Moreover, the APs comprised five different firing patterns  
557 (Figure 2B–B’), with 52% of APs were tonic (36/69), 17% phasic (12/69), 7% single (5/69), 13%  
558 delayed (9/69), and 10% irregular (7/69) (Figure 2B–B’, Table 1). These firing patterns resemble  
559 previously identified categories of mouse dorsal horn neurons in terms of AP patterns (Hu and

560 Gereau, 2003, 2011; Heinke et al., 2004). The tdTomato(+) neurons had an average rheobase of  
561  $22.4 \pm 2.8$  pA, an AP threshold of  $-30.9 \pm 1.1$  mV, and a peak AP of  $21.7 \pm 1.8$  mV. Inter-group  
562 comparison showed that only neurons with delayed AP patterns had lower resting membrane  
563 potentials. No differences were observed in all other measured electrophysiological properties  
564 among neurons in the five AP pattern categories (Table 1). Collectively, the *Gla3*-Cre populations  
565 constitute five categories of neurons according to their firing patterns, with homogenous intrinsic  
566 membrane properties. The presence of functional glycine receptors on the recorded neurons was  
567 determined by applying glycine to the recording chamber in a voltage clamp mode, where cells  
568 were held at  $-60$  mV. All glycine applied *Gla3*-Cre;tdTomato neurons showed hyperpolarizing  
569 currents (an average of  $-34.8 \pm 5.7$  pA), and the glycine-induced current was completely blocked by  
570 the glycine receptor antagonist strychnine (Figure 2C).

571 Two studies have described that GLRA3 is present in the superficial laminae of the dorsal horn  
572 (Harvey et al., 2004; Werynska et al., 2021), while a third study demonstrated that GLRA3  
573 immunoreactivity is also present in the ventral horn (Wang et al., 2018). The latter study is more  
574 consistent with our observations as the *Gla3*-Cre(+) populations were localized in both the dorsal  
575 and ventral laminae (Figure 1A–C), which is also consistent with mRNA expression of *Gla3*  
576 (Ceder et al., 2023). To investigate the dendritic localization of *Gla3*-Cre(+) neurons, we  
577 performed cell fillings (Figure 2D–E). Neurobiotin was used to fill the neurons and the morphology  
578 was revealed by staining the filled neuron with Alexa Fluor™ 488 streptavidin conjugate (Figure  
579 2D). Dendritic morphologies and locations are showed in Figure 2E. The dendritic tree of each  
580 filled neurons appeared to be local and without long projecting dendrites. All neurons showed  
581 vertical alignment, where the dendritic arbors projected predominantly in a dorsal-ventral direction.

582

583 *Adult Glra3-Cre(+) neurons are mainly located in laminae III–IV and selective chemogenetic*  
584 *activation induces spontaneous behaviors indicative of a role in nociception and pruriception*

585 After the analysis of *Glra3-Cre;tdTomato* neurons, we further investigated the neuronal profile and  
586 anatomical location of adult *Glra3-Cre(+) cells*. Theoretically, the *tdTomato* reporter line marks  
587 both developmental and adult *Glra3-Cre*-expressing cells. Therefore, to label the adult population  
588 exclusively, reporter virus AAV8.hSyn-DIO-mCherry was unilaterally microinjected into the  
589 lumbar 5/lumbar 6 (L5/L6) spinal segments (abbreviated *Glra3-Cre.mCherry*). First, the specificity  
590 of the reporter, and the DREADD viral vectors used for the subsequent sensory behavioral  
591 analyses, were investigated by examining mCherry expression in *Glra3-Cre(-)* control mice. No  
592 fluorescent cells were detected (Figure 3), thus the virally induced gene expression in subsequent  
593 analyses was Cre-dependent. The histological analysis (Figure 4A–C) was conducted in the same  
594 manner as in the *Glra3-Cre;tdTomato* analysis, showing that 89.2±3.9% (1807/2099) of the  
595 mCherry(+) cells co-expressed NEUN (Figure 4A, C). In consistency with the tdTomato analysis,  
596 the mCherry(+) population was predominantly located in the dorsal horn (86.4±3.2%, 1279/1524),  
597 with a minor subpopulation in the ventral horn (15.0±4.5%, 245/1524) (Figure 4B–C). In the dorsal  
598 horn, the mCherry(+) cells were mainly restricted to laminae III–IV (40.1±4.2%, 590/1524),  
599 followed by lamina I (14.2±2.7%, 179/1524), laminae V–VI (11.6±2.0%, 222/1524), the PKCγ(+)  
600 inner lamina II (11.1±1.2%, 166/1524), in which 21.3±5.4% (41/166) of the mCherry(+) neurons  
601 were PKCγ(+), and the IB4(+) outer lamina II (9.4±1.4%, 122/1524, Figure 4B–C).

602 Activation of spinal GLYT2 neurons decreases pain and itch behaviors (Foster et al., 2015), and  
603 the anatomical location of the *Glra3-Cre(+) neurons* showed herein indicates a sensory role of  
604 *Glra3(+) neurons*. To investigate this, *Glra3-Cre(+) mice* were unilaterally injected into L5/L6  
605 with AAV8.hSyn-DIO-hM3D(Gq)-mCherry (abbreviated *Glra3-Cre.hM3Dq*) and the behavioral

606 phenotype was compared with *Gla3-Cre.mCherry* mice (control) (Figure 3D–F). The mice were  
607 administered CNO to selectively activate the *Gla3-Cre* populations. After CNO administration,  
608 *Gla3-Cre.hM3Dq* mice displayed a higher duration and frequency of licking/biting of the  
609 ipsilateral hind paw compared with control mice (Figure 4D). In mice, licking of the hind paw is  
610 associated with pain, while biting is a sign of itch (LaMotte et al., 2011). Therefore, our phenotype  
611 indicated both a nociceptive and a pruriceptive role for the *Gla3-Cre* populations. Additionally,  
612 activation of the *Gla3-Cre.hM3Dq* population resulted in stomping (Casarrubea et al., 2019) and  
613 guarding (Wang and Wang, 2003; Mogil and Crager, 2004), which were not observed in control  
614 mice (Figure 4E–F). These behaviors further indicated nociceptive/pruriceptive-related roles of  
615 these populations. Collectively, activation of the lumbar spinal *Gla3-Cre* populations results in  
616 nocifensive and pruritofensive behaviors.

617  
618 *Chemogenetic silencing of the Gla3-Cre populations decreases chloroquine- and compound*  
619 *48/80-induced itch*

620 Since selective chemogenetic activation of *Gla3-Cre(+)* neurons induced spontaneous behaviors  
621 indicative of a role in pain/itch transmission, we sought to decipher the involvement of this  
622 population in different sensory modalities. For this purpose, adult *Gla3-Cre(+)* mice were  
623 unilaterally injected with AAV8-hSyn-DIO-hM4D(Gi)-mCherry in L5/L6 (abbreviated *Gla3-*  
624 *Cre.hM4Di*) to enable selective silencing while sensory behaviors were monitored. The results  
625 were compared with control virus-injected *Gla3-Cre.mCherry* mice (Figure 5A). First, the basal  
626 behavioral phenotype was investigated following CNO administration. Selective silencing of  
627 *Gla3-Cre(+)* neurons did not affect spontaneous licking/biting behaviors in duration nor frequency

628 during the 0–30- and 30–60-min intervals after CNO administration (Figure 5B). Stomping and  
629 guarding behaviors were not observed when silencing the *Gla3*-Cre populations (data not shown).

630 In consistency with the Bourane et al. (2015) study (Bourane et al., 2015), the mice were subjected  
631 to sensory testing 40min after CNO administration. The pruriceptive role of the spinal lumbar  
632 *Gla3*-Cre population was examined in hairy skin, for which mice were administered either control  
633 saline, compound 48/80, or chloroquine solution (chemical itch) subcutaneously into the calf  
634 (Figure 5C–E). Compound 48/80 activates sensory neurons both directly via MRGPRA1  
635 (Schemann et al., 2012; Azimi et al., 2016, 2017) and indirectly as a mast cell degranulator by  
636 binding MRGPRB2 (Azimi et al., 2016), resulting in the release of pro-inflammatory molecules  
637 and pruritogens, including histamine and serotonin (Gupta and Harvima, 2018). Chloroquine  
638 activates primary afferents expressing MRGPRA3 (Liu et al., 2009). Saline evoked no differences  
639 in the duration or frequency of licking/biting of the injected area (Figure 5C), showing that the  
640 *Gla3*-Cre populations do not convey sensory information associated with the injection itself.  
641 When administering compound 48/80, both the duration and frequency of licking/biting of the  
642 affected area were decreased following *Gla3*-Cre(+) silencing (Figure 5D). For chloroquine  
643 administration, the same results were observed as with compound 48/80 injection (Figure 5E).

644 The role of the *Gla3*-Cre populations in noxious mechanical transmission was examined using the  
645 Randall-Selitto test. To target the tail dermatome, AAV8-hSyn-DIO-hM4D(Gi)-mCherry or the  
646 control virus was injected in the sacral 2 (S2) segment (Bennett et al., 1999). The mechanical  
647 threshold for *Gla3*-Cre.hM4Di mice did not differ compared with *Gla3*-Cre.mCherry mice  
648 (Figure 5F). To investigate if the *Gla3*-Cre populations are involved in thermal transmission,  
649 Hargreaves and acetone drop tests were performed (Figure 5G–H). Withdrawal response times,  
650 within groups, induced by heat stimulation of the ipsilateral hind paw were not affected when

651 comparing pre- and post- CNO administration in *Gla3*-Cre.mCherry or *Gla3*-Cre.hM4Di mice  
652 (Figure 5G). When further comparing the withdrawal response times between the *Gla3*-  
653 Cre.mCherry and *Gla3*-Cre.hM4Di mice following CNO administration, no differences were  
654 observed (Figure 5G). Application of a drop of acetone solution to the plantar surface of the  
655 ipsilateral hind paw did not alter sensory responses, including flinching, withdrawal, or  
656 licking/biting of the paw (Figure 5H). In conclusion, the *Gla3*-Cre populations have a pro-pruritic  
657 role in compound 48/80- and chloroquine-evoked itch, while not involved in acute noxious  
658 mechanical or thermal transmission.

659

#### 660 *Spinal neurons activated by compound 48/80 or chloroquine co-express Gla3*

661 Based on the behavioral observations, we wanted to molecularly verify the proposed sensory role  
662 of spinal *Gla3*(+) neurons and subsequently relate it to the *Vglut2*(+) and *Viaat*(+) spinal *Gla3*-  
663 Cre subpopulations. To do so, sensory stimulations in anesthetized and awake C57BL/6J mice were  
664 performed, followed by RNAscope (Wang et al., 2012) analyses of *fos* (Sheng and Greenberg,  
665 1990), *Gla3*, and *Vglut2* or *Viaat* in the L4/L6 dorsal spinal cord. The mice were subjected to one  
666 of six possible stimuli: a subcutaneous injection of saline, compound 48/80, or chloroquine  
667 subcutaneously in the right dorsolateral calf, a noxious mechanical stimulus (pinch or scratching)  
668 of the right dorsolateral calf, or thermal (Hargreaves) stimulation of the right hind paw (Figure 6A–  
669 L', for separate channels see Figure 7 and Figure 8). Scratching of the calf is not a natural behavior  
670 of mice, however, this stimulation was conducted in this area to enable comparison with the other  
671 stimuli. To prevent transcriptional influence from pain- and itch-responsive behaviors, all  
672 stimulations were performed under urethane anesthesia, except for the Hargreaves test that was  
673 performed on awake freely moving mice. All stimuli, except saline, were found to have a higher

674 number of *fos*(+) cells on the ipsilateral side compared with the contralateral side: saline  
675 contralateral  $47 \pm 5$  (847) and ipsilateral  $48 \pm 2$  (862); compound 48/80 contralateral  $43 \pm 3$  (779) and  
676 ipsilateral  $75 \pm 5$  (1347); chloroquine contralateral  $24 \pm 5$  (426) and ipsilateral  $41 \pm 3$  (745); artificial  
677 scratching contralateral  $36 \pm 3$  (606) and ipsilateral  $52 \pm 4$  (889); pinch contralateral  $36 \pm 3$  (573) and  
678 ipsilateral  $52 \pm 12$  (834); and noxious heat (Hargreaves) contralateral  $21 \pm 3$  (378) and ipsilateral  
679  $27 \pm 2$  (485) (Figure 6M). *Fos*(+)*Glr3*(+)-expressing cells were found to be greater in number on  
680 the ipsilateral dorsal horn than the contralateral dorsal horn for both compound 48/80 and  
681 chloroquine (Figure 6N). The average number of *fos*(+)*Glr3*(+) cells in the ipsilateral dorsal horn  
682 after injection with compound 48/80 was higher than the average number of *fos*(+)*Glr3*(+) cells  
683 after saline injection, which was not observed for chloroquine administration (Figure 6N). Of *fos*(+)  
684 cells, more than half of compound 48/80- and chloroquine-activated cells expressed *Glr3*  
685 (compound 48/80=59% (795/1347); chloroquine=67% (502/745); saline=52% (449/862);  
686 scratch=50% (442/889); pinch=49% (218/443); Hargreaves=47% (230/486)). No difference in the  
687 number of *fos*(+)*Glr3*(+) expressing cells could be detected for scratch, pinch, or Hargreaves  
688 (comparing the ipsi- and contralateral sides) (Figure 6O). Altogether, these findings verify that  
689 *Glr3*(+) neurons are involved in the communication of compound 48/80- and chloroquine-induced  
690 itch, and that these neurons are not involved in acute mechanical or thermal transmission. Since  
691 *Glr3* is found in both excitatory and inhibitory neuronal populations (Häring et al., 2018; Zeisel  
692 et al., 2018), we further investigated the sensory-modality activation of these *fos*(+)*Glr3*(+)  
693 subpopulations after injections with saline, compound 48/80, or chloroquine, focusing on the  
694 ipsilateral dorsal horn (Figure 9A–H'''). All three stimuli led to the expression of *fos* in both  
695 *Glr3*(+)*Vglut2*(+) and *Glr3*(+)*Viaat*(+) populations (Figure 9B). Taken together, the  
696 transcriptional analysis shows that *Glr3* is expressed in compound 48/80- and chloroquine-  
697 activated neurons, suggesting a role in transmission of these two sensory stimuli. Moreover, the

698 sensory-modality activated *fos(+)**Gla3(+)* cells can be found in subpopulations expressing the  
699 excitatory marker *Vglut2(+)* or the inhibitory marker *Viaat(+)*.

700  
701 *Lumbar Gla3-Cre(+)* neurons receive monosynaptic input from excitatory and inhibitory local  
702 spinal neurons

703 After identifying a pro-pruritic role for *Gla3-Cre(+)* neurons via behavioral experiments and co-  
704 expression of *Gla3* in compound 48/80- and chloroquine-activated *fos(+)* cells, we investigated  
705 the connectivity of lumbar *Gla3-Cre(+)* neurons. Retrograde viral tracing and dorsal root  
706 stimulation were used to deduce the mono- and poly-synaptic neurons targeting the *Gla3-Cre*  
707 populations. To enable analysis of the monosynaptic connectivity, a two-step viral injection  
708 procedure was performed. First, the helper virus AAV8.Syn-flex-TVA-oG-GFP was injected,  
709 enabling *Gla3-Cre(+)* host cell entry and subsequent retrograde monosynaptic propagation of the  
710 secondly injected EnvA pseudotyped mCherry rabies virus. In the spinal cord of control *Gla3-*  
711 *Cre(-)* mice, no helper GFP(+)*mCherry(-)* nor starter GFP(+)*mCherry(+)* cells were detected. Two  
712 *mCherry(+)* cells were found in the cervical division (1 cell in the ipsilateral dorsal horn and 1  
713 *mCherry(+)* cell in the contralateral ventral horn (one in each mouse)) (Figure 10A–B). In the brain,  
714 no traced *mCherry(+)* cells were detected in control mice. In the lumbar DRG, 51 *mCherry(+)* cells  
715 (43 ipsilateral, 8 contralateral) were found in two mice (43 ipsilateral and 6 contralateral in one  
716 mouse and 2 contralateral in a second mouse), verifying the Cre-dependent robustness and  
717 reliability of this tracing system.

718 In the spinal cords of *Gla3-Cre(+)* mice, 94 starter GFP(+)*mCherry(+)* cells were localized in the  
719 lumbar enlargement (Figure 10C’, D). Furthermore, 526 traced *mCherry(+)* cells were found in



720 the ipsilateral lumbar enlargement, and in four out of five mice, 16 traced cells were found in the  
721 contralateral lumbar spinal cord. None of these mice had any starter GFP(+)mCherry(+) cells  
722 located on the contralateral side (Figure 10C–D). Thus, it is possible that the *Gla3*-Cre populations  
723 receive some input from the contralateral side in addition to abundant ipsilateral input. Also, one  
724 mCherry(+) cell was detected in the ipsilateral dorsal horn of the cervical division, while none were  
725 detected in either thoracic nor sacral divisions (Figure 10C–C’'), indicating that the *Gla3*-Cre  
726 populations receive mainly local spinal input.

727 To molecularly examine the starter and traced cells, co-localizations with NEUN and the inhibitory  
728 marker PAX2 (Larsson, 2017) were investigated. Starter cells overlapped 44% (17/39), whereas  
729 79% (191/241) of the traced cells co-localized with NEUN (Figure 11A–B). 30.9% (17/55) of the  
730 starter cells and 35.4% (101/285) of the traced cells overlapped with PAX2 (Figure 11C–D), which,  
731 in consistency with the RNAscope findings, further indicates that the *Gla3*-Cre population  
732 comprises an inhibitory subpopulation. In the dorsal-ventral axis, the mCherry(+) cells were mainly  
733 located in the dorsal horn (laminae I–VI, Figure 11E–F), suggesting that the spinal input to the  
734 *Gla3*-Cre populations predominately constitutes of sensory-related transmission. A smaller  
735 subpopulation of mCherry(+) cells was observed in the ventral horn (laminae VII–IX) and lamina  
736 X (Figure 11E–F), with the former suggesting that the *Gla3*-Cre populations potentially receive  
737 input from motor-related spinal neurons.

738

### 739 *Lumbar Gla3-Cre(+) neurons receive monosynaptic input from several brain areas*

740 In the brain, a total of 89 traced mCherry(+) cells were detected in seven out of ten *Gla3*-Cre(+) mice.  
741 One mouse had a traced cell in the ipsilateral and two mice had traced cells in the contralateral

742 motor cortices (M1, M2, n cell=9). In a third mouse, traced cells were located in the ipsilateral  
743 somatosensory cortex, barrel field (S1BF, n cells=2) area (Figure 12A). Three mice had  
744 mCherry(+) cells in the contralateral p1 reticular formation (p1Rt, n cells=7) (Figure 12B) and in  
745 the red nucleus magnocellular part/red nucleus parvocellular part (RPC/RMC, n cells=16 cells)  
746 (Figure 12C). In addition, traced cells were detected in the ipsilateral and contralateral pontine  
747 reticular nucleus, either in the oral (PnO, n cells=10) or caudal part (PnC, n cells=7) (Figure 12D),  
748 and bilaterally in the gigantocellular vestibular nucleus (Gi, n cells=8) (Figure 12E). This  
749 demonstrates that the lumbar *Gla3-Cre* populations receive monosynaptic input from several brain  
750 areas. For details regarding brain area localization of the traced mCherry(+) cells in the individual  
751 mice, see (Table 2).

752  
753 *The spinal Gla3-Cre populations receive monosynaptic information from multiple subgroups of*  
754 *primary afferents*

755 Mono- and pre-synaptic traced mCherry(+) cells were detected in lumbar DRG of *Gla3-Cre(+)*  
756 mice, indicating that these spinal populations receive peripheral monosynaptic input. The traced  
757 cells were mainly found ipsilateral, but a few mCherry(+) cells were also detected in contralateral  
758 lumbar DRG in two out of six mice (n cells=20). In *Gla3-Cre(+)* mice, traced cells were found in  
759 one ipsilateral thoracic DRG in two separate mice (n cells=47). In one of these mice, and in a third  
760 mouse, mCherry(+) cells (n cells=20) were found in one contralateral thoracic DRG. As mentioned  
761 above, mCherry(+) cells were observed in the contralateral DRG in two *Gla3-Cre(-)* mice,  
762 implying that the contralateral mCherry(+) cells found in the *Gla3-Cre(+)* mice may be false  
763 positives. To identify the *Gla3-Cre(+)* contacting primary afferents, overlap with the markers  
764 NF200, TRKA, CGRP, IB4, TH, *Mrgprd*, *Mrgpra3*, *SST*, *Nppb*, *Trpv1* and *Trpm8* (Averill et al.,

1995; Patapoutian et al., 2003; Li et al., 2011; Usoskin et al., 2015; Albisetti et al., 2017; Kupari and Ernfors, 2023) was examined (Figure 13A–N, for separate channels see Figure 14). Of the ipsilateral lumbar DRG mCherry(+) cells, 28.4% (591/2079) belonged to the neurofilament heavy myelinated NF200(+) group (Figure 13A, L), which is present in A $\delta$ - and A $\alpha$ / $\beta$ -fibers (Basbaum et al., 2009; Meltzer et al., 2021). CGRP is a pro-pruritic and -noxious neuropeptide (McCoy et al., 2012; Rogoz et al., 2014), which is highly co-expressed with noxious receptor TRKA (Woolf et al., 1994; Averill et al., 1995; McCoy et al., 2012; Barker et al., 2020), and both genes have little overlap with IB4-binding fibers (Averill et al., 1995; McCoy et al., 2012; Usoskin et al., 2015). 34.9% (687/1988) of mCherry(+) cells overlapped with the TRKA(+) population (Figure 14B, L) and 20.3% (213/1049) with CGRP(+) (Figure 13C, L). Furthermore, 26.6% (391/1472) of the mCherry(+) cells overlapped with small unmyelinated non-peptidergic neuronal binding marker IB4 (Figure 14D, L), and 9.2% (179/1951) with TH (Figure 13E, L), which is expressed in low-threshold mechanosensory C-fibers (Li et al., 2011). In contrast, 79.5% (591/743) of the NF200(+), 57.1% (687/1203) of TRKA(+), 58.0% (213/367) of CGRP(+), 57.9% (391/675) of IB4-binding, and 29.9% (179/598) of TH(+) neurons were mCherry(+) (Figure 13M). Not all primary sensory afferents are equally susceptible to retrograde tracing by rabies virus (Albisetti et al., 2017), however, the overlap of the traced mCherry(+) neurons with all markers indicates that the spinal *Gla3*-Cre populations receive monosynaptic peripheral information from several fiber subtypes.

To obtain a more detailed view of the peripheral input to lumbar *Gla3*-Cre(+) neurons, markers for receptor and neurotransmitter DRG subtypes were targeted (Kupari and Ernfors, 2023) (Figure 13F–M). Three pruriceptive molecular clusters have previously been identified, namely NP1, NP2, and NP3. *Mrgprd* is expressed in the NP1 cluster, *Mrgpra3* in the NP2, and *SST/Nppb* in the NP3 cluster (Usoskin et al., 2015), where *Sst* has little co-localization with IB4 (Usoskin et al., 2015;

788 Stantcheva et al., 2016). *Mrgprd* was detected in 37.5% (147/392) (Figure 13F, L), *Mrgpra3* in  
789 17.6% (99/392) (Figure 14G, L), SST in 21.4% (265/1239) (Figure 13H, L), and *Nppb* in 20.3%  
790 (72/354) (Figure 13I, L) of the traced mCherry(+) cells. Strikingly, mCherry was detected in a large  
791 portion of the pruriceptive sub-clusters: 46.5% (147/316) of the *Mrgprd*(+), 69.7% (69/99) of  
792 *Mrgpra3*(+), 66.9% (265/394) of SST(+), and 40.9% (72/176) of the *Nppb*(+) neurons (Figure  
793 14M), supporting the behavioral finding of the *Gla3*-Cre populations facilitating itch-related  
794 transmission. Lastly, the expressions of the temperature-sensitive channels *Trpv1* and *Trpm8* were  
795 investigated. *Trpv1* is activated by capsaicin and noxious temperatures ( $\geq 42^{\circ}\text{C}$ ), while *Trpm8* is  
796 activated by menthol and cooling temperatures ( $< 26\text{--}28^{\circ}\text{C}$ ) (Patapoutian et al., 2003). Herein,  
797 13.5% (53/392) and 2.3% (9/392) of the mCherry(+) cells expressed *Trpv1* or *Trpm8*, respectively  
798 (Figure 13J–L). In contrast, 13.2% (53/403) of the *Trpv1*(+) and 14.3% (9/63) of the *Trpm8*(+)  
799 populations expressed mCherry (Figure 13M). The low overlap of *Trpv1* in traced neurons is  
800 consistent with both the low co-expression of *Gla3* in Hargreaves-induced *fos*(+) cells and the  
801 lack of phenotype of DREADD-mediated inactivation of *Gla3*-Cre(+) neurons in the same test.

802 To further investigate and validate that *Gla3*-Cre(+) neurons receive peripheral monosynaptic  
803 input, patch-clamp recordings were conducted on *Gla3*-Cre(+) (reporter tdTomato(+)) and viral  
804 mCherry(+) neurons in combination with dorsal root stimulation (Figure 13N). The data revealed  
805 that the *Gla3*-Cre populations receive monosynaptic inputs from all afferent fiber subtypes. Half  
806 of the recorded neurons (16/32) received monosynaptic inputs from at least two afferent fibers,  
807 among which almost one-third (5/16) formed monosynaptic connections with all three fiber  
808 subtypes. Furthermore, the majority of synaptic inputs was delivered via A $\alpha$ / $\beta$  fibers (41%) or C-  
809 fibers (40%), while only 19% was transmitted by A $\delta$  fibers (Figure 13O). Collectively, these results  
810 confirmed that *Gla3*-Cre(+) neurons receive monosynaptic information from multiple afferent

811 fiber subtypes, including myelinated and itch-associated neurons, suggesting that the *Gla3-Cre*  
812 populations form complex monosynaptic connections with primary afferents.

813

JNeurosci Accepted Manuscript

## 814 **Discussion**

815

816 Herein, we report that the *Gla3*-Cre line labels excitatory and inhibitory primarily dorsal neuronal  
817 populations in the spinal cord that express *Gla3*. These populations respond to glycine and are  
818 heterogeneous in terms of AP firing patterns and homogenous in intrinsic membrane properties.  
819 Behavioral and expressional analyses revealed that spinal *Gla3*-Cre populations have a pro-  
820 pruritic role in compound 48/80- and chloroquine-evoked itch, and no role in the mechanical or  
821 thermal responses tested. Analyses using mono-synaptic retrograde tracing and dorsal root  
822 stimulations demonstrated that lumbar *Gla3*-Cre populations receive monosynaptic excitatory and  
823 inhibitory input from neurons within the lumbar division, several brain areas related to sensory and  
824 motor functions, and afferents belonging to the NF200(+), TRKA(+), IB4-binding, and TH(+)  
825 subpopulations. Furthermore, CGRP(+) and pruritic markers *Mrgprd*(+), *Mrgpra3*(+), SST(+), and  
826 *Nppb*(+) afferent populations were found to synapse on spinal *Gla3*-Cre(+) neurons. The  
827 multitude of sensory-modality input to this population was confirmed with dorsal root stimulations.  
828 Taken together, the data show that the spinal *Gla3*-Cre populations communicate compound 48/80  
829 and chloroquine-evoked itch.

830 The glycinergic system is a fast-response inhibitory system important for modulating motor and  
831 sensory reflex activity, muscle tone, and respiratory rhythms (Manzke et al., 2010; Cioffi, 2018).  
832 The glycinergic system serves a protective role in pain and itch, where activation of glycinergic  
833 neurons leads to attenuated pain and itch responses, and ablation causes nociceptive and  
834 pruriceptive hypersensitivity (Foster et al., 2015). Blocking spinal glycine receptors decreases the  
835 nociceptive counter-stimulation effect on persistent itch-mediated spontaneous activity in the  
836 spinal cord (Akiyama et al., 2011), implementing the importance of the glycinergic system in

837 sensory regulation. Our chemogenetic activation experiments indicate that the adult spinal *Gla3-*  
838 *Cre* populations have an acute sensory role as its activation evoked spontaneous sensory behaviors,  
839 such as licking/biting, stomping, and guarding of the affected dermatome, whereas silencing  
840 decreased compound 48/80- and chloroquine-induced itch, indicative of a pro-pruritic role.

841 In the retrograde rabies tracing experiment, we investigated overlap of traced neurons with primary  
842 afferent subtype markers to deduce the sensory-modality input to the spinal *Gla3-Cre* populations.  
843 Almost half of the NP1-*Mrgprd*(+) ( $\beta$ -alanine receptor (Liu et al., 2012)) and NP3-*Nppb*(+)/*Sst*(+)  
844 (Usoskin et al., 2015; Stantcheva et al., 2016) primary afferents synapse on *Gla3-Cre*(+) neurons.  
845 Activation of SST(+) primary afferents evokes pruritofensive behaviors and deletion of *Sst*  
846 attenuates itch evoked by pruritogens, such as compound 48/80 and chloroquine (Huang et al.,  
847 2018). Furthermore, SST(+) primary afferent ablation decreases histamine, chloroquine, IL-31-  
848 and serotonin-evoked scratching (Stantcheva et al., 2016). Herein, we found that almost 70% of  
849 SST(+) primary afferents and chloroquine receptor *Mrgpra3*(+) primary afferents, found in the  
850 NP2 cluster (Liu et al., 2009; Usoskin et al., 2015), synapse on *Gla3-Cre*(+) neurons. TRKA is  
851 the receptor of NGF $\beta$ , a neurotrophic protein important for hyperalgesia (Woolf et al., 1994; Barker  
852 et al., 2020) and CGRP is a neuropeptide with pro-pruritic and -noxious functions (McCoy et al.,  
853 2012; Rogoz et al., 2014). *Ntrk1* (gene encoding TRKA) and *Calca* (gene encoding CGRP) are  
854 highly co-expressed in non-peptidergic pruriceptive NP2 neurons and in nociceptive peptidergic  
855 PEP1–2 neurons. Our retrograde monosynaptic tracing showed that *Gla3-Cre*(+) neurons receive  
856 monosynaptic input from TRKA(+) and CGRP(+) primary afferents. The dorsal root stimulation  
857 further confirmed that these populations receive monosynaptic input from C-fibers, collectively  
858 implying that spinal *Gla3-Cre*(+) neurons are central for communicating itch.

859 Transcriptional validation of the behavioral involvement of spinal *Gla3*-Cre(+) neurons in  
860 different sensory modalities confirmed that *Gla3* is largely expressed in compound 48/80-evoked  
861 *fos*(+) neurons compared with saline-induced *fos*(+) cells. Compared with the contralateral side,  
862 chloroquine-activated *fos*(+) cells expressed *Gla3* but this effect could not be separated from the  
863 influence of the injection itself. However, the chloroquine-activated cells constitute a smaller  
864 population than the saline-activated group ( $p < .0001$ ), which may explain this result. Previous  
865 studies have found that itch-inducing compounds activate cells in the superficial dorsal horn (Doi-  
866 Saika et al., 1997; Nojima et al., 2003; Yao et al., 1992; Jinks and Carstens, 2000; Nakano et al.,  
867 2008; Gatto et al., 2021; Han et al., 2012; Akiyama et al., 2013), which is similar to our findings.

868 Consistent with the absence of thermal response alterations following *Gla3* deletion/mutation  
869 observed by the cited studies (Harvey et al., 2009; Werynska et al., 2021), chemogenetic silencing  
870 of *Gla3*-Cre neurons did not alter the withdrawal response in the Hargreaves test. Subsequent  
871 histological analysis showed that Hargreaves-activated *fos*(+) cells did not overlap with *Gla3*  
872 compared with the contralateral side in naïve mice. Moreover, silencing did not affect the response  
873 in the acetone drop test, further dismissing involvement of the spinal *Gla3*-Cre(+) neurons in acute  
874 thermal transmission. The retrograde rabies tracing revealed that the *Gla3*-Cre populations receive  
875 sparse monosynaptic input from *Trpm8*(+) primary afferents, while 13.5% of the traced DRG  
876 neurons overlapped with *Trpv1*. TRPV1(+) primary afferents are key mediators in itch-  
877 transmission (Mishra et al., 2011; Rogoz et al., 2014) and TRPV1-deficient mice show reduced  
878 responses to histamine (Imamachi et al., 2009). The *TrpVI*(+) primary afferent input to the lumbar  
879 *Gla3*-Cre populations may therefore be related to itch rather than thermal sensation. Silencing of  
880 GLYT2 neurons do however regulate both mechanical and thermal transmission (Foster et al.,  
881 2015) and activation of GLYT2 neurons has an anti-hyperalgesic effect on neuropathic-induced



882 mechanical allodynia (Foster et al., 2015). Meanwhile, deletion/mutation of *Gla3* does not affect  
883 the withdrawal response to mechanical and thermal stimulation following nerve injury (Harvey et  
884 al., 2009b; Werynska et al., 2021). Chemogenetic silencing of the *Gla3*-Cre populations did not  
885 affect the acute mechanical sensitivity in the Randall-Selitto test and scratch- or pinch-activated  
886 *fos*(+) cells did not express *Gla3* in higher occurrence compared with the contralateral side in  
887 naïve mice. Conclusively, our analyses indicate that the *Gla3*-Cre(+) neurons may not be the post-  
888 synaptic target of the GLYT2 population in regulation of noxious mechanical and thermal  
889 transmission. However, since GLRA3 has been connected to inflammatory-induced  
890 hypersensitivity (Harvey et al., 2009; Werynska et al., 2021), future investigations targeting the  
891 role of *Gla3*-Cre(+) neurons in inflammatory, neuropathic, thermal and mechanical allodynia are  
892 of interest.

893 Besides input from itch-related primary afferents, the monosynaptic tracing experiments and dorsal  
894 root stimulations revealed that the *Gla3*-Cre populations receive input from A $\alpha$ / $\beta$  fibers as partial  
895 overlap with NF200(+). As NF200 can be detected in A $\beta$  low-threshold mechanoreceptors  
896 (LTMRs), A $\beta$  high-threshold mechanoreceptors (HTMRs), and A $\delta$ -fibers (Djoughri and Lawson,  
897 2004; Nagi et al., 2019; Meltzer et al., 2021), thus, input from these neuronal sub-populations  
898 cannot be excluded. Furthermore, the overlap of mCherry(+) cells with TH(+) neurons, which  
899 convey low-threshold mechanical information and are possibly associated with pleasant touch (Li  
900 et al., 2011), proposes that the lumbar *Gla3*-Cre populations receive several categories of sensory  
901 input. In addition, traced cells were found in the ventral horn (laminae VII-IV), indicating that the  
902 *Gla3*-Cre populations may receive input from spinal motor-related neurons. Additionally, starter,  
903 lineage and virally labelled *Gla3*-Cre(+) cells were observed in the ventral horn. In line with these  
904 observations, we recently showed that *Gla3* is detected in the dorsal and ventral horns of the

905 lumbar division (Ceder et al., 2023). Thus, it remains unclear whether sensory-mediating *Gla3-*  
906 *Cre(+)* neurons receive motor input or if the ventrally located *Gla3-Cre* population have motor  
907 functions.

908 Traced cells were also detected in the brain, suggesting that the lumbar *Gla3-Cre(+)* neurons  
909 receive distant descending input. These brain areas included the contralateral motor cortices,  
910 ipsilateral primary somatosensory cortex, barrel area, contralateral p1 reticular formation,  
911 magnocellular and parvocellular parts of the red nucleus (RMC and RPC), ipsilateral oral and  
912 caudal part of the pontine reticular nucleus, and bilateral gigantocellular vestibular nucleus.  
913 Previous unilateral retrograde tracing from the cervical 1 and 2 segments in mouse shows a similar  
914 tracing pattern as observed in our tracing experiment (Liang et al., 2011). The RMC and reticular  
915 formations are related to analgesic functions (Prado et al., 1984; Martins and Tavares, 2017; Basile  
916 et al., 2021), and the RMC, RPC, and pontine reticular nucleus to motor functions (Morales et al.,  
917 1987; Kennedy, 1990; Basile et al., 2021). Moreover, a study in mice linked monosynaptic  
918 signalling from the motor and sensory cortices to distinct spinal dorsal and ventral interneuron  
919 populations, and further to different motoric functions. Here, scant monosynaptic inputs from the  
920 motor cortex to dorsal horn neurons and from the sensory cortex to ventral neurons were observed  
921 (Ueno et al., 2018), indicating that the ventrally located *Gla3-Cre(+)* neurons probably receive  
922 monosynaptic input from the motor cortex. Collectively, we showed that the spinal *Gla3-Cre*  
923 populations receive monosynaptic descending input from brain areas involved in sensory and/or  
924 motor functions.

925

926 *Conclusions*

927 Spinal GLYT2 neurons regulate itch (Foster et al., 2015), suggesting that the glycinergic system  
928 has potential as drug targets for itch. Nonetheless, thus far, the pruriceptive roles of the glycine  
929 receptor subunits have not been evaluated. Here, we successfully linked the *Gla3*-Cre populations  
930 to a pro-pruriceptive role in itch, indicating that GLRA3 may be a potential novel target for itch  
931 treatment. The spontaneous guarding behaviors observed from activating the *Gla3*-Cre  
932 populations are indicative of a role in sensory hypersensitivity (Wang and Wang, 2003; Mogil and  
933 Crager, 2004; Casarrubea et al., 2019) and raises questions regarding the hypersensitivity  
934 involvement of these populations for future investigations.

935

#### 936 *Methodological considerations*

937 From the monosynaptic retrograde viral tracing, the lumbar *Gla3*-Cre populations were found to  
938 receive both inhibitory PAX2(+) and presumably excitatory, PAX2(-) input, from the lumbar  
939 segments, where the majority of the traced mCherry(+) cells were PAX2(-). However, the NEUN  
940 overlap analysis revealed that 44% of starter cells, 79% of traced mCherry(+) cells, and 89% of  
941 virally marked *Gla3*-Cre.mCherry were NEUN(+), which can be compared with the 98%  
942 NEUN(+) overlap in the *Gla3*-Cre;*tdTomato* cells. The decrease in overlap may indicate that the  
943 viral injections affect expressional patterns in the infected cells, and therefore, the PAX2(+) overlap  
944 in the starter and traced cells may be underestimated.

946

## References

- 947 Akiyama T, Iodi Carstens M, Carstens E (2011) Transmitters and pathways mediating inhibition of spinal  
948 itch-signaling neurons by scratching and other counterstimuli. *PLoS ONE* 6:e22665.
- 949 Akiyama T, Tominaga M, Davoodi A, Nagamine M, Blansit K, Horwitz A, Carstens MI, Carstens E (2013)  
950 Roles for substance P and gastrin-releasing peptide as neurotransmitters released by primary  
951 afferent pruriceptors. *J Neurophysiol* 109:742–748.
- 952 Albisetti GW, Ghanem A, Foster E, Conzelmann K-K, Zeilhofer HU, Wildner H (2017) Identification of two  
953 classes of somatosensory neurons that display resistance to retrograde infection by rabies virus.  
954 *J Neurosci* 37:10358–10371.
- 955 Anderson CR, Ashwell KW, Collewijn H, Conta A, Harvey A, Heise C, Hodgetts S, Holstege G, Kayalioglu G,  
956 Keast JR, McHanwell S, McLachlan EM, Paxinos G, Plant G, Scremin O, Sidhu A, Stelzner D,  
957 Watson C (2009) The spinal cord: A christopher and dana reeve foundation text and atlas. In: *The*  
958 *Spinal Cord*, pp v. Elsevier. Available at:  
959 <https://linkinghub.elsevier.com/retrieve/pii/B9780123742476500018> [Accessed February 23,  
960 2021].
- 961 Averill S, McMahon SB, Clary DO, Reichardt LF, Priestley JV (1995) Immunocytochemical localization of  
962 trkA receptors in chemically identified subgroups of adult rat sensory neurons. *Eur J Neurosci*  
963 7:1484–1494.
- 964 Azimi E, Reddy VB, Pereira PJS, Talbot S, Woolf CJ, Lerner EA (2017) Substance P activates Mas-related G  
965 protein-coupled receptors to induce itch. *J Allergy Clin Immunol* 140:447-453.e3.
- 966 Azimi E, Reddy VB, Shade K-TC, Anthony RM, Talbot S, Pereira PJS, Lerner EA (2016) Dual action of  
967 neurokinin-1 antagonists on Mas-related GPCRs. *JCI Insight* 1:e89362.
- 968 Barker PA, Mantyh P, Arendt-Nielsen L, Viktrup L, Tive L (2020) Nerve growth factor signaling and its  
969 contribution to pain. *J Pain Res* 13:1223–1241.
- 970 Basbaum AI, Bautista DM, Scherrer G, Julius D (2009) Cellular and molecular mechanisms of pain. *Cell*  
971 139:267–284.
- 972 Basile GA, Quartu M, Bertino S, Serra MP, Boi M, Bramanti A, Anastasi GP, Milardi D, Cacciola A (2021)  
973 Red nucleus structure and function: from anatomy to clinical neurosciences. *Brain Struct Funct*  
974 226:69–91.
- 975 Bennett DJ, Gorassini M, Fouad K, Sanelli L, Han Y, Cheng J (1999) Spasticity in rats with sacral spinal cord  
976 injury. *J Neurotrauma* 16:69–84.
- 977 Berrocal YA, Almeida VW, Puentes R, Knott EP, Hechtman JF, Garland M, Pearse DD (2014) Loss of central  
978 inhibition: implications for behavioral hypersensitivity after contusive spinal cord injury in rats.  
979 *Pain Res Treat* 2014:178278.
- 980 Beyer C, Roberts LA, Komisaruk BR (1985) Hyperalgesia induced by altered glycinergic activity at the  
981 spinal cord. *Life Sciences* 37:875–882.

- 982 Bourane S, Duan B, Koch SC, Dalet A, Britz O, Garcia-Campmany L, Kim E, Cheng L, Ghosh A, Ma Q,  
983 Goulding M (2015) Gate control of mechanical itch by a subpopulation of spinal cord  
984 interneurons. *Science* 350:550–554.
- 985 Casarrubea, Aiello, Santangelo, Di Giovanni, Crescimanno (2019) Different Representation Procedures  
986 Originated from Multivariate Temporal Pattern Analysis of the Behavioral Response to Pain in  
987 Wistar Rats Tested in a Hot-Plate under Morphine. *Brain Sci* 9:233.
- 988 Ceder MM, Weman HM, Johansson E, Henriksson K, Magnusson KA, Roman E, Lagerström MC (2023) The  
989 glycine receptor alpha 3 subunit mRNA expression shows sex-dependent differences in the adult  
990 mouse brain. *BMC Neuroscience* 24:32.
- 991 Cioffi CL (2018) Modulation of Glycine-Mediated Spinal Neurotransmission for the Treatment of Chronic  
992 Pain. *J Med Chem* 61:2652–2679.
- 993 Djouhri L, Lawson SN (2004) Abeta-fiber nociceptive primary afferent neurons: a review of incidence and  
994 properties in relation to other afferent A-fiber neurons in mammals. *Brain Res Brain Res Rev*  
995 46:131–145.
- 996 Doi-Saika M, Tokunaga A, Senba E (1997) Intradermal 5-HT induces Fos expression in rat dorsal horn  
997 neurons not via 5-HT3 but via 5-HT2A receptors. *Neurosci Res* 29:143–149.
- 998 Dutertre S, Becker C-M, Betz H (2012) Inhibitory glycine receptors: an update. *J Biol Chem* 287:40216–  
999 40223.
- 1000 Foster E, Wildner H, Tudeau L, Haueter S, Ralvenius WT, Jegen M, Johannssen H, Hösli L, Haenraets K,  
1001 Ghanem A, Conzelmann K-K, Bösl M, Zeilhofer HU (2015) Targeted ablation, silencing, and  
1002 activation establish glycinergic dorsal horn neurons as key components of a spinal gate for pain  
1003 and itch. *Neuron* 85:1289–1304.
- 1004 Freitag FB, Ahemaiti A, Jakobsson JET, Weman HM, Lagerström MC (2019) Spinal gastrin releasing  
1005 peptide receptor expressing interneurons are controlled by local phasic and tonic inhibition. *Sci*  
1006 *Rep* 9:16573.
- 1007 Freitag FB, Ahemaiti A, Weman HM, Ambroz K, Lagerström MC (2021) Targeting barrel field spiny stellate  
1008 cells using a vesicular monoaminergic transporter 2-Cre mouse line. *Sci Rep* 11:3239.
- 1009 Gatto G, Bourane S, Ren X, Di Costanzo S, Fenton PK, Halder P, Seal RP, Goulding MD (2021) A functional  
1010 topographic map for spinal sensorimotor reflexes. *Neuron* 109:91-104.e5.
- 1011 Groemer TW, Triller A, Zeilhofer HU, Becker K, Eulenburg V, Becker CM (2022) Nociception in the glycine  
1012 receptor deficient mutant mouse spastic. *Front Mol Neurosci* 15:832490.
- 1013 Gupta K, Harvima IT (2018) Mast cell-neural interactions contribute to pain and itch. *Immunol Rev*  
1014 282:168–187.
- 1015 Han N, Zu JY, Chai J (2012) Spinal bombesin-recognized neurones mediate more nonhistaminergic than  
1016 histaminergic sensation of itch in mice. *Clin Exp Dermatol* 37:290–295.

- 1017 Häring M, Zeisel A, Hochgerner H, Rinwa P, Jakobsson JET, Lönnerberg P, La Manno G, Sharma N, Borgius  
1018 L, Kiehn O, Lagerström MC, Linnarsson S, Ernfors P (2018) Neuronal atlas of the dorsal horn  
1019 defines its architecture and links sensory input to transcriptional cell types. *Nat Neurosci* 21:869–  
1020 880.
- 1021 Harvey RJ, Depner UB, Wässle H, Ahmadi S, Heindl C, Reinold H, Smart TG, Harvey K, Schütz B, Abo-Salem  
1022 OM, Zimmer A, Poisbeau P, Welzl H, Wolfer DP, Betz H, Zeilhofer HU, Müller U (2004) GlyR  
1023 alpha3: an essential target for spinal PGE2-mediated inflammatory pain sensitization. *Science*  
1024 304:884–887.
- 1025 Harvey VL, Caley A, Müller UC, Harvey RJ, Dickenson AH (2009) A Selective Role for alpha3 Subunit  
1026 Glycine Receptors in Inflammatory Pain. *Front Mol Neurosci* 2:14.
- 1027 Heinke B, Ruscheweyh R, Forsthuber L, Wunderbaldinger G, Sandkühler J (2004) Physiological,  
1028 neurochemical and morphological properties of a subgroup of GABAergic spinal lamina II  
1029 neurones identified by expression of green fluorescent protein in mice. *J Physiol* 560:249–266.
- 1030 Hu H-J, Gereau RW (2003) ERK Integrates PKA and PKC Signaling in Superficial Dorsal Horn Neurons. II.  
1031 Modulation of Neuronal Excitability. *Journal of Neurophysiology* 90:1680–1688.
- 1032 Hu H-J, Gereau RW (2011) Metabotropic glutamate receptor 5 regulates excitability and Kv4.2-containing  
1033 K<sup>+</sup> channels primarily in excitatory neurons of the spinal dorsal horn. *J Neurophysiol* 105:3010–  
1034 3021.
- 1035 Huang J, Polgár E, Solinski HJ, Mishra SK, Tseng P-Y, Iwagaki N, Boyle KA, Dickie AC, Kriegbaum MC,  
1036 Wildner H, Zeilhofer HU, Watanabe M, Riddell JS, Todd AJ, Hoon MA (2018) Circuit dissection of  
1037 the role of somatostatin in itch and pain. *Nat Neurosci* 21:707–716.
- 1038 Imamachi N, Park GH, Lee H, Anderson DJ, Simon MI, Basbaum AI, Han S-K (2009) TRPV1-expressing  
1039 primary afferents generate behavioral responses to pruritogens via multiple mechanisms. *Proc*  
1040 *Natl Acad Sci U S A* 106:11330–11335.
- 1041 Jinks SL, Carstens E (2000) Superficial dorsal horn neurons identified by intracutaneous histamine:  
1042 chemonociceptive responses and modulation by morphine. *J Neurophysiol* 84:616–627.
- 1043 Kennedy PR (1990) Corticospinal, rubrospinal and rubro-olivary projections: a unifying hypothesis.  
1044 *Trends Neurosci* 13:474–479.
- 1045 Krashes MJ, Koda S, Ye C, Rogan SC, Adams AC, Cusher DS, Maratos-Flier E, Roth BL, Lowell BB (2011)  
1046 Rapid, reversible activation of AgRP neurons drives feeding behavior in mice. *J Clin Invest*  
1047 121:1424–1428.
- 1048 Kupari J, Ernfors P (2023) Molecular taxonomy of nociceptors and pruriceptors. *Pain* 164:1245–1257.
- 1049 LaMotte RH, Shimada SG, Sikand P (2011) Mouse models of acute, chemical itch and pain in humans. *Exp*  
1050 *Dermatol* 20:778–782.
- 1051 Larsson M (2017) Pax2 is persistently expressed by GABAergic neurons throughout the adult rat dorsal  
1052 horn. *Neurosci Lett* 638:96–101.

- 1053 Lein ES et al. (2007) Genome-wide atlas of gene expression in the adult mouse brain. *Nature* 445:168–  
1054 176.
- 1055 Li L, Rutlin M, Abraira VE, Cassidy C, Kus L, Gong S, Jankowski MP, Luo W, Heintz N, Koerber HR,  
1056 Woodbury CJ, Ginty DD (2011) The functional organization of cutaneous low-threshold  
1057 mechanosensory neurons. *Cell* 147:1615–1627.
- 1058 Li T, Mamillapalli R, Ding S, Chang H, Liu Z-W, Gao X-B, Taylor HS (2018) Endometriosis alters brain  
1059 electrophysiology, gene expression and increases pain sensitization, anxiety, and depression in  
1060 female mice. *Biol Reprod* 99:349–359.
- 1061 Liang H, Paxinos G, Watson C (2011) Projections from the brain to the spinal cord in the mouse. *Brain*  
1062 *Struct Funct* 215:159–186.
- 1063 Liu Q, Sikand P, Ma C, Tang Z, Han L, Li Z, Sun S, LaMotte RH, Dong X (2012) Mechanisms of itch evoked  
1064 by  $\beta$ -alanine. *J Neurosci* 32:14532–14537.
- 1065 Liu Q, Tang Z, Surdenikova L, Kim S, Patel KN, Kim A, Ru F, Guan Y, Weng H-J, Geng Y, Udem BJ, Kollarik  
1066 M, Chen Z-F, Anderson DJ, Dong X (2009) Sensory neuron-specific GPCR Mrgprs are itch  
1067 receptors mediating chloroquine-induced pruritus. *Cell* 139:1353–1365.
- 1068 Lynch JW (2004) Molecular structure and function of the glycine receptor chloride channel. *Physiol Rev*  
1069 84:1051–1095.
- 1070 Manzke T, Niebert M, Koch UR, Caley A, Vogelgesang S, Hülsmann S, Ponimaskin E, Müller U, Smart TG,  
1071 Harvey RJ, Richter DW (2010) Serotonin receptor 1A-modulated phosphorylation of glycine  
1072 receptor  $\alpha 3$  controls breathing in mice. *J Clin Invest* 120:4118–4128.
- 1073 Mariqueo T (2020) The Expression of Glycine Receptor  $\alpha 3$  Subunit is Differentially Regulated in Different  
1074 Types of Pain. *J Neurol Neurobiol* Available at:  
1075 [https://scholar.archive.org/work/pxkxm6bt35cdzon6ktqnppfily/access/wayback/http://sciforsch](https://scholar.archive.org/work/pxkxm6bt35cdzon6ktqnppfily/access/wayback/http://sciforschonline.org/journals/neurology/article-data/JNNB161/JNNB161.pdf)  
1076 [online.org/journals/neurology/article-data/JNNB161/JNNB161.pdf](https://scholar.archive.org/work/pxkxm6bt35cdzon6ktqnppfily/access/wayback/http://sciforschonline.org/journals/neurology/article-data/JNNB161/JNNB161.pdf) [Accessed March 23,  
1077 2022].
- 1078 Martins I, Tavares I (2017) Reticular formation and pain: the past and the future. *Front Neuroanat* 11:51.
- 1079 McCoy ES, Taylor-Blake B, Zylka MJ (2012) CGRP $\alpha$ -expressing sensory neurons respond to stimuli that  
1080 evoke sensations of pain and itch. *PLoS ONE* 7:e36355.
- 1081 McCracken LM, Lowes DC, Salling MC, Carreau-Vollmer C, Odean NN, Blednov YA, Betz H, Harris RA,  
1082 Harrison NL (2017) Glycine receptor  $\alpha 3$  and  $\alpha 2$  subunits mediate tonic and exogenous agonist-  
1083 induced currents in forebrain. *Proc Natl Acad Sci USA* 114:E7179–E7186.
- 1084 Meltzer S, Santiago C, Sharma N, Ginty DD (2021) The cellular and molecular basis of somatosensory  
1085 neuron development. *Neuron* 109:3736–3757.
- 1086 Mishra SK, Tisel SM, Orestes P, Bhangoo SK, Hoon MA (2011) TRPV1-lineage neurons are required for  
1087 thermal sensation. *EMBO J* 30:582–593.

- 1088 Mogil JS, Cragger SE (2004) What should we be measuring in behavioral studies of chronic pain in  
1089 animals? *Pain* 112:12–15.
- 1090 Morales F, Engelhardt J, Soja P (1987) Motoneuron properties during motor inhibition produced by  
1091 microinjection of carbachol into the pontine reticular formation of the decerebrate cat. *Journal*  
1092 *of ...* Available at: <https://journals.physiology.org/doi/abs/10.1152/jn.1987.57.4.1118> [Accessed  
1093 April 27, 2023].
- 1094 Nagi SS, Marshall AG, Makdani A, Jarocka E, Liljencrantz J, Ridderström M, Shaikh S, O’Neill F, Saade D,  
1095 Donkervoort S, Foley AR, Minde J, Trulsson M, Cole J, Bönnemann CG, Chesler AT, Bushnell MC,  
1096 McGlone F, Olausson H (2019) An ultrafast system for signaling mechanical pain in human skin.  
1097 *Sci Adv* 5:eaaw1297.
- 1098 Nakano T, Andoh T, Lee J-B, Kuraishi Y (2008) Different dorsal horn neurons responding to histamine and  
1099 allergic itch stimuli. *Neuroreport* 19:723–726.
- 1100 Nojima H, Simons CT, Cuellar JM, Carstens MI, Moore JA, Carstens E (2003) Opioid modulation of  
1101 scratching and spinal c-fos expression evoked by intradermal serotonin. *J Neurosci* 23:10784–  
1102 10790.
- 1103 Osakada F, Mori T, Cetin AH, Marshel JH, Virgen B, Callaway EM (2011) New rabies virus variants for  
1104 monitoring and manipulating activity and gene expression in defined neural circuits. *Neuron*  
1105 71:617–631.
- 1106 Pan H, Fatima M, Li A, Lee H, Cai W, Horwitz L, Hor CC, Zaher N, Cin M, Slade H, Huang T, Xu XZS, Duan B  
1107 (2019) Identification of a spinal circuit for mechanical and persistent spontaneous itch. *Neuron*  
1108 103:1135-1149.e6.
- 1109 Patapoutian A, Peier AM, Story GM, Viswanath V (2003) ThermoTRP channels and beyond: mechanisms  
1110 of temperature sensation. *Nat Rev Neurosci* 4:529–539.
- 1111 Paxinos G, Franklin K (n.d.) *The Mouse Brain in Stereotaxic Coordinates* Academic Press, San Diego.
- 1112 Peirs C, Patil S, Bouali-Benazzouz R, Artola A, Landry M, Dallel R (2014) Protein kinase C gamma  
1113 interneurons in the rat medullary dorsal horn: distribution and synaptic inputs to these neurons,  
1114 and subcellular localization of the enzyme. *J Comp Neurol* 522:393–413.
- 1115 Pinto V, Szûcs P, Derkach VA, Safronov BV (2008) Monosynaptic convergence of C- and Adelta-afferent  
1116 fibres from different segmental dorsal roots on to single substantia gelatinosa neurones in the  
1117 rat spinal cord. *J Physiol (Lond)* 586:4165–4177.
- 1118 Polgár E, Fowler JH, McGill MM, Todd AJ (1999) The types of neuron which contain protein kinase C  
1119 gamma in rat spinal cord. *Brain Res* 833:71–80.
- 1120 Prado WA, Raghbir R, Roberts MHT (1984) Long duration antinociception induced by red nucleus  
1121 stimulation in the rat. *Pain* 18:S329.
- 1122 Rogoz K, Andersen HH, Lagerström MC, Kullander K (2014) Multimodal use of calcitonin gene-related  
1123 peptide and substance P in itch and acute pain uncovered by the elimination of vesicular



- 1124 glutamate transporter 2 from transient receptor potential cation channel subfamily V member 1  
1125 neurons. *J Neurosci* 34:14055–14068.
- 1126 San Martin LS, Armijo-Weingart L, Araya A, Yévenes GE, Harvey RJ, Aguayo LG (2021) Contribution of glyr  
1127  $\alpha 3$  subunits to the sensitivity and effect of ethanol in the nucleus accumbens. *Front Mol*  
1128 *Neurosci* 14:756607.
- 1129 Schemann M, Kugler EM, Buhner S, Eastwood C, Donovan J, Jiang W, Grundy D (2012) The mast cell  
1130 degranulator compound 48/80 directly activates neurons. *PLoS ONE* 7:e52104.
- 1131 Sheng M, Greenberg ME (1990) The regulation and function of c-fos and other immediate early genes in  
1132 the nervous system. *Neuron* 4:477–485.
- 1133 Stantcheva KK, Iovino L, Dhandapani R, Martinez C, Castaldi L, Nocchi L, Perlas E, Portulano C, Pesaresi M,  
1134 Shirlekar KS, de Castro Reis F, Paparountas T, Bilbao D, Heppenstall PA (2016) A subpopulation of  
1135 itch-sensing neurons marked by Ret and somatostatin expression. *EMBO Rep* 17:585–600.
- 1136 Takazawa T, Choudhury P, Tong C-K, Conway CM, Scherrer G, Flood PD, Mukai J, MacDermott AB (2017)  
1137 Inhibition Mediated by Glycinergic and GABAergic Receptors on Excitatory Neurons in Mouse  
1138 Superficial Dorsal Horn Is Location-Specific but Modified by Inflammation. *J Neurosci* 37:2336–  
1139 2348.
- 1140 Todd AJ (2017) Identifying functional populations among the interneurons in laminae I-III of the spinal  
1141 dorsal horn. *Mol Pain* 13:1744806917693003.
- 1142 Tudeau L, Acuña MA, Albisetti GW, Neumann E, Ralvenius WT, Scheurer L, Poe M, Cook JM, Johannssen  
1143 HC, Zeilhofer HU (2020) Mice lacking spinal  $\alpha 2$ GABAA receptors: Altered GABAergic  
1144 neurotransmission, diminished GABAergic antihyperalgesia, and potential compensatory  
1145 mechanisms preventing a hyperalgesic phenotype. *Brain Res* 1741:146889.
- 1146 Ueno M, Nakamura Y, Li J, Gu Z, Niehaus J, Maezawa M, Crone SA, Goulding M, Baccei ML, Yoshida Y  
1147 (2018) Corticospinal Circuits from the Sensory and Motor Cortices Differentially Regulate Skilled  
1148 Movements through Distinct Spinal Interneurons. *Cell Rep* 23:1286-1300.e7.
- 1149 Usoskin D, Furlan A, Islam S, Abdo H, Lönnerberg P, Lou D, Hjerling-Leffler J, Haeggström J, Kharchenko  
1150 O, Kharchenko PV, Linnarsson S, Ernfors P (2015) Unbiased classification of sensory neuron types  
1151 by large-scale single-cell RNA sequencing. *Nat Neurosci* 18:145–153.
- 1152 Wang F, Flanagan J, Su N, Wang L-C, Bui S, Nielson A, Wu X, Vo H-T, Ma X-J, Luo Y (2012) RNAscope: a  
1153 novel in situ RNA analysis platform for formalin-fixed, paraffin-embedded tissues. *J Mol Diagn*  
1154 14:22–29.
- 1155 Wang H-C, Cheng K-I, Chen P-R, Tseng K-Y, Kwan A-L, Chang L-L (2018) Glycine receptors expression in rat  
1156 spinal cord and dorsal root ganglion in prostaglandin E2 intrathecal injection models. *BMC*  
1157 *Neuroscience* 19:72.
- 1158 Wang LX, Wang ZJ (2003) Animal and cellular models of chronic pain. *Adv Drug Deliv Rev* 55:949–965.
- 1159 Watson C, Paxinos G (2009) Chapter 16—Atlas of the Mouse Spinal Cord. *The Spinal Cord: A ...*

1160 Werynska K, Gingras J, Benke D, Scheurer L, Neumann E, Zeilhofer HU (2021) A Glra3 phospho-deficient  
1161 mouse mutant establishes the critical role of PKA-dependent phosphorylation and inhibition of  
1162 glycine receptors in spinal inflammatory hyperalgesia. Pain Available at:  
1163 <https://journals.lww.com/10.1097/j.pain.0000000000002236> [Accessed March 1, 2021].

1164 Woolf CJ, Safieh-Garabedian B, Ma QP, Crilly P, Winter J (1994) Nerve growth factor contributes to the  
1165 generation of inflammatory sensory hypersensitivity. Neuroscience 62:327–331.

1166 Yamamoto T, Yaksh TL (1993) Effects of intrathecal strychnine and bicuculline on nerve compression-  
1167 induced thermal hyperalgesia and selective antagonism by MK-801. PAIN 54:79.

1168 Yao GL, Tohyama M, Senba E (1992) Histamine-caused itch induces Fos-like immunoreactivity in dorsal  
1169 horn neurons: effect of morphine pretreatment. Brain Res 599:333–337.

1170 Zeilhofer HU (2005) The glycinergic control of spinal pain processing. Cell Mol Life Sci 62:2027–2035.

1171 Zeisel A et al. (2018) Molecular architecture of the mouse nervous system. Cell 174:999-1014.e22.

1172

JNeurosci Accepted Manuscript

1173 **Legends**

1174

1175 **Figure 1. *Gla3-Cre;tdTomato* neurons are predominantly located in laminae III–IV and the**  
1176 **adult *Gla3-Cre* population consists of a major excitatory and a minor inhibitory population.**

1177 **(A)** Overlap of spinal lumbar *Gla3-Cre;tdTomato* cells (magenta) and neuronal marker NEUN  
1178 (yellow). Yellow dotted circles display examples of tdTomato(+)NEUN(+) cells. **(B–B’)** Location  
1179 of tdTomato(+) cells (magenta) in IB4(+) outer lamina II (white), PKC $\gamma$ (+) inner lamina II  
1180 (yellow), laminae III–IV, V–VI, and ventral laminae defined from The Spinal Cord atlas (Anderson  
1181 et al., 2009). Yellow dotted circles represent examples of tdTomato(+)PKC $\gamma$ (+) cells. **(C)** Scatter  
1182 bar plot of the occurrence of tdTomato(+)NEUN(+) and tdTomato(+) cells in different spinal areas  
1183 (2 females, n images: NEUN: 10; 2 females, n images: PKC $\gamma$ /IB4: 13). **(D)** Schematic illustration  
1184 of AAVDJ.Ef1a-DIO-HTB lumbar 5/lumbar 6 (L5/L6) microinjection into *Gla3-Cre*(+) mice. **(E–**  
1185 **E’)** Overlap of *Gla3* (magenta) and *Vglut2* (white) in adult *Gla3-Cre*.HTB neurons (cyan).  
1186 Yellow dotted circles indicate *Gla3*(+) *Vglut2*(+), magenta dotted circles denote *Gla3*(+) *Vglut2*(-  
1187 ), and white circles represent *Gla3*(-) *Vglut2*(+) in *Gla3-Cre*.HTB(+) cells. **(F)** Scatter bar plot of  
1188 percentages of *Gla3-Cre*.HTB(+) neurons expressing analyzed genes when targeting *Vglut2* (2  
1189 males, n sections: 6, images: 12) **(G–G’)** *Gla3-Cre*.HTB neurons’ expression of *Gla3* (magenta)  
1190 and *Viaat* (white). Yellow dotted circles indicate *Gla3*(+) *Viaat*(-), white dotted circles represent  
1191 *Gla3*(-) *Vglut2*(+), and blue dotted circles show *Gla3*(-) *Vglut2*(-) in *Gla3-Cre*.HTB(+) cells. **(H)**  
1192 Scatter bar plot displaying percentages of *Gla3-Cre*.HTB(+) neurons expressing analyzed genes  
1193 when targeting *Viaat* (3 females, n sections: 7, images: 15). Scale bar: (A, B’, E, G): 100 $\mu$ m, (B):  
1194 150 $\mu$ m, (enlargement in A, E’, G’): 50 $\mu$ m, (enlargement in B): 75 $\mu$ m. The observational dots in

1195 the scatter bar plots (C, F, H) represent a unilateral part of the spinal cord and the different dot  
1196 colors signify different mice. Results are presented as mean±SEM.

1197

1198 **Figure 2. *Gla3-Cre;tdTomato* neurons respond to glycine and the populations display a**  
1199 **heterogeneous firing pattern. (A)** Patch-clamp recordings of spinal *Gla3-Cre;tdTomato* neurons  
1200 (magenta). A schematic patch pipette is indicated with a white arrowhead. Scale bar: 50µm. The  
1201 image on the right represents a recording of action potential firing (above) upon stimulation with a  
1202 depolarizing current for a duration of 500ms (below). **(B)** Pie chart of the distribution of different  
1203 action potential firing patterns (8 females, 7 males, n cells: 69). **(B')** Representative recording of  
1204 each firing pattern. The scale bar applies to all five traces. **(C)** Representative recordings of the  
1205 hyperpolarizing current induced by glycine (300µM, n cells: 13, above) and blockage by strychnine  
1206 (10µM, n cells: 6, below). The scale bar applies to both traces. **(D)** A Neurobiotin™ filled neuron  
1207 in a mouse spinal cord slice. Magenta(+) cells are *Gla3-Cre;tdTomato* neurons, PKCγ staining is  
1208 presented in white, blue is DAPI staining (scale bar: 50µm). The zoomed in image shows the  
1209 Neurobiotin™ filled neuron stained with Alexa Fluor™ 488 streptavidin conjugate (in green, scale  
1210 bar: 20µm). **(E)** Morphological and locational reconstruction of all Neurobiotin™ filled neurons  
1211 (n cells: 13, scale bar: 100µm). Laminae are defined from The Spinal Cord atlas (Anderson et al.,  
1212 2009).

1213

1214 **Figure 3. mCherry and chemogenetic viral vector fluorescent genes are not expressed in**  
1215 ***Gla3-Cre(-)* wildtype injected mice.** Low mCherry fluorescence detection, but no positive cells,  
1216 could be visualized in close proximity to the L5/L6 injection site of AAV8.hSyn-DIO-mCherry

1217 (control virus, 2 females and 1 male) (A), AAV8.hSyn-DIO-hM3D(Gq)-mCherry (1 female and 2  
1218 males) (B), or AAV8.hSyn-DIO-hM4D(Gi)-mCherry (2 females and 1 male) (C) injected mice,  
1219 demonstrating the Cre-dependent specificity of the viral vectors. Scale bars: 150 $\mu$ m.

1220  
1221 **Figure 4. Adult *Gla3*-Cre(+) neurons are mainly located in laminae III–IV and selective**  
1222 **chemogenetic activation induces spontaneous behaviors indicative of a role in nociception**  
1223 **and pruriception**

1224 (A) Expression of NEUN (yellow) in *Gla3*-Cre.mCherry (magenta) lumbar spinal cord. Yellow  
1225 dotted circles represent mCherry(+)NEUN(+) overlap and magenta dotted circles specify  
1226 mCherry(+)NEUN(-) cells. (B–B') mCherry(+) co-localization with outer lamina II marker IB4  
1227 (white), inner lamina II marker PKC $\gamma$  (yellow), and its expression in laminae III–IV, V–VI, and  
1228 ventral laminae defined from The Spinal Cord atlas (Anderson et al., 2009). The white dotted  
1229 circles show mCherry(+) expression in the IB4 band and magenta dotted circles indicate  
1230 mCherry(+)PKC $\gamma$ (-) cells in the PKC $\gamma$  band. mCherry(+)PKC $\gamma$ (+) cells are not shown in this  
1231 image. (C) Scatter bar plot of percentages of mCherry(+)NEUN(+) and laminae layer localization  
1232 of mCherry(+) neurons (2 females, 2 males, n sections: NEUN: 31; PKC $\gamma$ /IB4: 16). Scale bars: (A,  
1233 B): 100 $\mu$ m, (zoomed images): 50 $\mu$ m. The observational dots in the scatter bar plots represent a  
1234 unilateral part of the spinal cord, different dot colors signify different mice. Results are presented  
1235 as mean $\pm$ SEM. (D–F) Spontaneous behaviors, including licking/biting, stomping, and guarding of  
1236 the corresponding dermatome (hind paw/leg), were observed in *Gla3*-Cre.hM3Dq mice (7+8  
1237 mice; 7 females, 8 males) after 0.1 mg/kg intraperitoneal administration of CNO. (D) Chemogenetic  
1238 activation of the *Gla3*-Cre populations increased total duration and frequency of licking/biting of  
1239 the ipsilateral hind paw compared with *Gla3*-Cre.mCherry mice in the 30min time window post-

1240 CNO injection (duration  $p=.0006$ , frequency  $p=.0002$ ). **(E)** Spontaneous stomping behavior was  
1241 observed in *Gla3-Cre.hM3Dq* mice following CNO injection, which was not seen in *Gla3-*  
1242 *Cre.mCherry* mice (duration and frequency,  $p<.0001$ ). **(F)** *Gla3-Cre.hM3Dq* mice displayed  
1243 guarding behaviors not observed in control mice. Both guarding duration and frequency were  
1244 affected by *Gla3-Cre* populations activation ( $p<.0001$ ). Results are presented as mean $\pm$ SEM.  
1245 Mann-Whitney u test was performed in **D** and Chi-square test in **E–F** to compare the group means.  
1246 \*\* $p<.001$ , \*\*\* $p<.0001$ .

1247  
1248 **Figure 5. Chemogenetic silencing of *Gla3-Cre(+)* neurons decreases histaminergic and**  
1249 **chloroquine-induced itch.**

1250 **(A)** Dendritic and cytosolic expression of mCherry (magenta) after AAV8.hSyn-DIO-mCherry  
1251 microinjection (upper). Dendritic and cytosolic localization of hM4D(Gi)-mCherry (yellow) after  
1252 microinjection of AAV8.hSyn-DIO-hM4D(Gi)-mCherry (lower). **(B)** Intraperitoneal  
1253 administration of CNO (0.1mg/kg) did not induce spontaneous licking/biting of the affected  
1254 dermatome in the 0–30min or 30–60min intervals post-injection (duration: 0–30min:  $p=.7463$ , 30–  
1255 60min:  $p=.4589$ ; frequency: 0–30min:  $p=.4109$ , 30–60min:  $p=.3945$ , 8 mice/group; 11 females, 5  
1256 males). **(C)** Neither licking duration nor frequency were affected by saline administration (10 $\mu$ l,  
1257 duration  $p=.7923$ ; frequency  $p=.9405$ , 8 mice/group; 9 females, 7 males). **(D)** Silencing *Gla3-*  
1258 *Cre(+)* neurons attenuated the licking/biting duration and frequency following compound 48/80  
1259 (20 $\mu$ g, 10 $\mu$ l) injection (duration  $p=.0037$ ; frequency  $p=.0028$ , 8 mice/group; 8 females, 8 males).  
1260 **(E)** *Gla3-Cre.hM4Di* mice displayed lower licking/biting duration and frequency following  
1261 chloroquine (10mM, 10 $\mu$ l) injection (duration  $p=.0117$ ; frequency  $p=.0084$ , 8 mice/group; 9  
1262 females, 7 males). **(F)** Silencing of sacral *Gla3-Cre(+)* neurons did not affect the mechanical

1263 threshold in the tail ( $p=.5110$ , 7 mice/group, 7 females, 7 males). **(G–H)** *Gla3*-Cre(+) neurons are  
1264 not involved in thermal transmission. **(G)** Thermal stimulation (Hargreaves) of the ipsilateral hind  
1265 paw did neither affect the withdrawal latency in post-CNO administrated *Gla3*-Cre.hM4Di mice  
1266 compared with *Gla3*-Cre.mCherry mice, nor the response pre- and post-administration of CNO in  
1267 *Gla3*-Cre.hM4Di mice (*Gla3*-Cre.mCherry pre vs post CNO:  $p=.9981$ ; *Gla3*-Cre.hM4Di pre vs  
1268 post CNO:  $p=.9659$ ; *Gla3*-Cre.mCherry vs *Gla3*-Cre.hM4Di post CNO:  $p=.5326$ , 8 mice/group;  
1269 11 females, 5 males). **(H)** Application of acetone solution (9:1 in water) did not affect the aversive  
1270 response when silencing *Gla3*-Cre(+) neurons ( $p=.1145$ , 8 mice/group; 8 females, 8 males). Scale  
1271 bars (A): 100 $\mu$ m. All results are presented as mean $\pm$ SEM. To compare the mean values, Mann-  
1272 Whitney u test was performed in C (saline duration) and E, unpaired two-tailed Student t-test was  
1273 performed in C (saline frequency), D, F and H. In G, and a one-way ANOVA with Šidák's multiple  
1274 comparisons test was used. \* $p<.05$ , \*\* $p<.01$ .

1275  
1276 **Figure 6: Spinal neurons activated by compound 48/80 or chloroquine co-express *Gla3*.**

1277 C57BL/6J mice were subjected to different sensory stimuli, whereafter the *Gla3* (magenta) and  
1278 *fos* (cyan) co-expressional patterns were investigated (DAPI (dark blue)). **(A–B')** Saline (10 $\mu$ l) (1  
1279 female, 2 males), **(C–D')** compound 48/80 (20 $\mu$ g, 10 $\mu$ l; 1 female, 2 males), **(E–F')** chloroquine  
1280 (20mM, 10 $\mu$ l; 1 female, 2 males), **(G–H')** scratch (30sec, approximately 300mN (30.6g); 2  
1281 females, 1 male) and **(I–J')** pinch (5 times for 5sec; 1 female, 2 males) in urethane anesthetized  
1282 mice (2g/kg). **(K–L')** Hargreaves (stimulated 3 times; 2 females, 1 male) in awake and freely  
1283 moving mice. **(A–L)** Representative images of the contralateral and ipsilateral (stimulated side)  
1284 dorsal horns for each stimulus, with close ups. *Fos*(+)*Gla3*(+) cells are depicted by a dotted  
1285 magenta circle. Scale bars: (A–L): 100 $\mu$ m, (zoomed in A–B, E–J): 20 $\mu$ m, (zoomed in C–D, K–L):

1286 50 $\mu$ m. To obtain high resolution, two images of each dorsal horn were acquired and later merged  
1287 together, to a composited representative image of the dorsal horn, using Adobe Photoshop 22.3.  
1288 (A'–L') Schematic illustrations of the *fos*(+) and *fos*(+)*Glra3*(+) cells, where each cell is illustrated  
1289 by a circle; *fos*(+) in cyan and *fos*(+)*Glra3*(+) in magenta (n sections; saline:16, compound 48/80:  
1290 17, chloroquine: 17, artificial scratching: 16, pinch: 17 and Hargreaves: 18). (M) Scatter bar plot  
1291 of the average number of *fos*(+) cells per dorsal horn for each stimulus on the contralateral (white  
1292 bar) and ipsilateral (grey bar) side. (N–O) Scatter bar plot of the average number of *fos*(+)*Glra3*(+)  
1293 cells per dorsal horn for each stimulus on the contralateral (white bar) and ipsilateral (grey bar)  
1294 side. Results are presented as mean $\pm$ SEM. Individual mice are marked with magenta, yellow, and  
1295 cyan in M–O to display the spread between sections and mice. Paired two-tailed Student t-tests  
1296 were performed in M–O, and a one-way ANOVA with Šidák's multiple comparisons test to check  
1297 for differences between saline, compound 48/80, and chloroquine injections. M. Contralateral vs.  
1298 ipsilateral: saline p=.8372; compound 48/80 p<.0001; chloroquine p<.0001; artificial scratching  
1299 p<.0001; pinch p=.0014; and noxious heat (Hargreaves) p=.0218. N. The number of *fos*(+)*Glra3*(+)  
1300 cells was higher on the ipsilateral side when injecting compound 48/80 or chloroquine compared  
1301 with the contralateral side (saline p=.5194, compound 48/80 p<.0001 and chloroquine p<.0001).  
1302 Compared with saline injections, only compound 48/80 injection resulted in a higher number of  
1303 *fos*(+)*Glra3*(+) cells (p<.0001). O. No differences in the number of *fos*(+)*Glra3*(+) neurons were  
1304 detected for scratch (p=.6817), pinch (p=.0617), or Hargreaves (p=.1092). For separate channels,  
1305 see Figure 7. For overlap with *fos*, *Glra3* and *Vglut2* or *Viaat* for the following stimuli: scratching,  
1306 pinch and Hargreaves, see Figure 8.

1307



1308 **Figure 7. Expression of *Glr3* and *fos* in the contralateral L5/L6 dorsal horn following calf**  
1309 **or paw stimulation in anesthetized or awake freely moving mice. (A–F)** The expression of  
1310 *Glr3* (magenta) in the contralateral L5/L6 dorsal horn following sensory stimulation. (A’–F’)  
1311 Expression of *fos* (cyan) in the contralateral L5/L6 dorsal horn after sensory stimulation. **A–A’**  
1312 Saline (10µl, 1 female, 2 males) injection in urethane (2g/kg) anesthetized mice. **B–B’** Compound  
1313 48/80 (20µg, 10µl, 1 female, 2 males) injection in urethane anesthetized mice. **C–C’** Chloroquine  
1314 (20mM, 10µl, 1 female, 2 males) injection in urethane anesthetized mice. **D–D’** Scratching (30sec  
1315 with 2Hz and approximately 300mN (30.6g), 2 females, 1 male) in urethane anesthetized mice. **E–**  
1316 **E’** Pinching (5 times for 5sec, 1 female, 2 males) in urethane anesthetized mice. **F–F’** Hargreaves  
1317 (stimulated 3 times, 2 females and 1 male) in freely moving awake mice. Scale bars: 50µm. To  
1318 obtain high resolution, two images of each dorsal horn were acquired and later merged together to  
1319 a composited representative image of the dorsal horn using Adobe Photoshop 22.3.

1320

1321 **Figure 8. The expression of *Glr3*, sensory modality-induced *fos* cells, and *Vglut2* or *Viaat* in**  
1322 **L5/L6 after dorsolateral calf or paw mechanical or heat stimulation in anesthetized or awake**  
1323 **freely moving mice. (A–E’’) Expressional view (A–F) of *Glr3* (’, magenta), *fos* (’’, cyan), and**  
1324 ***Vglut2* or *Viaat* (’’, white) in the L5/L6 ipsilateral dorsal horn after sensory stimulation of the**  
1325 **dorsolateral calf in urethane (2g/kg) anesthetized mice (Scratch: 30sec with 2Hz and approximately**  
1326 **300mN (30.6g), 2 females, 1 male; Pinch: 5 times for 5sec; 1 female, 2 males). (a–e’’) Zoomed in**  
1327 **view of the respective marker genes after stimulation. (F–F’’) Expressional view (F) of *Glr3* (F’,**  
1328 **magenta), *fos* (F’’, cyan), and *Vglut2* or *Viaat* (F’’, white) in the L5/L6 ipsilateral dorsal horn after**  
1329 **noxious heat stimulation of the hind paw (stimulated 3 times with 20sec cut-off time; 2 females, 1**  
1330 **male) in awake freely moving mice. (f–f’’) Zoomed in view of the respective marker genes after**

1331 noxious heat stimulation. Magenta dotted circles show *fos(+)**Glr3(+)*, light pink indicates  
1332 *fos(+)**Viaat(+)*, and dark magenta shows *fos(+)**Glr3(+)**Vglut2(+)*. Scale bars: (A–F): 50µm, (a–  
1333 f’’’): 20µm. To obtain high resolution, two images of each dorsal horn were acquired and later  
1334 merged together to a composited representative image of the dorsal horn using Adobe Photoshop  
1335 22.3.

1336

1337 **Figure 9. Compound 48/80- and chloroquine-induced *fos* cells expressing *Glr3* are both**  
1338 **excitatory and inhibitory.** Expression of *fos*, *Glr3*, and *Vglut2* or *Viaat*, and the ipsilateral L5/L6  
1339 dorsal horn spatial location of cells expressing these genes (3 mice of mixed sex/stimulation, n  
1340 sections/mice: 2–4), following control saline (10µl, n sections: 9), compound 48/80 (20µg, 10µl, n  
1341 sections: *Vglut2*: 8; *Viaat*: 9), or chloroquine (20mM, 10µl, n sections: *Vglut2*: 9; *Viaat*: 9) calf  
1342 injections in urethane (2g/kg) anesthetized mice. (A) Schematic illustration of calf injections. (B)  
1343 The co-expression of *Vglut2* or *Viaat* in saline, compound 48/80- and chloroquine-activated  
1344 *fos(+)**Glr3(+)* cells. Both excitatory *Glr3(+)**Vglut2(+)* and inhibitory *Glr3(+)**Viaat(+)* neurons  
1345 are activated following saline, compound 48/80, and chloroquine administration. Saline-activated  
1346 *fos(+)**Glr3(+)* population showed 40.9±3.6% (94/231) co-expression with *Vglut2* and 56.1±4.4%  
1347 (124/218) with *Viaat*; compound 48/80 displayed 53.2±4.9% (208/373) and 45.7±3.2% (196/422)  
1348 co-expression with *Vglut2* and *Viaat*, respectively. Chloroquine-activated *fos(+)**Glr3(+)* neurons  
1349 co-expressed both *Vglut2* and *Viaat* in similar proportions: 40.8±4.6% (98/238) and 40.9±3.5%  
1350 (107/264), respectively. The graph presents data as mean±SEM. (C–H’’’’’) Each panel shows the  
1351 overview of the expression of the targeted genes with nucleus marker DAPI (dark blue) first,  
1352 followed by *Glr3* (’, magenta), sensory stimulation-induced *fos* (’’, cyan), and *Vglut2* or *Viaat*  
1353 (’’’, white). Magenta dotted circle: *fos(+)**Glr3(+)* cells; white dotted circle:

1354 *fos(+)**Glr3(+)**Vglut2(+)* or *fos(+)**Glr3(+)**Viaat(+)* cells. The schematic images in (') show the  
1355 spatial localization of the sensory-induced *fos(+)* cells (cyan), *fos(+)**Glr3(+)* (magenta), and  
1356 *fos(+)**Glr3(+)**Vglut2(+)* (C'', E'', G''; purple) or *fos(+)**Glr3(+)**Viaat(+)* (D'', F'', H'';  
1357 light pink) cells. (C'', D'') Saline injection resulted in a widespread *fos(+)* cell pattern in the  
1358 dorsal horn, and overlapping cells with *Glr3(+)* could be found in the whole dorsal horn.  
1359 Moreover, the saline-activated *fos(+)**Glr3(+)**Vglut2(+)* neurons were found to be located more to  
1360 the lateral part of the dorsal horn, while the saline-activated *fos(+)**Glr3(+)**Viaat(+)* cells were  
1361 more spread over the dorsal horn, with some clustering in the medial part of the dorsal horn. (E'',  
1362 F'') Compound 48/80-activated *fos(+)* cells were clustered in the superficial layer of the  
1363 dorsolateral horn, where *Glr3(+)**Vglut2(+)* cells (E'') and *Glr3(+)**Viaat(+)* cells (F'') were  
1364 found in the same area. (G'', H'') Chloroquine-activated *fos(+)* cells clustered in similar  
1365 patterns as observed for compound 48/80, but the chloroquine *fos(+)* cells were fewer in number  
1366 compared with compound 48/80. *Fos(+)**Glr3(+)**Vglut2(+)* cells (G'') were found more  
1367 dorsolateral, similar to *fos(+)**Glr3(+)**Viaat(+)* cells (H''), which were found mostly dorsolateral  
1368 but with a higher degree of scattering. Scale bars: (C, D, E, F, G, H): 100µm; (c, d, e, f, g, h): 50µm.  
1369 To obtain high resolution, two images of each dorsal horn were acquired and later merged together  
1370 to a composited representative image of the dorsal horn using Adobe Photoshop 22.3.

1371  
1372 **Figure 10. Starter and traced cells were mainly found in the lumbar division in *Glr3-Cre(+)***  
1373 **mice and only a few cells were detected in *Glr3-Cre(-)* mice. (A–A'').** No starter  
1374 GFP(+)mCherry(+) or traced mCherry(+) cells were detected in the thoracic (A'), lumbar (A'') or  
1375 sacral (A''') divisions in *Glr3-Cre(-)* mice. Two mCherry(+) cells were found in the cervical (A)  
1376 division in two separate mice, where 1 mCherry(+) cell was found in the contralateral ventral horn

1377 and 1 cell in the ipsilateral dorsal horn (3 females, 3 males, every sixth section analyzed). These  
1378 cells are not depicted in the image. **(B)** No starter GFP(+)mCherry(+) or traced mCherry(+) cells  
1379 were observed at the injection site of *Gla3-Cre(-)* mice. **(C)** Starter GFP(+)mCherry(+) and traced  
1380 mCherry(+) cells were found in the lumbar division (C'') and 1 mCherry(+) cell was observed in  
1381 the distant cervical (C), whereas no traced cells were located in the thoracic (C') or sacral (C''')  
1382 divisions in *Gla3-Cre(+)* mice (5 females, 5 males, every sixth section analyzed). **(D)** Starter  
1383 GFP(+)mCherry(+) and traced mCherry(+) cells were detected at the injection site of *Gla3-Cre(+)*  
1384 mice. The blue dotted circles represents GFP(+)mCherry(-) cells and the yellow dotted circles show  
1385 GFP(+)mCherry(+) starter cells. Traced mCherry(+) is not displayed in images. GFP is displayed  
1386 as cyan and mCherry as magenta (DAPI as yellow). Scale bars: (A–A'', C–C''): 300µm; (B, D):  
1387 150µm. For high resolution, images were acquired in 10x and were thereafter merged for  
1388 representation in Adobe Photoshop 22.3.

1389

1390 **Figure 11. Lumbar *Gla3-Cre(+)* neurons receive monosynaptic input from excitatory and**  
1391 **inhibitory local spinal neurons. (A)** Co-expression of NEUN (yellow) in *Gla3-Cre* starter  
1392 GFP(+)mCherry(+) and traced mCherry(+) cells. **(B)** Pie charts of NEUN overlap in ipsilateral  
1393 starter *Gla3-Cre(+)* (top chart) and traced cells (bottom chart) (3 females, 2 males, n images: 29).  
1394 **(C)** Co-localization of PAX2 (yellow) in *Gla3-Cre* starter GFP(+)mCherry(+) and traced  
1395 mCherry(+) cells. GFP is displayed as cyan and mCherry as magenta. **(D)** Pie charts of co-  
1396 expression of PAX2 in the starter *Gla3-Cre(+)* (top chart) and traced cells (bottom chart) (3  
1397 females, 2 males, n images: 31). Scale bars: (A, C): 150µm; (zoomed images): 75µm. **(E)**  
1398 Schematic illustration of the spatial localization of NEUN(+) and NEUN(-) *Gla3-Cre* starter  
1399 GFP(+)mCherry(+) and traced mCherry(+) cells in the ipsi- and contralateral spinal lumbar

1400 division. **(F)** Schematic illustration of *Gla3*-Cre starter GFP(+)mCherry(+) and traced mCherry(+)   
1401 cell localizations and overlap with PAX2 in the ipsi- and contralateral spinal lumbar division. The   
1402 marker(+) starter cells are shown as cyan dots and the marker(-) starter cells as grey dots, whereas   
1403 the marker(+) traced cells are depicted as yellow dots and marker(-) traced cells as magenta dots.   
1404 The schematic image was acquired from Atlas of the Mouse Spinal Cord (Watson and Paxinos,   
1405 2009). For starter and traced cells in *Gla3*-Cre(-) mice and the cervical, thoracic and sacral   
1406 divisions of the spinal cord in *Gla3*-Cre(+) mice, please see Figure 11.

1407   
1408 **Figure 12. Lumbar *Gla3*-Cre(+) neurons receive monosynaptic input from several brain**   
1409 **areas. (A–D)** Schematic illustrations of the mono- and pre-synaptic traced mCherry(+) cells found   
1410 in several brain areas (n cells=89 from 7 out of the ten mice; 5 females, 5 males; 3 females and 4   
1411 males had traced mCherry(+) cells). The brain areas with more than one mCherry(+) cell or the   
1412 brain areas with mCherry(+) cells in more than one mouse are shown in the figure. The coloring of   
1413 the dots represents the different mice and the schematic images were acquired from The Mouse   
1414 Brain Atlas in *Stereotaxic Coordinates* (Paxinos and Franklin, n.d.). **(A)** Traced mCherry(+) cells   
1415 in the ipsilateral and contralateral primary and secondary motor cortices (M1, M2) (bregma: -0.94–   
1416 (-)1.22mm; 2 females) and in the ipsilateral somatosensory cortex, barrel field (S1BF) (bregma:   
1417 0.38–(-)1.34mm; 1 male). **(B)** mCherry(+) cells were observed in the contralateral p1 reticular   
1418 formation (p1Rt) (bregma:-3.08–(-)3.16mm; 3 females). **(C)** The contralateral localization of   
1419 mCherry(+) cells in the magnocellular and parvicellular parts (RMC and RPC) (bregma: -3.08–(   
1420 )4.04mm; 3 females). **(D)** The ipsilateral and contralateral localization of traced mCherry(+) cells   
1421 in the oral and caudal part of the pontine reticular nucleus (PnO and PnC) (bregma: -4.24–(

1422 )5.23mm; 2 females, 2 males). **(E)** mCherry(+) cells were bilaterally localized in the gigantocellular  
1423 vestibular nucleus (Gi) (bregma: -5.88–(-)6.97mm; 2 females, 2 males). Scale bars: 100µm.

1424

1425 **Figure 13. The spinal *Gla3*-Cre populations receive monosynaptic information from**  
1426 **multiple subgroups of primary afferents. (A–K)** Co-expression of markers (yellow) in lumbar  
1427 DRG mCherry(+) traced cells (magenta). The cyan dotted circles indicate mCherry(+)marker(+) and the magenta dotted circles show examples of mCherry(+)marker(-) cells. **(A)** NF200: 2  
1428 females, 2 males. **(B)** TRKA: 2 females, 2 males. **(C)** CGRP: 1 female, 2 males. **(D)** IB4: 3 females,  
1429 1 male. **(E)** TH: 4 females, 2 males. **(F)** *Mrgprd*: 1 female, 2 males. **(G)** *Mrgpra3*: 1 female, 2  
1430 males. **(H)** SST: 2 females, 1 male. **(I)** *Nppb*: 1 female, 2 males. **(J)** *Trpv1*: 1 female, 2 males. **(K)**  
1431 *Trpm8*: 1 female, 2 males. Scale bars: 100µm. **(L)** Bar plot of the proportion of marker co-  
1432 expression in mCherry(+) DRG cells. **(M)** Bar plot of the occurrence of mCherry(+) in marker-  
1433 expressing DRG cells. The results are shown as total percentages of overlap. **(N)** Schematic  
1434 illustration of a root stimulation combined patch-clamp recording, where red dots indicate *Gla3*-  
1435 Cre(+) neurons. The traces in the middle are representative patch-clamp recordings of  
1436 monosynaptic inputs from different afferent fibers. **(O)** Venn diagram illustrating the distribution  
1437 of monosynaptic inputs from the different afferent fiber subtypes. The overlapping areas denote  
1438 neurons that received monosynaptic inputs from multiple afferent fiber subtypes. For separate  
1439 channels, see Figure 14.

1441

1442 **Figure 14. Spinal *Gla3*-Cre traced mCherry(+) co-localization with the marker genes and**  
1443 **tested proteins, relating to Figure 13.** Separate channel view of the different DRG markers from

1444 Figure 9. (A–K) The lumbar *Gla3*-Cre traced mCherry(+) cells in the DRG (magenta). (A'–K')

1445 Marker genes and proteins. Scale bars: 100µm.

JNeurosci Accepted Manuscript

1447 **Table 1. Membrane and firing properties of *Gla3-Cre:tdTomato* neurons**

| <b>Firing pattern</b>           | <b>Tonic<br/>(n=36)</b> | <b>Delayed<br/>(n=9)</b> | <b>Phasic<br/>(n=12)</b> | <b>Irregular<br/>(n=7)</b> | <b>Single<br/>(n=5)</b> | <b>Total<br/>(n=69)</b> |
|---------------------------------|-------------------------|--------------------------|--------------------------|----------------------------|-------------------------|-------------------------|
| Resting membrane potential (mV) | -59.37±1.54             | <b>-72.33*±3.15</b>      | -56.33±2.78              | -58.14±1.83                | -52.40±3.17             | -59.91±1.22             |
| Input resistance (MΩ)           | 1010.6±119.1            | 732.78±123.53            | 796.33±119.4             | 718.71±150                 | 649.60±110.31           | 879.43±70.08            |
| Capacitance (pF)                | 56.79±7.12              | 79.22±7.38               | 48.42±6.84               | 51.71±7.54                 | 26.40±6.23              | 55.07±4.34              |
| Rheobase (pA)                   | 21.24±2.82              | 23.33±3.51               | 19.00±4.55               | 20.43±2.89                 | 41.40±12.82             | 22.56±2.03              |
| AP threshold (mV)               | -31.38±1.55             | <b>-30.84±2.73</b>       | -28.34±2.88              | -36.69±1.65                | -25.14±6.51             | -30.94±1.12             |
| AP rising time (ms)             | 1.08±0.12               | 1.35±0.08                | 1.98±0.35                | 1.39±0.12                  | 1.27±0.32               | 1.34±0.10               |
| AP peak (mV)                    | 21.43±2.69              | 28.43±2.77               | 20.80±5.15               | 17.16±5.16                 | 19.59±7.68              | 21.71±1.85              |

\*: *Delayed AP group showed lower resting membrane potential (numbers in bold red) compared to all the other groups in two tailed one-way ANOVA followed by Turkey's Multiple Comparison Test.*



1449 **Table 2. Brain areas containing spinal lumbar *Gla3-Cre(+)* retrogradely traced neurons.**

| Sex    | Animal ID | Bregma        | Brain Structure Abbreviation | Brain Structure   | Number of cells | Ipsi/Contra |
|--------|-----------|---------------|------------------------------|---|-----------------|-------------|
| Female | 1         | -3.08–(-4.04) | RMC                          | Red nucleus, magnocellular part                                 | 5               | Contra      |
|        |           | -3.08         | p1Rt/REth                    | p1 reticular formation/retroethmoid nucleus                     | 1               | Contra      |
|        |           | -3.16         | p1Rt                         | p1 reticular formation  | 1               | Contra      |
|        |           | -3.52         | RMC/RPC                      | Red nucleus, magnocellular part/red nucleus, parvicellular part | 1               | Contra      |
|        |           | -3.80         | PaR                          | Pararubal nucleus   | 1               | Contra      |
|        |           | -5.80         | IRt                          | Intermediate reticular nucleus                                  | 2               | Contra      |
|        |           | -5.88         | MVeMC                        | Medial vestibular nucleus, magnocellular part                   | 1               | Ipsi        |

|        |   |       |         |   |   |        |
|--------|---|-------|---------|---|---|--------|
|        |   | -5.88 | MVePC   | Mmedial vestibular<br>nucleus,<br>parvicellular part                      | 2 | Contra |
|        |   | -6.12 | Gi      | Gigantocellular<br>vestibular nucleus                                     | 1 | Contra |
|        |   | -6.96 | MVe     | Medial vestibular<br>nucleus  | 1 | Contra |
| Female | 2 | -0.94 | M1      | Primary motor<br>cortex   | 3 | Contra |
|        |   | -0.94 | M2      | Secondary motor<br>cortex   | 3 | Contra |
|        |   | -1.22 | M1/M2   | Primary motor<br>cortex/ secondary<br>motor cortex                        | 1 | Ipsi   |
|        |   | -3.08 | p1Rt    | p1 reticular<br>formation   | 2 | Contra |
|        |   | -3.16 | RMC/RPC | Red nucleus,<br>mangocellular part/<br>red nucleus,<br>parvicellular part | 2 | Contra |
|        |   | -3.40 | RMC     | Red nucleus,<br>magnocellular part  | 2 | Contra |
|        |   | -4.04 | LPAG    | Lateral<br>periaqueductal gray  | 1 | ipsi   |

|               |          |  |   |                     |
|---------------|----------|--|---|---------------------|
| -4.04         | Su3      | Supraoculomotor<br>periaqueductal gray   | 1 | Ipsi                |
| -4.24         | mRT      | Mesencephalic<br>reticular formation   | 1 | Contra              |
| -4.24         | PTg/PnO  | Reticulotegmental<br>nucleus of the pons/<br>pontine reticular<br>nucleus, oral part | 1 | Contra              |
| -4.48–(-4.60) | PnO      | Pontine reticular<br>nucleus, oral part  | 7 | 1 ipsi, 6<br>contra |
| -5.20         | PnC      | Pontine reticular<br>nucleus, caudal part  | 2 | 1 ipsi, 1<br>contra |
| -5.20         | PO       | Paraolivary nucleus  | 1 | Contra              |
| -5.68         | SuVe     | Superior vestibular<br>nucleus   | 1 | Contra              |
| -5.88         | SuVe/LVe | Superior vestibular<br>nucleus/lateral<br>vestibular nucleus                         | 1 | Contra              |
| -5.88–(-7.08) | Gi       | Gigantocellular<br>vestibular nucleus  | 5 | 2 ipsi, 3<br>contra |
| -6.24–(-7.08) | SpVe     | spinal vestibular<br>nucleus   | 3 | 1 ipsi, 2<br>contra |
| -6.96         | C1       | C1 adrenaline cells  | 1 | Ipsi                |
| -7.08         | Sol      | Solitary tract   | 1 | Ipsi                |

|        |       |   |      |  |   |        |
|--------|-------|---|------|--|---|--------|
| Female | 3     | -1.22   | M1   | Primary motor cortex                   | 1 | Contra |
|        |       | -1.22   | M2   | Secondary motor cortex                 | 1 | Contra |
|        |       | -3.08   | p1Rt | p1 reticular formation                 | 3 | Contra |
|        |       | -3.28   | mRt  | Mesencephalic reticular formation      | 2 | Ipsi   |
|        |       | -3.28   | RMC  | Red nucleus, magnocellular part        | 1 | Contra |
|        |       | -3.28   | RPC  | Red nucleus, parvicellular part        | 5 | Contra |
|        |       | -4.24–(-4.60)                                 | PnO  | Pontine reticular nucleus, oral part   | 2 | Contra |
|        |       | -4.60   | Pa4  | Paratrochlear nucleus                  | 1 |        |
|        |       | -5.20   | PnC  | Pontine reticular nucleus, caudal part | 2 | Contra |
|        |       | -5.20   | PnR  | Pontine raphe nucleus                  | 1 | Ipsi   |
| -5.88  | MVeMC | Medial vestibular nucleus, magnocellular part | 1    | Contra                                 |   |        |
| Male   | 4     | -0.7  | RSD  | Retrosplenial dysgranular cortex       | 2 | Contra |

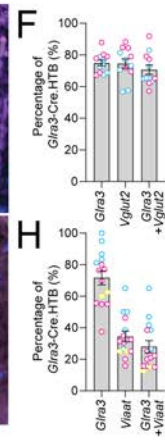
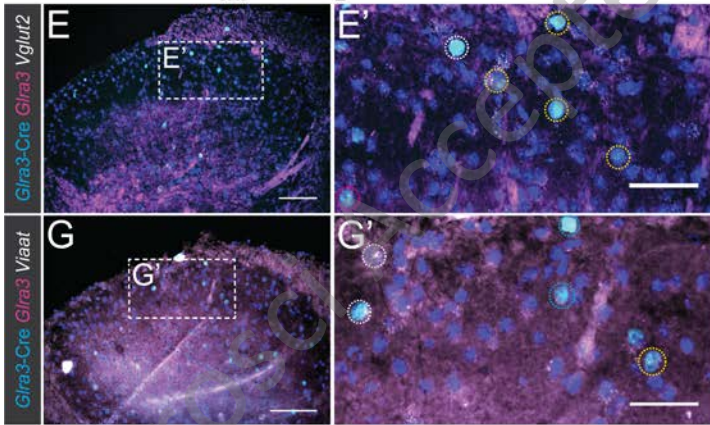
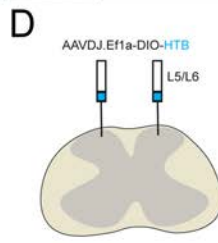
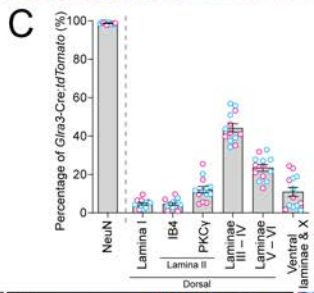
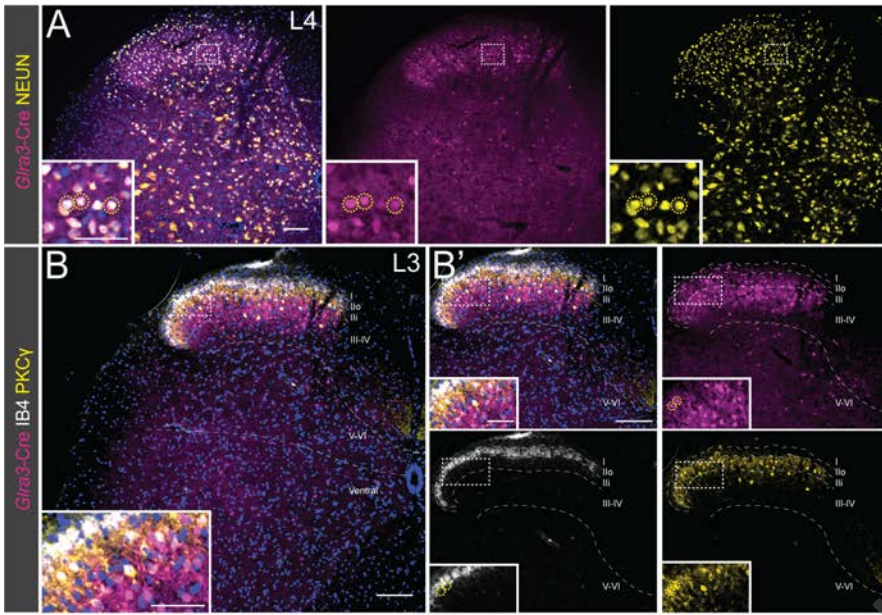
|      |   |       |                |  |   |        |
|------|---|-------|----------------|--|---|--------|
|      |   | -1.34 | S1BF           | Primary<br>somatosensory<br>cortex, barrel   | 1 | Ipsi   |
|      |   | 0.38  | S1BF/S1U<br>Lp | Primary<br>somatosensory<br>cortex, barrel/<br>Primary<br>somatosensory<br>cortex, upper lip | 1 | Ipsi   |
|      |   | -0.7  | S1HL           | Primary<br>somatosensory<br>cortex, hindleg  | 1 | Contra |
|      |   | -6.97 | Gi             | Gigantocellular<br>vestibular nucleus  | 1 | Ipsi   |
| Male | 5 | -5.23 | PnC            | Pontine reticular<br>nucleus, caudal part  | 2 | Contra |
|      |   | -6.64 | Gi             | Gigantocellular<br>vestibular nucleus  | 1 | Contra |
| Male | 6 | -4.16 | mRt            | Mesencephalic<br>reticular formation   | 1 | Contra |
|      |   | -6.0  | LVe            | Lateral vestibular<br>nucleus  | 1 | Contra |
|      |   | -7.78 | MdV            | Medullary reticular<br>nucleus, ventral part   | 1 | Contra |

|      |   |       |      |   |   |        |
|------|---|-------|------|---|---|--------|
| Male | 7 | -5.20 | PnC  | Pontine reticular<br>nucleus, caudal part | 1 | Contra |
|      |   | -5.88 | LPGi | Lateral<br>paragigantocellular<br>nucleus | 1 |        |

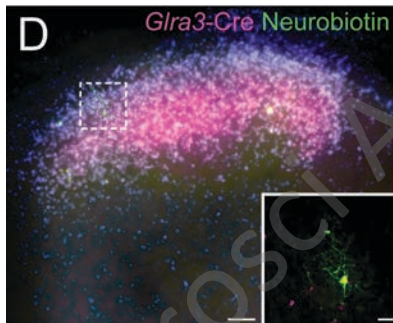
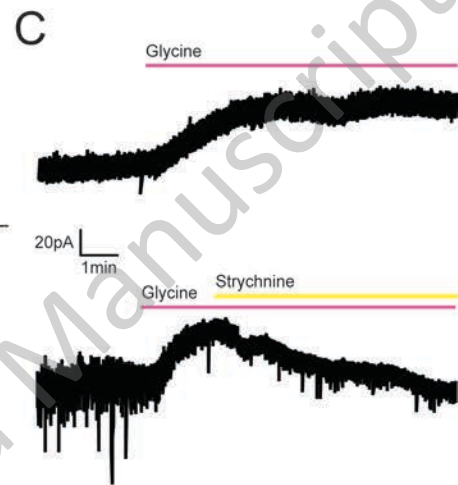
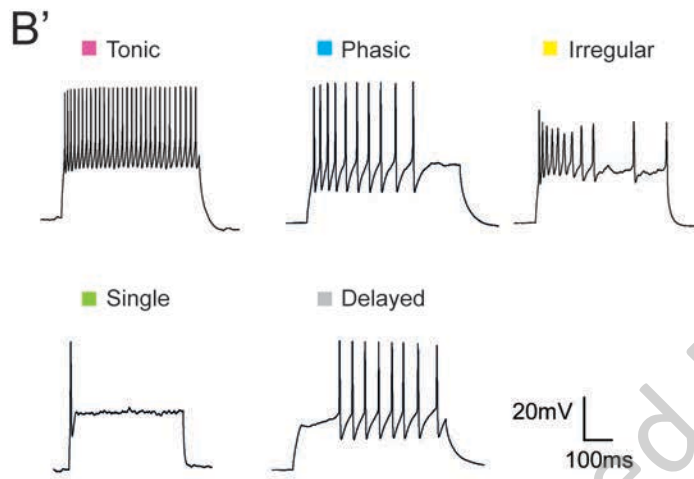
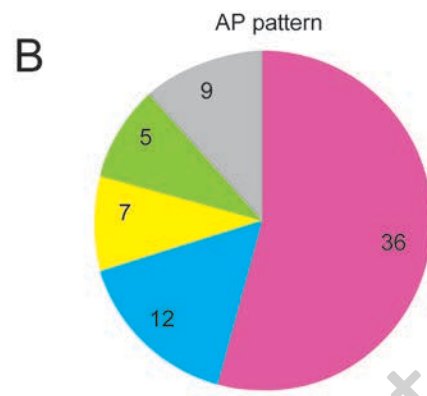
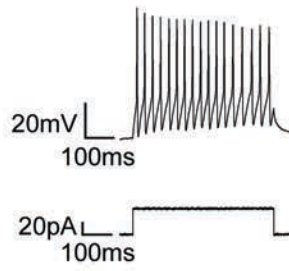
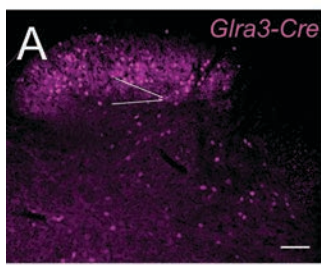
1450

1451

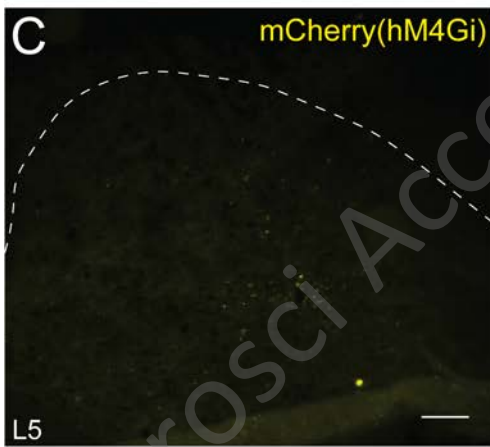
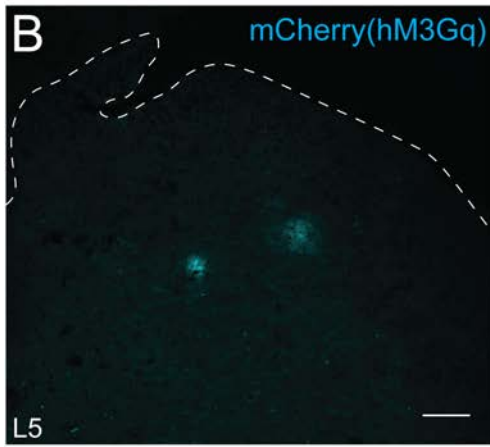
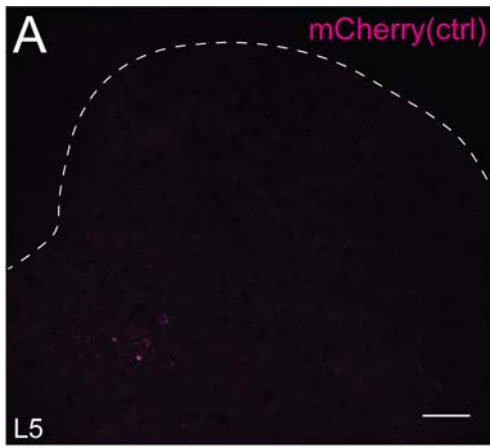
JNeurosci Accepted Manuscript



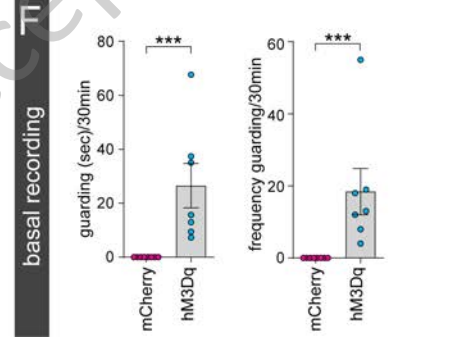
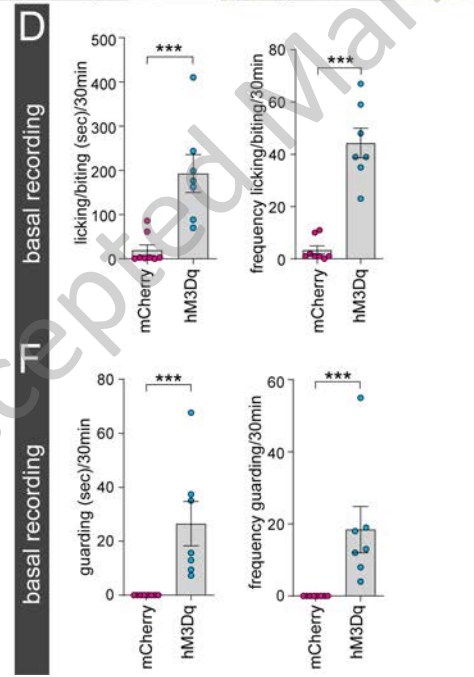
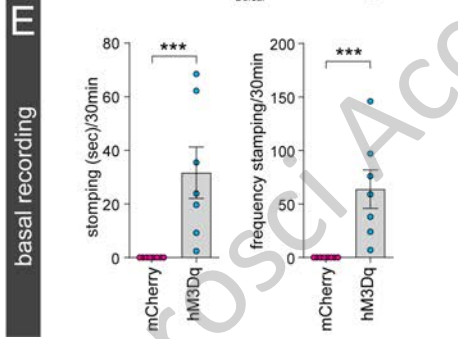
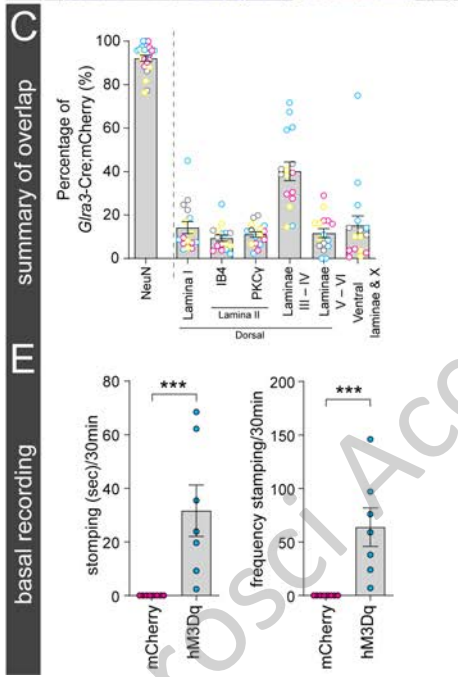
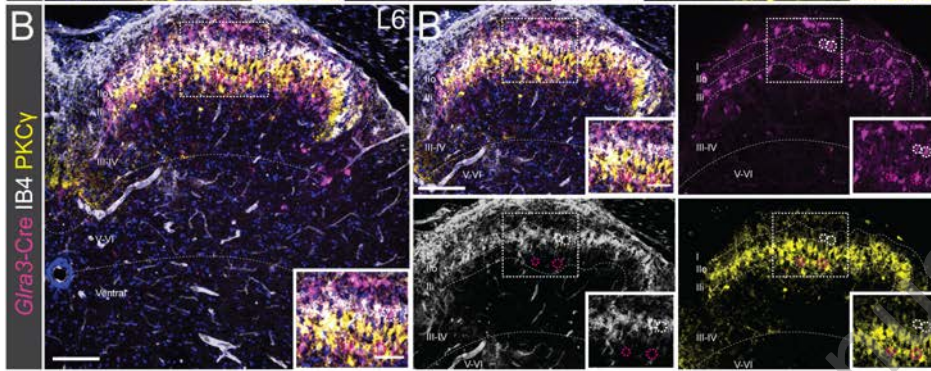
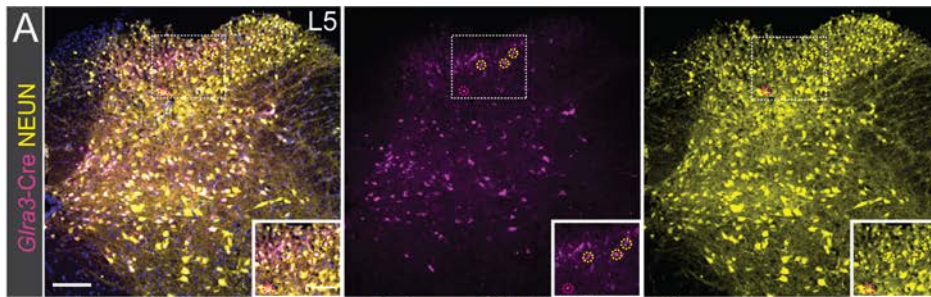
JNeurosci Accepted Manuscript



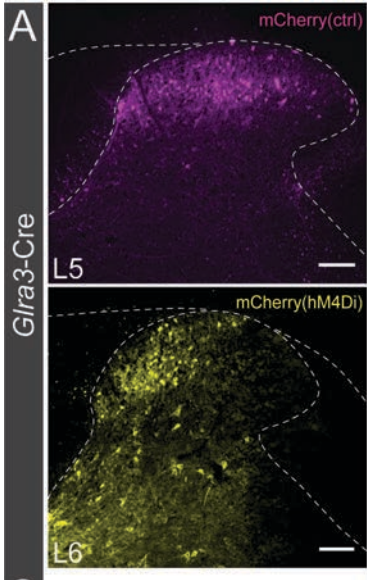




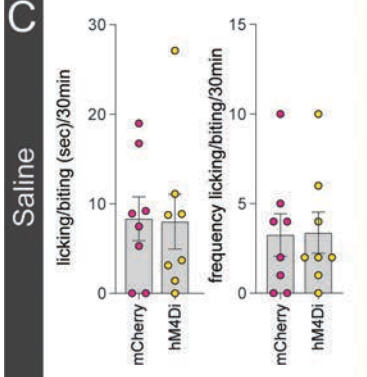
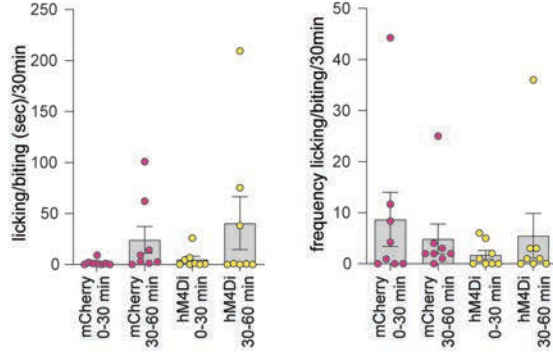
JNeurosci Accepted Manuscript



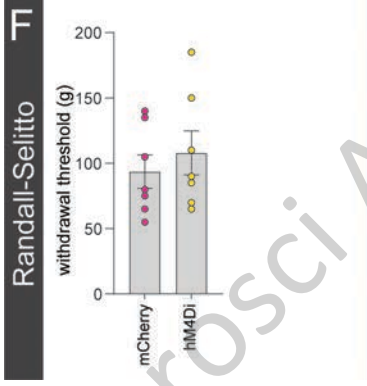
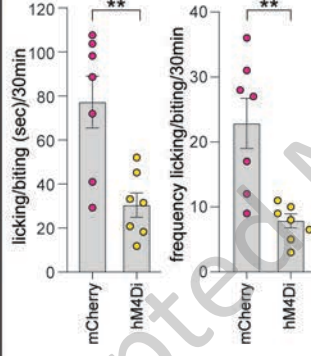
JNeurosci Accepted Manuscript



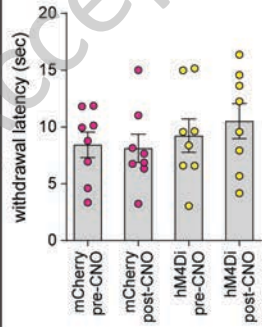
**B** Basal behavior



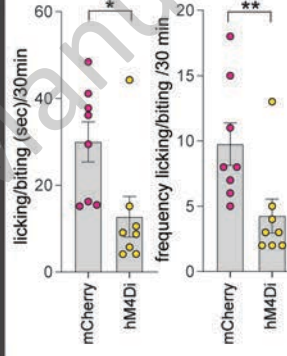
**D** Compound 48/80



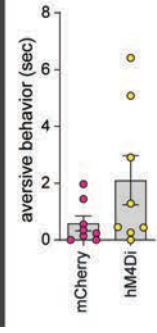
**F** Hargreaves



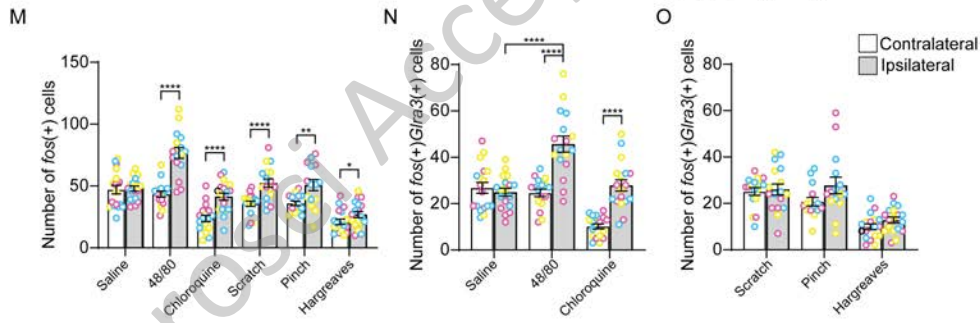
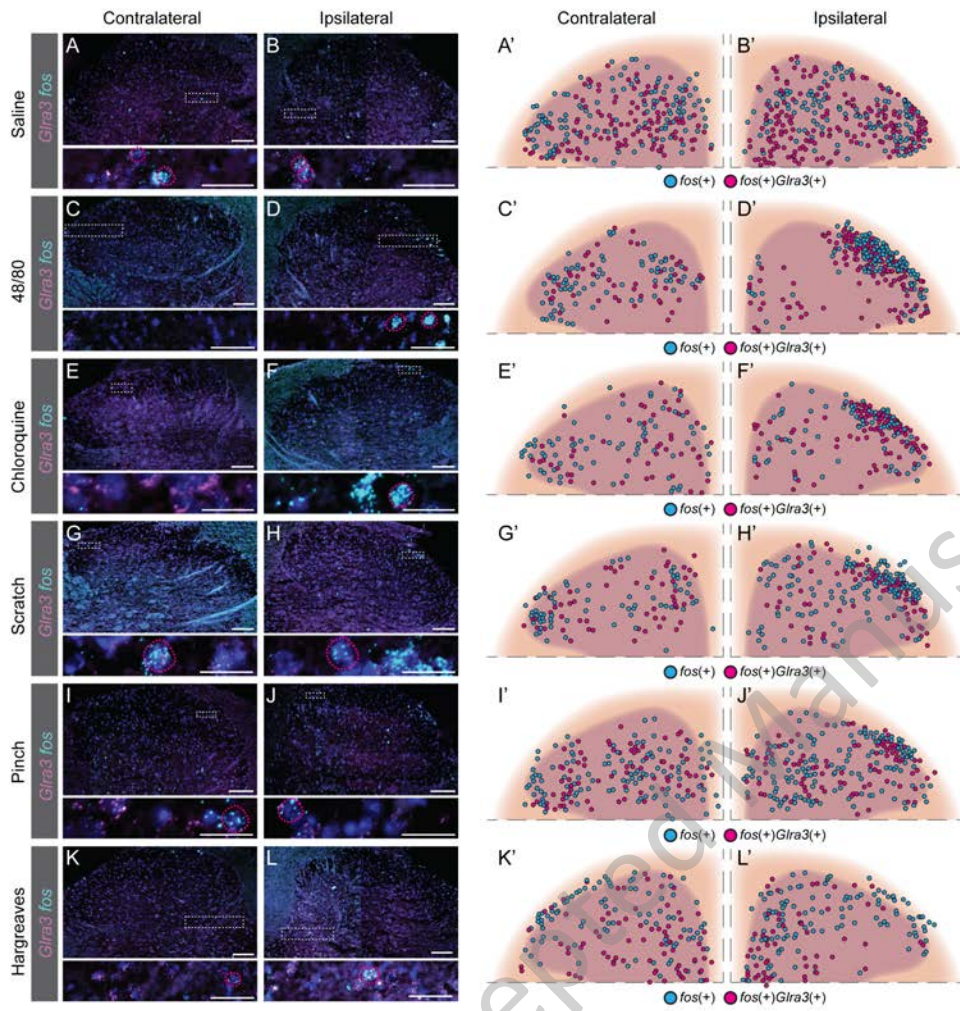
**G** Chloroquine

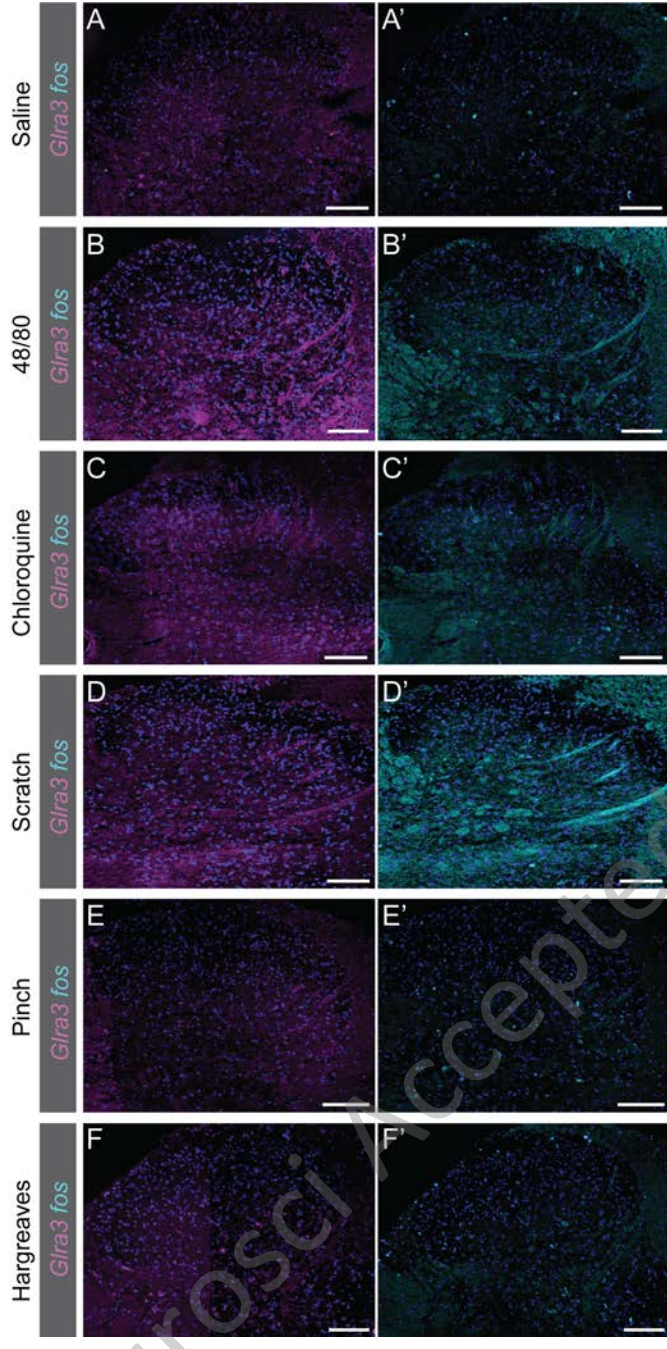


**H** Acetone

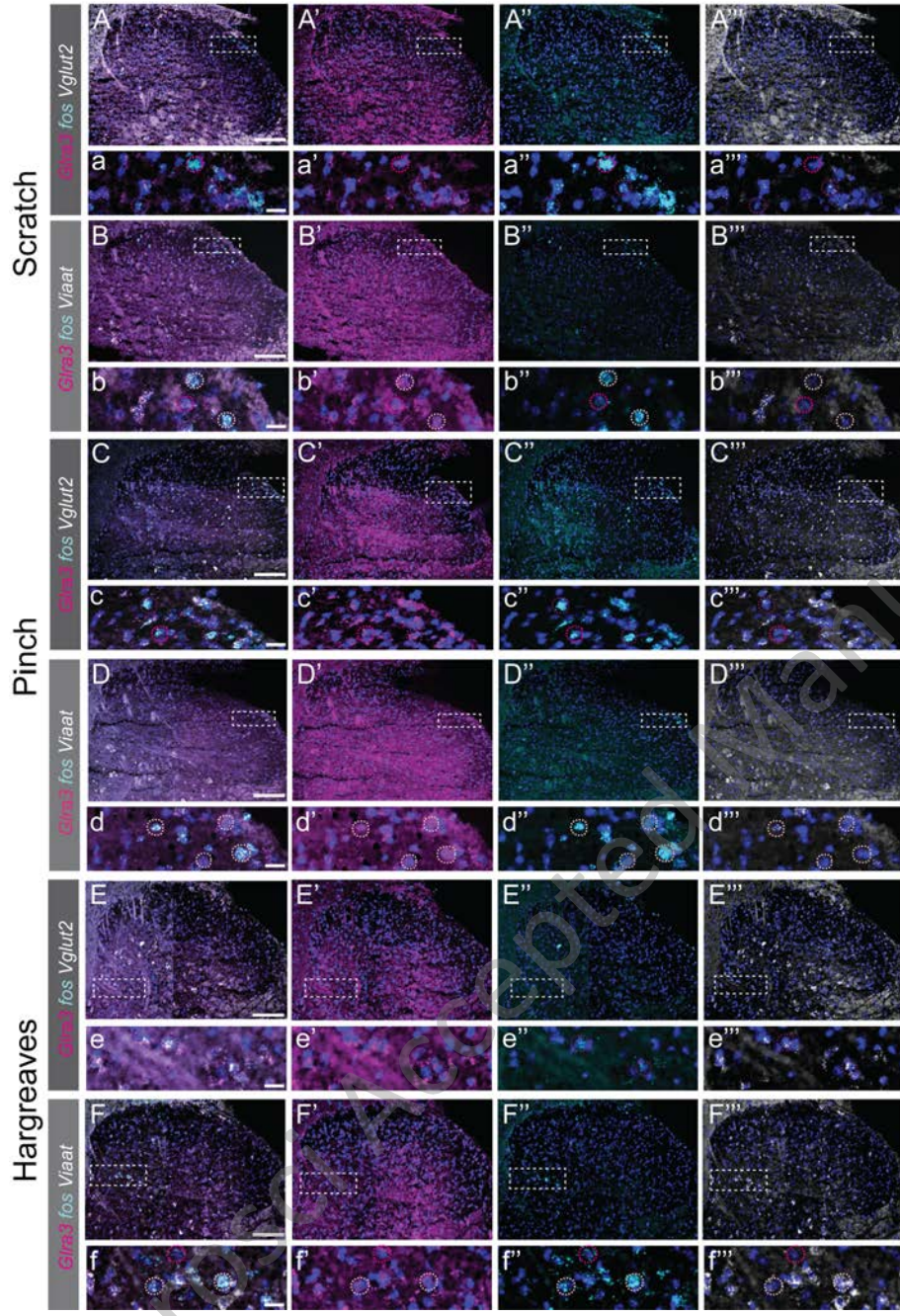


JNeurosci Accepted Manuscript

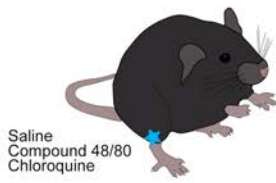




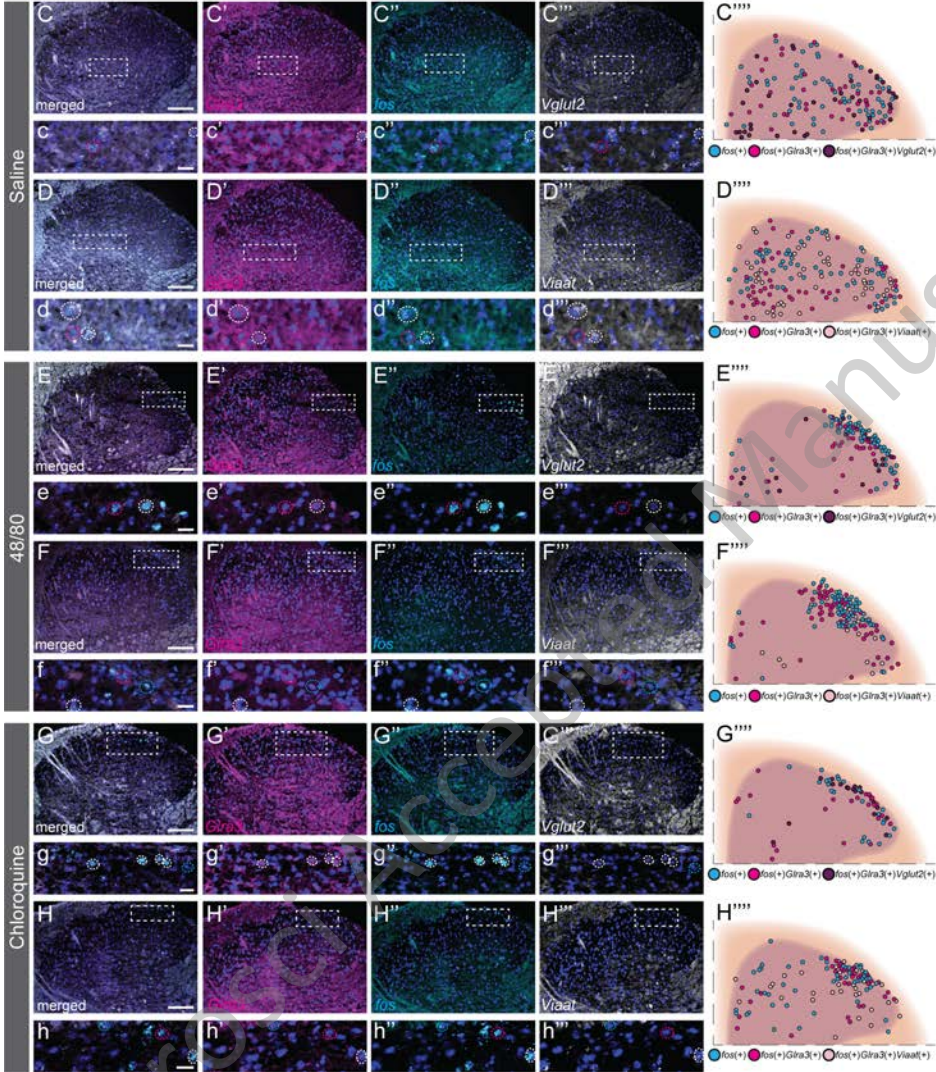
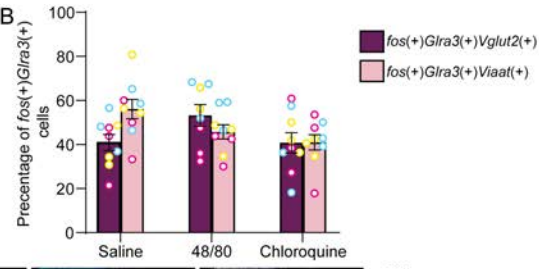
JNeurosci Accepted Manuscript



A

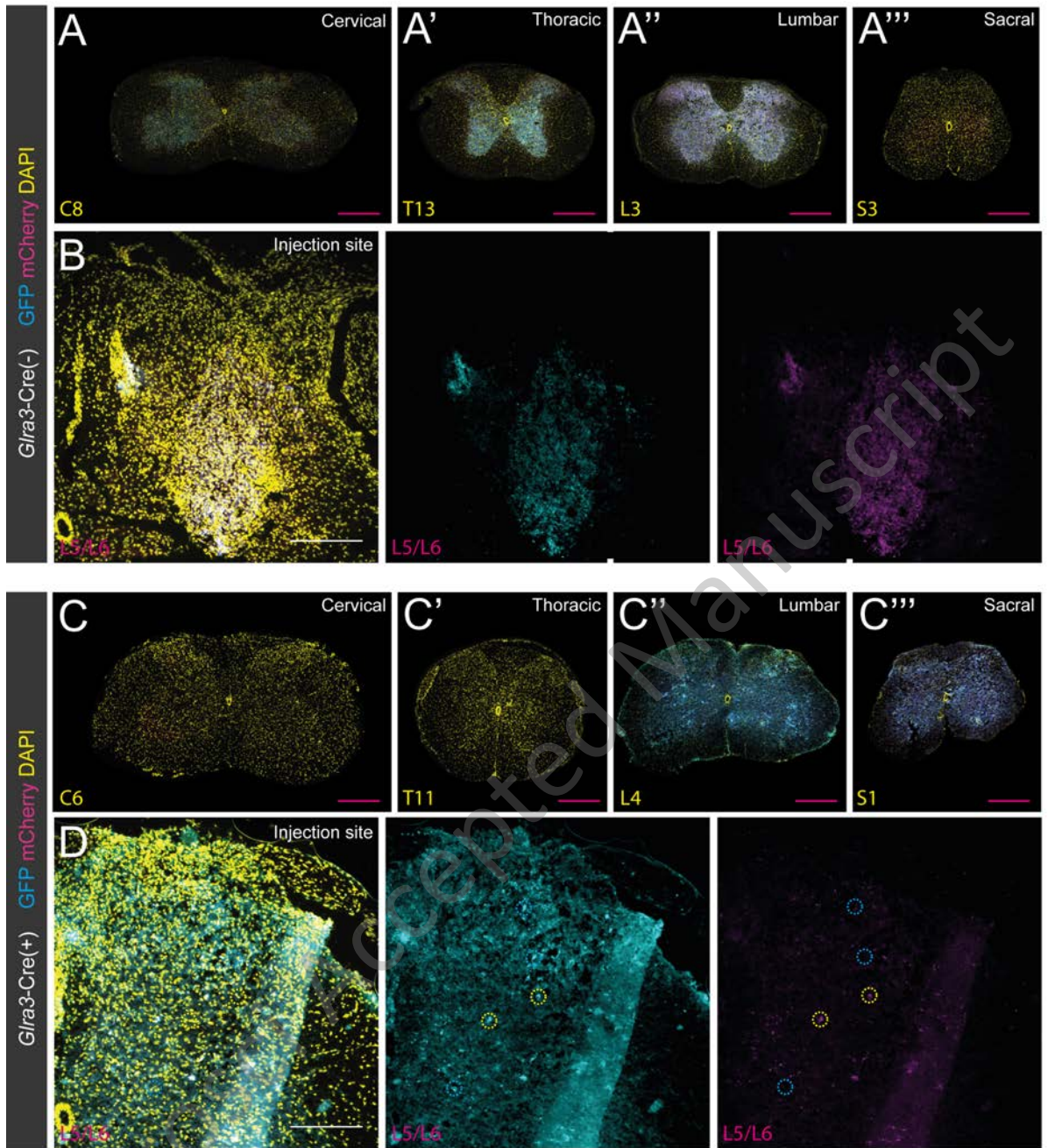


B

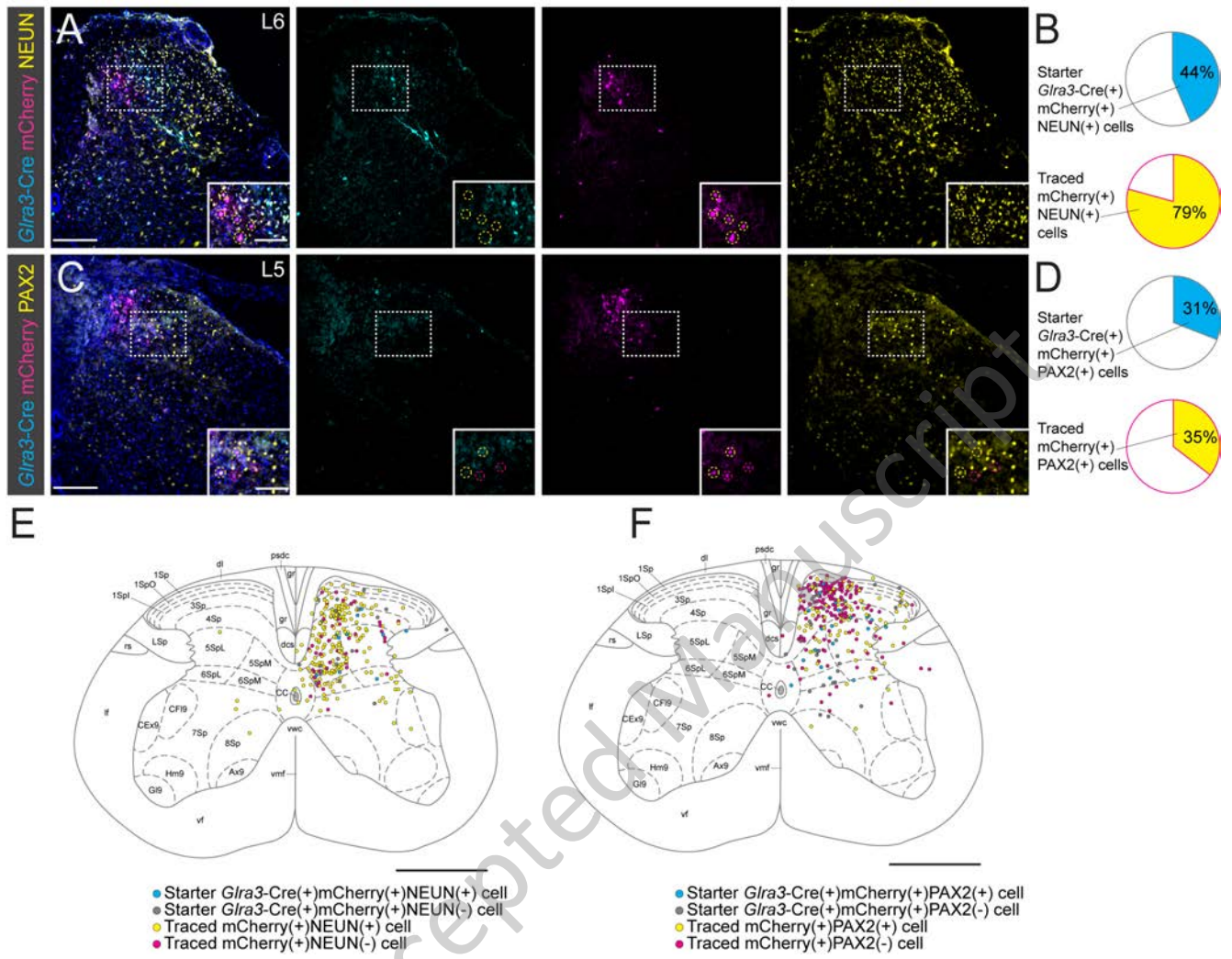


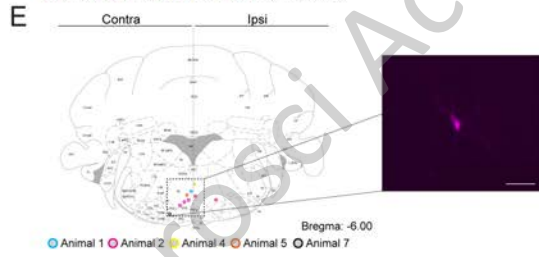
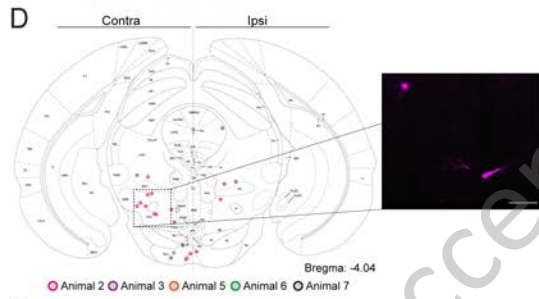
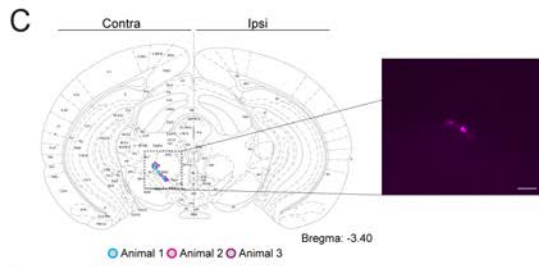
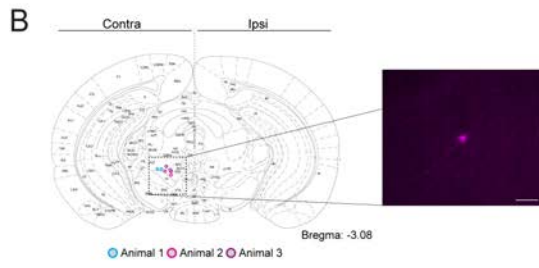
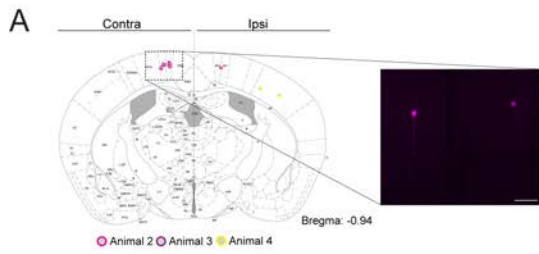
JNeurosci

Manuscript

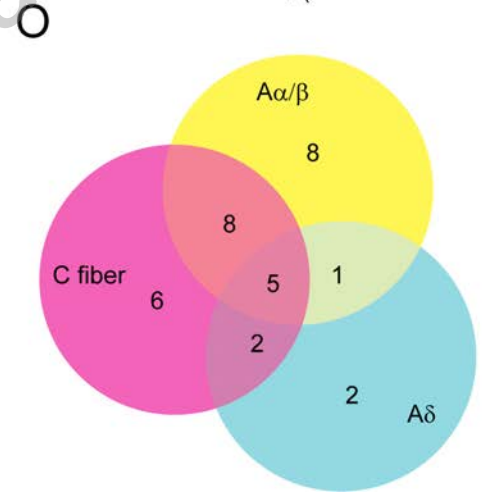
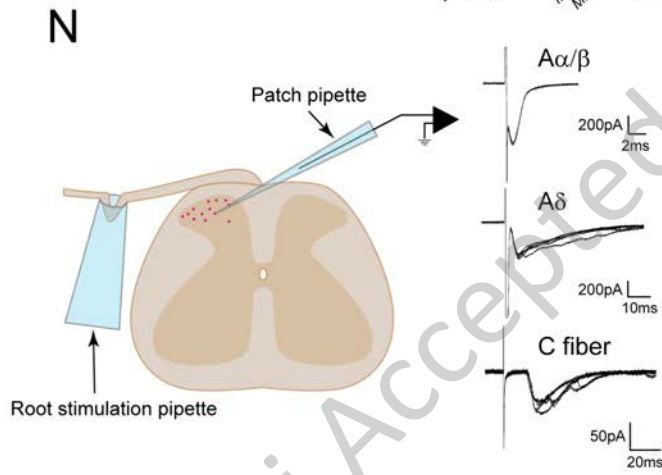
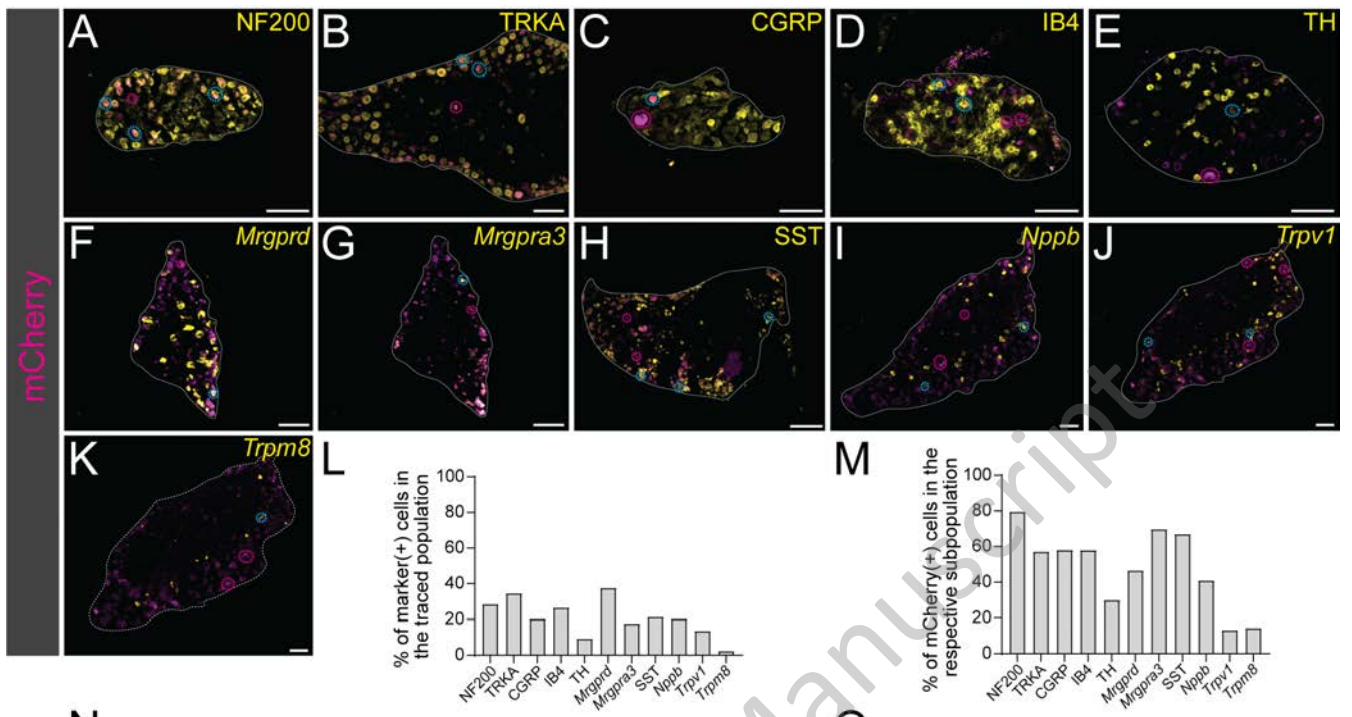








JNeurosci Accepted Manuscript



JNeurosci Accepted Manuscript

